A multiplexed Cas13-based assay with point-of-care attributes for simultaneous COVID-19 diagnosis and variant surveillance

Maturada Patchsung[1,†], Aimorn Homchan[1,2,†], Kanokpol Aphicho[1,†], Surased Suraritdechachai[1,†], Thanyapat Wanitchanon[1,5], Archiraya Pattama[3], Khomkrit Sappakhaw[1], Piyachat Meesawat[1], Thanakrit Wongsatit[1], Artittaya Athipanyasilp[1,3], Krittapas Jantarug[1], Niracha Athipanyasilp[3], Juthamas Buahom[3], Supapat Visanpattanasin[2], Nootaree Niljianskul[4], Pimchai Chaiyen[1], Ruchanok Tinikul[2], Nuanjun Wichukchinda[5], Surakameth Mahasirimongkol[5], Rujipas Sirijatuphat[6], Nasikarn Angkasekwinai[6], Michael A. Crone[7,8,9], Paul S. Freemont[7,8,9], Julia Joung[10,11,12,13,14], Alim Ladha[10,11,12,13,14], Omar Abudayyeh[12], Jonathan Gootenberg[12], Feng Zhang[10,11,12,13,14], Claire Chewapreecha[15,16] , Sittinan Chanarat[2], Navin Horthongkham[3,*], Danaya Pakotiprapha[2,*], Chayasith Uttamapinant[1,*]

[1]School of Biomolecular Science and Engineering, Vidyasirimedhi Institute of Science and Technology (VISTEC), Rayong, Thailand.
[2]Department of Biochemistry and Center for Excellence in Protein and Enzyme Technology, Faculty of Science, Mahidol University, Bangkok, Thailand.
[3]Department of Microbiology, Faculty of Medicine Siriraj Hospital, Mahidol University, Bangkok, Thailand.
[4]PTT Public Company Limited, Bangkok, Thailand.
[5]Division of Genomic Medicine and Innovation Support, Department of Medical Sciences, Ministry of Public Health, Nonthaburi, Thailand.
[6]Department of Medicine, Faculty of Medicine Siriraj Hospital, Mahidol University, Bangkok, Thailand.
[7]London Biofoundry, Imperial College Translation and Innovation Hub, White City Campus, 84 Wood Lane, London, UK.
[8]Section of Structural and Synthetic Biology, Department of Infectious Disease, Imperial College London, London, UK.
[9]UK Dementia Research Institute Centre for Care Research and Technology, Imperial College London, London, UK.
[10]Howard Hughes Medical Institute, Cambridge, MA, USA.
[11]Broad Institute of MIT and Harvard, Cambridge, MA, USA.
[12]McGovern Institute for Brain Research at MIT, Cambridge, MA, USA.
[13]Department of Biological Engineering, MIT, Cambridge, MA, USA.
[14]Department of Brain and Cognitive Sciences, MIT, Cambridge, MA, USA.
[15]Mahidol-Oxford Tropical Medicine Research Unit, Faculty of Tropical Medicine, Mahidol University, Bangkok, Thailand.
[16]Wellcome Sanger Institute, Hinxton, UK.
[†]These authors contributed equally to this work
[*]Corresponding authors: danaya.pak@mahidol.ac.th; navin.hor@mahidol.edu; chayasith.u@vistec.ac.th

Abstract

Point-of-care (POC) nucleic acid detection technologies are poised to aid gold-standard technologies in controlling the COVID-19 pandemic, yet shortcomings in the capability to perform critically needed complex detection—such as multiplexed detection for viral variant surveillance—may limit their widespread adoption. Herein, we developed a robust multiplexed CRISPR-based detection using LwaCas13a and PsmCas13b to simultaneously diagnose SARS-CoV-2 infection and pinpoint the causative SARS-CoV-2 variant of concern (VOC)—including globally dominant VOCs Delta (B.1.617.2) and Omicron (B.1.1.529)—all while

51   maintaining high levels of accuracy upon the detection of multiple SARS-CoV-2 gene targets.
52   The platform has several attributes suitable for POC use: premixed, freeze-dried reagents for
53   easy use and storage; convenient direct-to-eye or smartphone-based readouts; and a one-pot
54   variant of the multiplexed detection. To reduce reliance on proprietary reagents and enable
55   sustainable use of such a technology in low- and middle-income countries, we locally produced
56   and formulated our own recombinase polymerase amplification reaction and demonstrated its
57   equivalent efficiency to commercial counterparts. Our tool—CRISPR-based detection for
58   simultaneous COVID-19 diagnosis and variant surveillance which can be locally
59   manufactured—may enable sustainable use of CRISPR diagnostics technologies for COVID-
60   19 and other diseases in POC settings.

61

62   **Introduction**
63   The recurrent emergence of new severe acute respiratory syndrome coronavirus 2 (SARS-
64   CoV-2) variants emphasizes the need of broad genomic and variant surveillance to monitor
65   SARS-CoV-2 characteristics and evolution. Genomic and variant surveillance is critical to the
66   understanding of the public health risk posed by new variants, as well as to the re-design and
67   continual improvements of vaccines, therapeutics, and diagnostic technologies. Low- and
68   middle-income countries (LMICs) are hotspots where several SARS-CoV-2 variants of
69   concern (VOCs) are postulated to emerge from (Bi et al., 2022), yet LMICs are at a distinct
70   disadvantage in ramping up variant surveillance capacity, due to resources being more limited,
71   mismanaged, or both. The majority (77%) of LMICs sequenced a minuscule fraction (<0.5%)
72   of their COVID-19 cases; 20 LMICs do not have any sequencing activity reported in public
73   databases (Brito et al., 2021). Together, this calls for a robust and affordable genomic
74   surveillance for LMICs.

75

76   Beyond genomic/variant surveillance activity, LMICs have limited access to the newest crisis
77   management technologies; lack the capacity and infrastructure to manufacture and distribute
78   crisis-critical products; and rely heavily on imports of these products which are subjected to
79   constraints in the supply chain. Efforts to strengthen genomic/variant surveillance activity of
80   LMICs in a sustainable manner—through the development of simple-to-use surveillance tools
81   that can be locally manufactured–should be a global priority. Ideally, diagnostics and
82   genomic/variant surveillance should be combined in the same technological platform to
83   maximize disease detection and variant surveillance capacity while optimizing resource use.

84

85   Genetic surveillance of SARS-CoV-2 can either target the whole viral genome or specific
86   genetic variations such as single nucleotide polymorphisms and indels through the use of next-
87   generation sequencing or quantitative real-time PCR with reverse transcription (RT-qPCR)
88   (European Centre for Disease et al., 2021). However, both sequencing- and PCR-based
89   investigations could be slow in returning results, thereby delaying an effort to contain the
90   outbreak especially for VOCs with greater transmissibility such as Delta (B.1.617.2; R_0 of 5-7
91   (Burki, 2021; Liu & Rocklöv, 2021) and Omicron (B.1.1.529; R_0 estimated to be as high as 10
92   (Burki, 2022)). Most importantly, current surveillance technologies require complicated,
93   expensive instruments and expertise in handling and data analysis, resulting in the limited use
94   of these technologies in LMICs (Brito et al., 2021) where disease detection and variant
95   surveillance are critically needed.

96

97   The collateral activity of clustered regularly interspaced short palindromic repeats (CRISPR)-
98   associated 12/13 (Cas12/13) nucleases (Chen et al., 2018; Gootenberg et al., 2018; Gootenberg
99   et al., 2017; Harrington et al., 2018) has recently been used as a basis for nucleic acid detection,
100   including that of SARS-CoV-2 (Broughton et al., 2020; Fozouni et al., 2020; Joung et al., 2020;

101   Patchsung et al., 2020). CRISPR-based detection has many attributes suitable for use in LMICs
102   especially in point-of-care settings: the assay does not need complicated equipment and
103   provides fast-to-return results, while maintaining high levels of diagnostic accuracy and
104   complex testing capabilities characteristic of laboratory-based diagnostic technologies.
105   CRISPR-based detection is particularly amenable to multiplexing, due to orthogonal cleavage
106   preferences of bystander nucleic acid probes by different Cas enzymes—particularly the Cas13
107   family—each of which can be programmed for sequence-specific detection by its
108   corresponding crRNA (Gootenberg et al., 2018). Due to its high sequence specificity (when
109   carefully designed and/or optimized), CRISPR-based detection has been explored as a tool to
110   map key SARS-CoV-2 mutations. A few reported technologies use equipment-heavy PCR (He
111   et al., 2022) and Fluidigm microfluidics (Welch et al., 2022) to amplify genetic materials and
112   increase the assay throughput, respectively. While such technologies drastically enhance the
113   ability to profile multiple mutations of SARS-CoV-2 and other viruses, the reliance on
114   extensive equipment may exclude them from utility in resource-poor settings. Equipment-light
115   CRISPR-based detection is considered highly practical for several reasons: these platforms
116   often combine an isothermal amplification step—compatible with a simple heating apparatus
117   like a water bath and obviating the need of a PCR thermocycler—with a CRISPR-Cas-based
118   detection step for maximal sensitivity and specificity. While discrimination of SARS-CoV-2
119   VOCs can be achieved with POC CRISPR-based detection, current POC CRISPR-based assays
120   have diminished sensitivity (a trade-off upon using a simplified protocol (Arizti-Sanz et al.,
121   2021) and lack multiplexed detection capability (Arizti-Sanz et al., 2021; Fasching et al., 2022).
122
123   Here we develop multiplexed CRISPR-based detection with point-of-care characteristics to
124   clinically diagnose SARS-CoV-2 infection and inform the causative VOCs in the same
125   reaction, while maintaining high sensitivity of detection (Figure 1). To do so, we extensively
126   optimized components and reaction conditions of the reverse-transcription recombinase
127   polymerase amplification (RT-RPA) to enable multiplexed amplification of two SARS-CoV-
128   2 genes, *n* and *s* (Figure 1A, B). We explored several Cas13 enzymes including an engineered
129   variant for multiplexed, orthogonal CRISPR-Cas13-based detection, and further screened
130   different parameters for improved detection sensitivity. We lyophilized premixed amplification
131   and CRISPR reactions and stored them in freeze-dried forms, which can be reconstituted
132   simply through addition of buffered nucleic acid analytes. The freeze-dried reagent format
133   enables convenient field deployment as well as longer reagent shelf-life. We further developed
134   a highly sensitive one-pot reaction which combines multiplexed RT-RPA and Cas13-based
135   detection in the same tube and demonstrated a simple visualization setup for multiplexed gene
136   detection. Finally, our system was successfully validated in suspected SARS-CoV-2 samples
137   from the real clinical setting; an indicative of both feasibility and robustness of our multiplexed
138   Cas13-based assay.
139
140   After assessing cross-reactivity and the limit of detection (LoD), we clinically validated the
141   multiplexed CRISPR-based detection of SARS-CoV-2 *n* and *s* genes (Figure 1B, top) on 136
142   clinical samples containing a full range of threshold cycle values (13-39). We found the
143   multiplexed CRISPR-based detection of SARS-CoV-2 obtained from nasopharyngeal and
144   throat swabs of infected patients to be 100% specific and 95-97% sensitive compared to RT-
145   qPCR. Within the characterized LoD (Ct ~37) the method is 100% specific and 100% sensitive.
146   To allow for broader implementation of the technology during the pandemic, we submitted the
147   most sensitive version of our freeze-dried, multiplexed CRISPR-based detection of SARS-
148   CoV-2 RNA for technological evaluation with the Food and Drug Administration (FDA) of
149   Thailand, and received full approval on September 22, 2021.
150

151   With emerging VOCs, we re-designed our multiplexed detection platform—with minimal
152   adjustments to our FDA-approved protocol beyond new primers and crRNAs—to concurrently
153   diagnose SARS-CoV-2 infection—via pan-variant detection of the *n* gene—and discriminate
154   the highly transmissible Delta (B.1.617.2) and Omicron (B.1.1.529) via variant-specific
155   detection of the *s* gene (Figure 1B, bottom). Our best design for multiplexed Delta variant
156   detection showed excellent sensitivity (LoD at C_t ~37) and specificity, with no cross-reactivity
157   toward wild-type, Alpha (B.1.1.7), and Omicron SARS-CoV-2. Our Omicron variant
158   detection—which detected the HV69-70 deletion also found in the now extinct Alpha strain—
159   was slightly less sensitive (LoD at C_t ~34) and exhibited minimal cross-reactivity with wild-
160   type and Delta SARS-CoV-2.
161
162   To sustain SARS-CoV-2 detection and variant surveillance capability in LMICs, we also report
163   here an RT-RPA reaction in which all protein components of RPA were locally produced in
164   Thailand, and demonstrated similar amplification efficiency, including for multiplexed
165   detection, of the locally produced RPA to commercial RPA. Our overall setup (Figure 1C)—
166   an equipment-light, field-deployable, and easy-to-use multiplexed CRISPR-based assay
167   capable of simultaneous detection of SARS-CoV-2 and VOC identification, while maintaining
168   high specificity and sensitivity—can now be prepared with locally manufactured components,
169   providing affordable access of critical reagents for diagnostic and variant surveillance assays
170   to the most vulnerable populations.
171

Results
Developing multiplexed reverse-transcription RPA for SARS-CoV-2 RNA detection
174   Standard SARS-CoV-2 laboratory diagnostics include the detection of at least two loci, often
175   in a multiplexed manner, as a precaution against escape mutations (Tang et al., 2020); we
176   wished to first confer this multiplexed detection capability to our platform. We focused our
177   optimization of multiplexed isothermal amplification on the RPA technique, as we and others
178   (Bao et al., 2020) found another popular isothermal amplification technique, LAMP, to be
179   highly susceptible to carryover contamination, likely due to its generation of large concatemer
180   amplicons that are highly amplificative and resistant to degradation. RPA can also be
181   performed at lower, near ambient temperature, making it more easily deployed for point-of-
182   care or field applications. Our previous work identified four sets of RPA primer pairs which
183   enable amplification of the spike (*s*), nucleocapsid (*n*), and two regions within the replicase
184   polyprotein 1ab (*orf1ab*) genes of SARS-CoV-2 (Patchsung et al., 2020) (Figure 1–figure
185   supplement 1A). Their amplification rates were variable, with the primer pair detecting the *s*
186   gene being the most sensitive (Patchsung et al., 2020). We found that simply combining two
187   of these primer pairs did not result in amplification of both targets, as the fast-amplifying
188   product of one gene would dominate the reaction (Figure 1–figure supplement 1). In order to
189   achieve simultaneous amplification of two targets, the amplification rates of both targets should
190   match (Jauset-Rubio et al., 2018), and be as high as possible for maximal sensitivity. We
191   decided to focus on improving the amplification of the *n* gene to match that of the *s* gene. The
192   *n* gene has relatively fewer mutations over time (Dutta et al., 2020) and consistently provides
193   the most sensitive detection in many nucleic acid-based detection assays due to its presence in
194   many subgenomic RNA forms (Alexandersen et al., 2020). Screening of 12 RPA primer pair
195   combinations identified a new *n* primer pair (F4-R1) with similar sensitivity of amplification
196   to our *s* gene primers (Figure 1–figure supplement 1B-C). Combining the optimized *n* and *s*
197   primers in the same reverse-transcription RPA (RT-RPA) reaction containing SARS-CoV-2
198   RNA as a template allowed us to detect both *n* and *s* amplicons with similar efficiency (Figure
199   1–figure supplement 1D). Beyond primer design, we optimized the primer concentration and
200   fine-tuned the *n*:*s* primer pair ratio by increasing the *n* primer pair amount 1.25-1.5-fold, and

201 found the *n* gene detection at these slightly skewed primer pair ratios to improve and match
202 that of the *s* gene at all RNA concentrations tested (Figure 1–figure supplement 2).
203
204 Consistent with previous reports (Patchsung et al., 2020; Qian et al., 2020), we found that
205 RNase H improves RT-RPA efficiency, but reducing RNase H amount in RT-RPA 4-8 fold
206 compared to what we initially reported (Patchsung et al., 2020) further enhanced the reaction
207 (Figure 1–figure supplement 2C). We reasoned that while RNase H can remove RNA from the
208 RNA:DNA duplex product of RT and accelerate subsequent RPA, excess RNase H may
209 degrade the SARS-CoV-2 RNA template in the starting RNA:primer complex and dampen the
210 enzyme's beneficial effect.
211
212 **Optimizing multiplexed CRISPR-based detection for SARS-CoV-2 RNA**
213 We established a readout platform for multiplexed RNA amplification, via a multiplexed
214 CRISPR-Cas reaction. Cas13 enzymes with orthogonal collateral cleavage preferences are well
215 characterized; among the variants, Cas13a from *Leptotrichia wadei* (LwaCas13a) and Cas13b
216 from *Prevotella* sp. MA2016 (PsmCas13b) have already been demonstrated to work well in
217 tandem, and have been used in combination with multiplexed RPA to detect two synthetic
218 DNA targets (Gootenberg et al., 2018). We previously set up LwaCas13a-based detection of
219 SARS-CoV-2 RNA, primarily for the *s* gene, utilizing a FAM-labeled polyU reporter
220 (Patchsung et al., 2020). To extend the detection to two genes, we expressed and purified
221 PsmCas13b (Figure 1–figure supplement 3), designed its CRISPR RNA (crRNA) to target the
222 *n* gene of SARS-CoV-2, and prepared a Cy5-labeled polyA reporter to match with adenine
223 cleavage preference of PsmCas13b.
224
225 We confirmed that PsmCas13b exhibits collateral cleavage of the polyA reporter, thereby
226 eliciting Cy5 fluorescence when its *n* gene target is present. We empirically optimized the
227 enzyme:crRNA amount used in the detection reaction, as well as the polyA reporter
228 concentration (Figure 1–figure supplement 4). Generally, more enzyme, crRNA, and the
229 reporter are needed for the PsmCas13b-based detection compared to conditions used for
230 LwaCas13a, reflecting poorer collateral cleavage kinetics of PsmCas13b, which was
231 previously documented (Gootenberg et al., 2018) and which we also confirmed by performing
232 side-by-side detection reactions with PsmCas13b vs LwaCas13a on the same RPA product
233 (Figure 1–figure supplement 5). Despite the slower kinetics of PsmCas13b, we demonstrated
234 that PsmCas13b and LwaCas13a can function orthogonally in a multiplexed reaction, to detect
235 *n* and *s* genes of SARS-CoV-2 respectively (Figure 1–figure supplement 2D).
236
237 We also explored Cas13d from *Ruminococcus flavefaciens* (RfxCas13d), which is the most
238 catalytically active of Cas13 orthologs in mammalian applications (Konermann et al., 2018),
239 as well as its engineered variant, RfxCas13d-RBD, which has an RNA binding domain (RBD)
240 from human protein kinase R fused to RfxCas13d to improve RNA binding (Yin et al., 2020).
241 However, both RfxCas13d variants exhibited the polyU cleavage efficiency that was lower
242 than that of LwaCas13a (Figure 1–figure supplement 6). Therefore, we decided to proceed with
243 the current best enzyme pair, LwaCas13a and PsmCas13b, and determine the system's clinical
244 performance in the multiplexed gene detection of SARS-CoV-2 (Figure 1–figure supplement
245 6).
246
247 We screened solubility/stability-enhancing additives in the reactions to improve the efficiency
248 of the multiplexed RT-RPA and CRISPR reaction. Triglycine boosted the multiplexed RPA
249 reaction the most, consistently increasing the positive rates (Figure 1–figure supplement 7A)
250 and betaine monohydrate consistently increased the fluorescence signal generated from both

Cas13a- and Cas13b-mediated cleavage by around 2-fold (Figure 1–figure supplement 7B and Figure 1–figure supplement 8). The beneficial effect of betaine in the Cas detection step can be combined with that of triglycine in the multiplexed RPA step, and we obtained the best signal-to-noise upon multiplexed detection when both additives were used in their respective reactions. (Figure 1–figure supplement 7C). Empirical adjustments to the Cas:crRNA ratio and total amount, and reaction buffers further improved the multiplexed Cas reactions (Figure 1–figure supplement 9).

Lyophilized RPA and CRISPR-Cas reaction pellets for portable SARS-CoV-2 RNA detection

We simplified liquid handling steps involved in the amplification and detection reactions and increased the shelf-lives of protein/RNA components of the reactions by storing them in lyophilized forms. All components required for either multiplexed RT-RPA or the CRISPR-LwaCas13a-based detection, aside fr6om potassium acetate and magnesium acetate for RT-RPA, and magnesium chloride for CRISPR-Cas reaction, can be lyophilized together in the presence of cryoprotective trehalose with minimal loss of activity upon reconstitution (Figure 1–figure supplement 10 and Figure 1–figure supplement 11). Trehalose may help the lyophilized RPA and Cas reactions through two mechanisms: it is known to help stabilize proteins for long-term storage and, from our additive screens, also helps boost the efficiency of both RPA and CRISPR-Cas13 reactions (Figure 1–figure supplement 7A, B).

Freeze-dried RT-RPA pellet can simply be rehydrated by direct addition of the RNA extract from clinical samples, along with KOAc and Mg(OAc)$_2$. The use of all-in-one freeze-dried RT-RPA pellets has an added benefit in that at least twice the volume of RNA can be used as input, resulting in even higher detection sensitivity compared to our conventional protocol where all reaction components are supplied in liquid form and the RNA input volume is restricted (Figure 1–figure supplement 11). In addition, increasing the quantity of components in RPA pellets by adding another RPA pellet (RT-2xRPA) boosted the analytical sensitivity of detection in samples with C_t as high as 37 (Figure 1–figure supplement 2E)

Analysis of clinical specificity, analytical sensitivity (the limit of detection) and clinical sensitivity of the multiplexed detection of SARS-CoV-2 RNA

We performed clinical validation with a lyophilized premixed RT-2xRPA formulation, as it had the highest detection sensitivity and suitable features for POC use. We found that the multiplexed RPA and Cas13a/b-based detection are specific for the *s* and *n* genes of SARS-CoV-2, and exhibited no cross-reactivity upon using RNA input from other common human coronaviruses, including human coronavirus OC43 (hCoV-OC43), hCoV-NL63, and hCoV-229E (Figure 2A). Using serially diluted RNA extracts from cultured SARS-CoV-2 in Vero cells (clinical isolate hCoV-19/Thailand/Siriraj_5/2020; GISAID accession ID: EPI_ISL_447908), we determined the limit of detection (LoD) of the optimized multiplexed detection of the SARS-CoV-2 *s* and *n* genes to be at C_t ~37 (Figure 2B).

The clinical performance of the multiplexed detection platform on RNA extracts from 136 nasopharyngeal and throat swab clinical samples, 91 of which are SARS-CoV-2 positive by RT-qPCR (C_t of the *n* gene ranging from ~13-39), matched well with the characterized specificity and LoD (Figure 2C-G). We were able to identify all 45 SARS-CoV-2-negative samples (100% specificity, Figure 2C). Among 91 RT-qPCR-positive samples, we were able to detect both *s* and *n* genes in 85 samples and at least either the *s* or the *n* gene in three other one sample, within 60 min of the multiplexed CRISPR reaction (Figure 2D, E). We were able to detect both genes in samples with C_t as high as 37.5 (Figure 2F). The clinical sensitivity of

301   our multiplexed detection within the determined LoD (C_t ~37) is 100% for the detection of
302   either the *s* or *n* gene of SARS-CoV-2, and 95% for the detection of both genes (Figure 2G).
303   For the full range of C_t's we encountered in clinical samples, the clinical sensitivity is 95-97%
304   for at least one gene detected. Due to extensive optimizations, the limit of detection of our
305   multiplexed detection scheme with lyophilized reagents are even higher than those of freshly
306   prepared singleplex RPA and CRISPR reactions for SARS-CoV-2 *s* gene we previously
307   reported (Patchsung et al., 2020) (LoD C_t ~33.5).
308
309   In addition to performing multiplexed detection with LwaCas13a and PsmCas13b, we explored
310   the use of LwaCas13a and crRNA combinations to detect both *s*- and *n*-gene RPA amplicons
311   (Figure 2B-G, LwaCas13a-based dual S/N gene detection). In this scheme, the use of multiple
312   primer pairs targeting different regions of the template could increase the probability of
313   successful amplification by at least one primer pair, especially at very low template
314   concentrations. Specific amplicons generated can all be detected by LwaCas13a—the Cas
315   enzyme with highest collateral activity known to date—programmed with a mixture of crRNAs
316   targeting all desired amplicons. Indeed, the clinical sensitivity for this combined output
317   approach is better than that of the conventional multiplexed detection, reaching 95% for the
318   full C_t range in our clinical samples, allowing for highly sensitive detection of SARS-CoV-2
319   RNA, while maintaining 100% specificity. The high level of detection accuracy was
320   maintained upon testing with different SARS-CoV-2 variants (Figure 2–figure supplement 1).
321   This lyophilized, LwaCas13-based dual-gene detection of SARS-CoV-2 RNA served as a basis
322   for our submission for technological evaluation with the Food and Drug Administration (FDA)
323   of Thailand, who specified precise specificity (no cross-reactivity with Influenza A and B;
324   MERS-CoV; and respiratory syncytial virus) and sensitivity (4,000 SARS-CoV-2 viral
325   copies/mL) requirements for non-PCR molecular tests for SARS-CoV-2. Our test received full
326   approval from the Thai FDA on September 22, 2021.
327
328   **A multiplexed CRISPR-based assay for simultaneous universal SARS-CoV-2 detection**
329   **and SARS-CoV-2 variant differentiation**
330   With suitable RPA primers and crRNA designs incorporating PAM requirements and synthetic
331   mismatches, CRISPR-based detection should have the ability to differentiate single-nucleotide
332   differences (Chen et al., 2021; Gootenberg et al., 2018; Gootenberg et al., 2017; Myhrvold et
333   al., 2018; Ooi et al., 2021; Shinoda et al., 2021; Teng et al., 2019; Zhou et al., 2020) found in
334   pathogen subtypes, including SARS-CoV-2 variants. In practice, cross-detection of highly
335   similar sequences could not be eliminated; this reduced specificity necessitates the use of
336   combinatorial detection of multiple signature mutations to provide high-confidence variant
337   identification (Welch et al., 2022). Here, we sought to be judicious in our target sequence
338   selection and crRNA design such that one CRISPR-Cas reaction is sufficient to identify a
339   SARS-CoV-2 variant. A multiplexed CRISPR-based detection combining a pan-strain
340   detection reaction with a variant differentiation one would be a cost-effective way to
341   simultaneously diagnose COVID-19, and track the emergence and spread of a known VOC in
342   a population.
343
344   In selecting target sequences for variant differentiation, we prioritized indel mutations (range
345   3-9 base-pairs per mutation) over substitution mutations (a single base-pair per mutation), as
346   the number of bases affected by indel mutations likely result in greater number of mismatches
347   which improves specificity for crRNA discrimination. However, the optimal indel length
348   mismatch between a crRNA and its target is unclear; 1- to 5-nucleotide indels were linked to
349   off-target activation of Cas9 (Lin et al., 2014), while a Cas13-based detection has been shown
350   to tolerate up to 15-nucleotide deletion in the target sequence (Gootenberg et al., 2018). While

351 sequence context likely plays a key role, short mismatches may still permit non-cognate
352 crRNA: target recognition, and longer mismatches may allow formation of RNA bulges which
353 minimally interfere with crRNA:target base pairing, also resulting in non-cognate target
354 recognition and Cas activation. We thus decided to empirically test three different indel lengths
355 when we selected SARS-CoV-2 variant-specific mutations: a three-nucleotide deletion (S:
356 Y144Δ, specific for Alpha); two six-nucleotide deletions (*s*:HV69/70Δ, specific for Alpha and
357 Omicron BA.1 and BA.3; and *s*:EF156/157ΔR158G; specific for Delta); and a nine-nucleotide
358 deletion (*orf1ab*:SGF3675-3677Δ; specific for Alpha) (Figure 3A and Figure 3–figure
359 supplement 1). We also tested the detection of one single-nucleotide substitution (S:T22917G,
360 resulting in L452R mutation; specific for Delta) and incorporated a synthetic mismatch in our
361 crRNA design (Figure 3–figure supplement 2).
362
363 We designed corresponding RPA primers and LwaCas13a crRNAs for all five mutation-
364 specific CRISPR-based detection (Figure 3–figure supplement 2 and Figure 3–figure
365 supplement 3), and first tested their specificity (Figure 3B, Figure 3–figure supplement 4). The
366 five SARS-CoV-2 variant-specific mutation detection reactions showed SARS-CoV-2 RNA-
367 dependent signal but exhibited different levels of selectivity for their target variants. The two
368 six-nucleotide deletion detections performed the best: EF156/157ΔR158G was highly specific
369 for Delta, with no cross-reactivity with Wuhan, Alpha, or Omicron strains; HV69/70Δ was also
370 highly specific for Alpha and Omicron as designed, but showed low-level cross-reactivity with
371 Wuhan and Delta. Y144Δ, SGF3675-3677Δ and L425R showed clear detection preference for
372 Alpha, Alpha, and Delta respectively, but background signals from other strains were
373 significant. We thus proceeded with the two best-performing variant-specific detection
374 reactions—EF156/157ΔR158G and HV69/70Δ—for subsequent experiments.
375
376 We characterized the limit of detection of the singleplex EF156/157ΔR158G-based detection
377 using a dilution series of RNA extracted from cultured SARS-CoV-2 Delta strain, and found
378 the detection to have an excellent LoD, capable of detecting Delta RNA with C_t of up to ~38
379 (Figure 3–figure supplement 5A). Further evaluation revealed robust detection in clinical
380 samples (C_t 15-37) (Figure 3–figure supplement 5B). We then combined the LwaCas13a-based
381 Delta-specific detection of the *s* gene with the PsmCas13b-based pan-SARS-CoV-2-strain
382 detection of the *n* gene in a multiplexed format (Figure 1B). Using the premixed, lyophilized
383 and multiplexed formulation as previously described, we confirmed that the excellent LoD of
384 Delta-specific reaction was maintained in the multiplexed format (Figure 3C and Figure 3–
385 figure supplement 6). Furthermore, the LwaCas13a-based Delta-specific multiplexed detection
386 was able to correctly identify all of twenty Delta patient specimens (C_t 13-27), with no cross-
387 reactivity toward ten Alpha clinical specimens (C_t 17-31) (Figure 3D). The PsmCas13b-based
388 pan-strain detection was fully functional, detecting the presence of SARS-CoV-2 in this same
389 set of thirty clinical samples.
390
391 With the recent emergence of the Omicron variant, we explored the use of the HV69/70Δ-
392 based detection for Omicron identification. We also performed additional cross-reactivity
393 evaluation with higher RNA titer at C_t ~25 since we observed sporadic cross-reactivity in the
394 previous experiment (Figure 3B and Figure 3–figure supplement 7). We found that the
395 HV69/70Δ-based detection was able to distinguish Alpha and Omicron variants from other
396 variants even at higher RNA titer. Next, we demonstrated that the singleplex HV69/70Δ-based
397 detection was sensitive to RNA with C_t up to ~34 upon testing with a dilution series of Omicron
398 variant RNA (Figure 3–figure supplement 5C) and was able to detect all Omicron variant
399 clinical samples (Figure 3–figure supplement 5D). Using serially diluted RNA from an
400 Omicron clinical extract, we demonstrated sensitive detection of the Omicron variant at up to

Ct ~34 in a multiplexed format (LwaCas13-based detection of Omicron HV69/70Δ *s* signature, and PsmCas13b-based pan-strain *n* gene detection) (Figure 3E, Figure 3–figure supplement 6). In addition, we were able to detect the HV69/70Δ *s* mutation as well as the SARS-CoV-2 *n* gene in fifteen Omicron clinical specimens (C_t 16-22), using the HV69/70Δ-based multiplexed detection approach (Figure 3F).

Combining multiplexed RPA and Cas13-based detection in a single step

To simplify usage and minimize the risk of carryover contamination, we formulated a one-pot protocol which combined components of multiplexed RPA and Cas13-based detection in a single reaction tube. We first tested a previously reported one-pot SHINE protocol (Arizti-Sanz et al., 2020) for the detection of SARS-CoV-2 S gene, but saw that its analytical sensitivity is poorer than our conventional two-step amplification and detection in separate pots by ~10-100-fold. Realizing that concentrations of RPA components in SHINE are diluted by 2-fold compared to the two-step variant, potentially hampering performance of RPA in the one-pot reaction, we re-formulated a one-pot recipe in which final concentrations of all components are as close to those in our optimized two-step variant as possible. We also switched the reaction temperature to be 39 °C, found to be optimal for combined RPA and Cas13-based detection (Figure 4–figure supplement 1). We tested the optimized one-pot multiplexed RPA amplification of the *s* and *n* genes and concurrent detection by LwaCas13a programmed with *s*- and *n*-targeted crRNAs, and found its analytical sensitivity to be on par with the two-step protocol (Figure 4A).

Direct visualization of multiplexed Cas13-based detection

To facilitate the use of a multiplexed CRISPR reaction in point-of-care settings, we switched the fluorophore labels of the PsmCas13b-polyA reporter, from Cy5 to rhodamine X (ROX). The ROX-based polyA reporter generates slightly higher levels of signal-to-noise upon PsmCas13b-mediated cleavage compared to the Cy5-based reporter (Figure 4–figure supplement 2). Moreover, ROX and fluorescein (FAM, on the LwaCas13a-polyU reporter) can be efficiently excited using a single blue LED light source(Ball et al., 2016), under which Cy5 gives no signal. ROX and FAM emissions can then be simultaneously monitored using different combinations of colored plastic filters (Figure 4B, Figure 4–figure supplement 3 and Figure 4–figure supplement 4). The emissions are easily readable by eye and ultimately, can be coupled to a portable smartphone-based detection (Priye et al., 2018; Priye et al., 2017; Samacoits et al., 2021) for quantitative analysis.

Establishing a fully configurable RPA reaction

Given the bottleneck experienced by many labs in procuring and affording commercial RPA, we sought to produce protein components and formulate efficient RPA in house. We expressed the four main protein components of the RPA reaction—bacteriophage T4 recombinase UvsX (UvsX), bacteriophage T4 recombinase loading factor UvsY (UvsY), bacteriophage T4 single-stranded binding protein Gp32 (Gp32), and *Bacillus subtilis* DNA Polymerase I, large fragment (Bsu LF)—in *Escherichia coli* and purified them to about 95% purity (Figure 4C). The activity of our laboratory-made RPA, formulated using a previously reported condition (Piepenburg et al., 2006), was tested via the amplification of a synthetic DNA representing the *s* gene of SARS-CoV-2, which showed clear amplification across different input concentrations under this standard condition (Figure 4–figure supplement 5). We next titrated the concentrations of the four main protein components of the RPA reaction in order to improve the amplification and found optimal concentrations for each component as follows: 2–3 μM UvsX; 2–11 μM UvsY, 26–35 μM Gp32, and 2-3 μM Bsu LF (Figure 4D). We combined optimized protein concentrations with the triglycine additive to successfully amplify the *n* gene of SARS-CoV-2

451 from either DNA or RNA samples for subsequent CRISPR-Cas13a detection (Figure 4E-4F).
452 The optimized in-house RT-RPA can be used in a multiplexed amplification reaction of the *s*
453 and *n* genes, coupled to LwaCas13a-based detection with *s*- and *n*-targeted crRNAs (G) and
454 can be lyophilized without loss in detection sensitivity (Figure 4H).
455
456 **Discussion and outlook**
457 Many advances in point-of-care nucleic acid detection technologies for SARS-CoV-2 RNA—
458 from crude lysate preparation (Arizti-Sanz et al., 2020; Joung et al., 2020; Qian et al., 2020),
459 nucleic acid enrichment post-lysis to enhance sensitivity (Joung et al., 2020), multiple options
460 of isothermal amplification (Subsoontorn et al., 2020), amplification-free detection (Fozouni
461 et al., 2020), multiple modes of detection (Chaibun et al., 2021; Patchsung et al., 2020) to
462 mobile, automated readouts of results (Fozouni et al., 2020)—have collectively pushed toward
463 large-scale practical uses of these technologies for the surveillance of the ongoing pandemic.
464 Here, we extend the utility of CRISPR-based detection—already shown to be among the most
465 sensitive and specific isothermal nucleic acid tests—toward robust multiplexed detection of
466 SARS-CoV-2 RNA. Multi-parameter optimizations of multiplexed RPA and CRISPR-Cas
467 reaction resulted in a highly specific and sensitive detection platform for the *s* and *n* genes of
468 SARS-CoV-2. We critically evaluated its performance on a large set of clinical samples and
469 demonstrated the high sensitivity (95-97%) and specificity (100%) of the multiplexed
470 CRISPR-based detection of SARS-CoV-2 RNA. Our enhanced multiplexed CRISPR-based
471 reaction can be re-designed to simultaneously provide COVID-19 diagnosis and identify the
472 causative SARS-CoV-2 variant of concern, including Delta and Omicron, with high specificity
473 and sensitivity. Beyond variant surveillance, our platform can be used for other multiplexed
474 combinations, including the detection of one SARS-CoV-2 gene and a human gene/RNA
475 control, and the detection of SARS-CoV-2 with another virus, such as influenza, whose
476 infection can co-occur with COVID-19 and present similar symptoms (Mayuramart et al.,
477 2021).
478
479 Beyond complex detection, we also improve the usability and portability of the enhanced
480 multiplexed CRISPR-based detection platform through freeze-dried reaction mixtures and a
481 one-pot configuration. While the current sensitivity of our enhanced multiplexed platform is
482 already high, we think the key to further improve the test accuracy while maintaining the ease
483 of use of the detection technology lies in the ability to tinker with the RPA reaction itself. The
484 ability to manufacture this key reagent at high quality in the lab has enabled us to make progress
485 toward this goal, first by improving the ease of use through tailored lyophilization of reaction
486 components. In addition to increasing sensitivity, engineering RPA such that the reaction can
487 function directly and robustly in diverse biological fluids could make RPA and CRISPR-based
488 detection viable testing platforms in very limited-resource settings—even at home—for
489 currently circulating or newly emerging SARS-CoV-2 and other infectious agents. Beyond
490 improving technology characteristics, local manufacturing of test kit components creates
491 opportunities for economic and research development, which could lead to sustainable use of
492 these technologies in disease monitoring and diagnosis especially in developing countries.
493
494 Both RPA and CRISPR-Cas reactions contain primarily enzyme components; in this study, we
495 started to explore the use of an engineered Cas13 enzyme to improve the reactions. Continual
496 efforts to engineer these enzyme components and their substrates as recently demonstrated with
497 Cas12a (Nguyen, Rananaware, et al., 2020) and its crRNA (Nguyen, Smith, et al., 2020), along
498 with integration with automation platforms for high-throughput assay development, could pave
499 way for substantially improved detection platforms.
500

Materials and Methods
Cloning methods for RPA expression plasmids
Nucleic acid sequences codon optimized for *E. coli* expression for T4 UvsX, T4 UvsY, T4 gp32, and Bsu DNA polymerase large fragment (Bsu LF) were ordered as plasmids from GeneArt (ThermoFisher Scientific). Bsu LF and *uvsY* were cloned into the pET28a backbone using Circular Polymerase Extension Cloning (CPEC) (Quan & Tian, 2011). *Gp32* and *uvsX* were cloned into the pET28a backbone using Type IIS assembly (Engler et al., 2008). Plasmids were sequence verified (Eurofins Genomics) and are available on Addgene as follows: pET28a-MH6-Bsu LF (Plasmid #163911); pET28a-gp32-H6 (Plasmid #163912); pET28a-uvsX-H6 (Plasmid #163913); and pET28a-MH6-uvsY (Plasmid #163914).

Expression and purification of protein components of RPA
We used near-identical expression and cell lysis protocols for UvsX, UvsY, gp32, and Bsu LF, but the purification step and final storage buffer conditions were different for each enzyme, as given below.

An expression plasmid for UvsX, UvsY, gp32, or Bsu LF was transformed into *E. coli* BL21(DE3) cells. The cells were grown in LB medium at 37°C until OD_{600} reached 0.7–0.8. Protein expression was induced using the following concentrations of isopropyl-β-D-thiogalactopyranoside (IPTG): 1 mM for UvsX and UvsY; 0.2 mM for gp32; and 0.5 mM for Bsu LF. The cells were grown for additional 16 hours at 16°C and harvested by centrifugation. The cell pellet was resuspended in lysis buffer (50 mM sodium phosphate pH 8.0, 500 mM sodium chloride, 10 mM imidazole). Phenylmethylsulfonyl fluoride (PMSF) was added into resuspended solution at 1 mM final concentration followed by sonication for a total burst time of 3 minutes (3 sec on for short burst and 9 sec off for cooling). The cell lysate was clarified by centrifugation at 27,000×g for 30 minutes at 4 °C. Nickel-nitrilotriacetic acid (Ni-NTA) agarose beads (Qiagen) was washed with two column volumes of water and equilibrated with lysis buffer. The clarified cell lysate was incubated with the Ni-NTA agarose beads (Qiagen) at 4 °C for 40 minutes. The column was washed with ten column volumes (CVs) of washing buffer (50 mM sodium phosphate pH 8.0, 500 mM sodium chloride, and 20 mM imidazole), and the bound proteins were eluted with elution buffer (50 mM sodium phosphate pH 8.0, 500 mM sodium chloride, 250 mM imidazole).

For UvsX, the protein was further purified by Heparin Sepharose Fast Flow (GE Healthcare Life Sciences) with a linear gradient of 0.1–1 M NaCl in Buffer A (20 mM Tris-HCl pH 8, 5 mM β-mercaptoethanol (βME)). Proteins were concentrated and stored in 20 mM Tris-HCl pH 8.0, 500 mM NaCl, and 40% (v/v) glycerol at −20 °C.

For UvsY, the protein was further purified by Heparin Sepharose Fast Flow (GE Healthcare Life Sciences) with a linear gradient of 0.1–1 M NaCl in Buffer A (20 mM Tris-HCl pH 8, 5 mM βME). Afterward, proteins were dialyzed against 20 mM Tris-HCl pH 7.5, 400 mM NaCl, 20% (v/v) glycerol and 5 mM βME, and the glycerol concentration adjusted to be 50% (v/v) with the addition of UvsY freezing buffer (20 mM Tris-HCl pH 7.5, 400 mM NaCl, and 80% (v/v) glycerol). Protein aliquots were stored in 20 mM Tris-HCl pH 7.5, 400 mM NaCl, and 50% (v/v) glycerol at −20 °C.

For gp32, eluted protein fractions were dialyzed against 20 mM Tris-HCl pH 7.5, 400 mM NaCl, and 5 mM βME, and the glycerol concentration adjusted to be 50% (v/v). Protein aliquots were stored in 10 mM Tris-HCl pH 7.5, 200 mM NaCl, and 50% (v/v) glycerol at −20 °C.

551
552 For Bsu LF, eluted protein fractions were concentrated and dialyzed against 50 mM Tris-HCl
553 pH 7.5, 50 mM KCl, 1 mM DTT, 0.1 mM EDTA, and 20% (v/v) glycerol. Glycerol
554 concentration was adjusted to be 50% (v/v) with the addition of Bsu LF freezing buffer (50
555 mM Tris-HCl pH 7.5, 50 mM KCl, 1 mM DTT, 0.1 mM EDTA, and 90% (v/v) glycerol).
556 Protein aliquots were stored in 50 mM Tris-HCl pH 7.5, 50 mM KCl, 1 mM DTT, 0.1 mM
557 EDTA, and 50% (v/v) glycerol at −20 °C.
558
559 **Expression and purification of Cas enzymes**
560 *LwaCas13a expression and purification*
561 LwaCas13a was expressed from pC013-His$_6$-Twinstrep-SUMO-LwaCas13a (Addgene:
562 #90097) and purified as previously described (Patchsung et al., 2020).
563
564 *PsmCas13b expression and purification*
565 *Escherichia coli* BL21 (DE3) transformed with pC0061-His$_6$-Twinstrep-SUMO-PsmCas13b
566 (Addgene: #115211) were grown in LB media containing 25 µg/mL ampicillin, and the protein
567 expression induced by the addition of 500 µM IPTG at 16 °C for overnight. Cells were
568 collected by centrifugation at 8,000 rpm for 20 min at 4 °C and the supernatant was discarded.
569 The cell pellet was resuspended in extraction buffer (50 mM Tris-HCl, 500 mM NaCl, 1 mM
570 DTT, 1x protease inhibitor cocktail, 0.25 mg/mL lysozyme, 5 mM imidazole, pH 7.5) then
571 lysed by sonication (Sonics Vibracell VCX750) using 40-60% pulse amplitude (on 10 s and
572 off 20 s until completely lysed). The lysate was centrifuged at 15,000 rpm for 45 min at 4 °C,
573 and the soluble fraction filtered through a 0.45 µm polyethersulfone membrane and loaded into
574 Chelating Sepharose^{TM} Fast Flow column which was pre-loaded with 0.2 M NiSO$_4$ and pre-
575 equilibrated with binding buffer (50 Tris-HCl, 500 mM NaCl, 5 mM imidazole pH 7.5). The
576 column was washed with 5 column volumes of binding buffer, 6 column volumes of washing
577 buffer (50 Tris-HCl, 500 mM NaCl, 50 mM imidazole pH 7.5) and eluted with 6 column
578 volumes of elution buffer (50 Tris-HCl, 500 mM NaCl, 500 mM imidazole pH 7.5). The
579 fractions containing His-Twinstrep-SUMO-PsmCas13b were pooled and exchanged with
580 SUMO cleavage buffer (20 mM Tris-HCl, 150 mM NaCl, pH 8.0) at 4 °C overnight.
581
582 The SUMO tag was cleaved with Ulp1 SUMO protease (Addgene #64697) using 10:1 of
583 SUMO substrate by incubation at room temperature for 5 h. The reaction was adjusted to pH
584 6.0 and filtered with 0.45 µm polyethersulfone membrane before loading into HiTrap SP HP
585 column which was equilibrated with binding buffer (50 mM phosphate pH 6.0, 200 mM NaCl).
586 The protein was washed and eluted with 50 mM phosphate, 200 mM NaCl with pH ranging
587 from 6.0, 6.5, 7.0, 7.5, and 8.0, followed by 50 mM Tris pH 8.0, 1 M NaCl. The PsmCas13b
588 fractions were pooled, concentrated, exchanged buffer using centricon 30k, diluted to a
589 concentration of 1.2 mg/mL, and stored at -80 °C in storage buffer (50 mM Tris-HCl, 600 mM
590 NaCl, 5 % glycerol, 2 mM DTT).
591
592 *RfxCas13d and RfxCas13d-RBD expression and purification*
593 *E. coli* BL21 (*DE3*) cells transformed with CMS1371 (for His$_6$-MBP-RfxCas13d expression)
594 or CMS1372 (for His$_6$-MBP-RfxCas13d-dsRBD) plasmid were grown in LB media containing
595 100 µg/mL ampicillin, and the recombinant gene expression induced by the addition of 500
596 µM IPTG at 16 ºC for overnight. Cells were collected and lysed as for PsmCas13b. Following
597 lysate clarification, the soluble fraction was filtered through 0.2 µm polyethersulfone
598 membrane and purified by HisTrap FF column connected to FPLC system. The column was
599 pre-equilibrated with binding buffer (50 mM Tris-HCl, 500 mM NaCl, 5 mM imidazole; pH
600 7.5). The soluble fraction was loaded at 2 mL/min, washed with 5 column volumes of binding

601 buffer. The recombinant protein was eluted in linear gradient of elution buffer (50 mM Tris-
602 HCl, 0.5 M NaCl, and 0.5 M imidazole; pH 7.5). The eluted fractions were pooled and dialyzed
603 with 50 mM Tris-HCl, 0.5 mM EDTA, 1 mM DTT and 200 mM NaCl; pH 7.5 at 4 ºC for 3
604 hours, before proceeding to MBP tag removal.

605

606 The MBP tag was cleaved with ultraTEV protease using 20:1 substrate: protease ratio in 50
607 mM Tris-HCl, 0.5 mM EDTA, 1 mM DTT and 200 mM NaCl; pH 7.5. The reaction mixture
608 was incubated at 4 ºC for overnight with gentle shaking before applied onto HisTrap column,
609 which was pre-equilibrated with (50 mM Tris-HCl, 500 mM NaCl, 5 mM imidazole; pH 7.5).
610 The flow-through and unbound fractions containing RfxCas13d and RfxCas13d-dsRBD
611 protein were then collected while retained MBP and other contaminants were later washed out
612 with high concentration of imidazole. The purified protein was exchanged against 40 mM Tris,
613 400 mM NaCl; pH 7.5 in DEPC-treated water and concentrated using centricon 30k, and
614 diluted to a concentration of 1.22 mg/mL (for RfxCas13d) and 1.89 mg/mL (for RfxCas13d-
615 RBD).

616

617 **RPA primers, crRNAs, and RNA reporters**
618 The oligonucleotides used are listed in Table S2. The crRNAs used for variant detection were
619 synthesized via *in vitro* transcription. The T7-3G oligonucleotide (at the final concentration of
620 0.5 µM) and the ssDNA crRNA template (at the final concentration of 0.5 µM) were subjected
621 to 34 cycles of 50 µL Q5® High-Fidelity DNA Polymerase reaction (New England Biolabs).
622 PCR products were purified using DNA Clean & Concentrator-5 kits (Zymo Research) and
623 eluted in 20 µL of nuclease-free water. Four picomoles of the purified dsDNA crRNA template
624 were used in *in vitro* transcription reactions using RiboMAX Large Scale RNA Production
625 System–T7 (ProMega) or MEGAshortscript™ T7 Transcription Kit (Invitrogen). The reactions
626 were performed at 37 ºC overnight, treated with DNase I, and purified using phenol-chloroform
627 extraction and alcohol precipitation. 15% acrylamide/7.5 M urea PAGE with GelRed®
628 (Biotium) staining was used to assess the size and purity of the transcribed product. Gels were
629 imaged on ImageQuant™ LAS 4000 (GE Healthcare); quantifications of produced crRNAs
630 were performed by measuring band densitometries using Fiji ImageJ software (Schindelin et
631 al., 2012) and comparing to RNA standards.

632

633 **Design of RPA primers and crRNAs**
634 *General RPA primers and crRNAs design*
635 RPA primers and crRNA were designed according to a published protocol (Kellner et al.,
636 2019).

637

638 *Design of RPA primers and crRNA targeting specific SARS-CoV-2 mutations*
639 Representative genome sequences of Alpha (n = 1,100), Beta (n = 126), Gamma (n = 729), and
640 Delta (n = 1,329) were retrieved from NCBI SARS-CoV-2 data packages using PANGO
641 designations (Rambaut et al., 2020) as queries (dates of data retrieval, 27 April and 5 May
642 2021). Retrieved sequences were aligned using MAFFT (Katoh & Standley, 2013). The
643 alignments were visualized and used to create consensus sequence for each variant using
644 Jalview (Waterhouse et al., 2009). The four consensus sequences along with the SARS-CoV-
645 2 isolate Wuhan-Hu-1 NCBI reference genome (Accession ID NC_045512.2) were re-aligned
646 using MAFFT and visualized in SnapGene software (Insightful Science). Using visualized
647 multiple sequence alignment, RPA primers and crRNAs were manually designed to cover
648 regions spanning the target mutation while avoiding regions with genetic variations among
649 SARS-CoV-2 variants. The design and chosen regions are shown in Figure 3–figure
650 supplement 2 and Figure 3–figure supplement 3.

651

Exclusivity evaluation of designed crRNAs

653 crRNA spacer sequences and their complementary sequences were searched against a BLAST
654 database of Betacoronavirus nucleotide sequences (Betacoronavirus BLAST,
655 https://blast.ncbi.nlm.nih.gov/Blast.cgi?PAGE_TYPE=BlastSearch&BLAST_SPEC=Betacor
656 onavirus), with the maximal number of target sequences set to 5000. The results were filtered
657 to include complete genomes (>29,000 nt) with 90-100% query coverage and 90-100% identity
658 (date of data retrieval 1 March 2022). The clade assignment of genomes was done using
659 NextClade (https://clades.nextstrain.org) (Aksamentov et al., 2021). The genomes with bad and
660 mediocre NextClade overall quality control status were excluded. The analysis was
661 summarized in Figure 3–figure supplement 8. The associated dataset was available in Figure
662 3–source data 1.

663

Inclusivity evaluation of designed primers and crRNAs

665 GenBank accession lists of SARS-CoV-2 variant genomes sampling by the NextStrain
666 COVID-19 global analysis open-data build were acquired by applying filter data by clade
667 before downloading author metadata (date of data retrieval, 3 March 2022); Alpha (n = 110),
668 Beta (n = 30), Gamma (n = 31), Delta (n = 1,044), and Omicron (n = 785)). FASTA files
669 comprising listed genomes were downloaded from GenBank and aligned using MAFFT. The
670 resulted alignments were visualized and inspected using JalView (Aksamentov et al., 2021).
671 The prevalence of the sequences aligned with primers and crRNAs in different variants were
672 calculated as a percentage of genomes with the complete matched sequence observed in the
673 alignments and represented by the frequency of the sequence among the variant isolates (%F).
674 Consensus sequences of each variant along with their %F values are provided in Figure 3–
675 figure supplement 3 for primers and Figure 3–figure supplement 2 for crRNAs. The associated
676 dataset was available in Figure 3–source data 2.

677

678 The NextStrain Clades or PANGO lineages were designated to each WHO classified variant
679 of concern as described in Table S1

680

681 **RPA Primer and primer combination screening with colorimetric lateral-flow Cas13a-**
682 **based readout** (for **Figure 1–figure supplement 1**)
683 RT-RPA was set up as previously described (Patchsung et al., 2020) using TwistAmp Basic
684 Kit (TwistDx) and EpiScript reverse transcriptase (Lucigen). Sequences of RPA primers used
685 were given in Table S2. LwaCas13a-based detection reactions were also set up exactly as
686 previously described (Patchsung et al., 2020), then visualized with HybriDetect lateral-flow
687 strips (Milenia Biotec). Sequences of LwaCas13a-crRNAs for each amplicon were given in
688 Table S2.

689

690 **Optimized multiplexed RT-RPA**
691 The optimized reaction condition for multiplexed RT-RPA for the amplification of *s* and *n*
692 genes of SARS-CoV-2 with TwistAmp Basic RPA is as follows. The protocol is for the
693 preparation of 5 multiplexed RPA reactions at a time from one lyophilized RPA pellet
694 (TwistAmp Basic kit, TwistDx). Working multiplexed RPA contained 2.5 μM *s*-gene forward
695 RPA primer, 2.5 μM *s*-gene reverse RPA primer, 3.1 μM *n*-gene F4 forward RPA primer, and
696 3.1 μM *n*-gene R1 forward RPA primer.

697

698 One RPA pellet was resuspended with 29.5 μL of the rehydration buffer from the kit. 1 μL
699 EpiScript reverse transcriptase (200 U/μL stock; Lucigen), 0.36 μL RNase H (5 U/μL stock;
700 NEB), 5 μL triglycine (570 mM stock, Sigma), and 5 μL multiplexed RPA primer mix were

added to the RPA resuspension. A portion of 8.2 μL of the RPA-primer-enzyme master-mix was aliquoted into five precooled 1.5 ml Eppendorf tubes. 5.3 μL RNA extract from nasopharyngeal and throat swab samples was then added to each aliquot. Lastly, 0.7 μL magnesium acetate (280 mM stock) was added to initiate the amplification. The reactions were incubated at 42 °C for 25 min, then placed on ice before proceeding to the Cas-based detection step.

Optimized multiplexed Cas13-based detection with fluorescence readout
Each multiplexed Cas13-based detection reaction can be assembled as follows, and making a mastermix by multiplying the amount given is possible: 2 μL HEPES (200 mM stock, pH 6.8), 0.8 μL ribonucleoside triphosphate mix (rNTPs, 25 mM stock, NEB), 0.6 μL NxGen T7 RNA polymerase (50 U/μL stock, Lucigen), 2.5 μL FAM-polyU-IABkFQ reporter (2 μM stock, IDT), 2.5 μL Cy5-polyA-IABkRQ or ROX-polyA-IABkRQ reporter (4 μM stock, IDT), 1 μL LwaCas13a-crRNA for the *s* gene (10 ng/μL stock, Synthego), 1 μL PsmCas13b-crRNA for the *n* gene (30 ng/μL stock, Synthego), 1 μL LwaCas13a enzyme (126 μg/mL; 900 μM working stock in enzyme storage buffer), 1 μL PsmCas13b enzyme (420 μg/mL; 2700 μM working stock in enzyme storage buffer), 3 μL betaine monohydrate (5 M stock, Sigma), 1 μL magnesium chloride (480 mM stock), and 1.3 μL DEPC-treated water.

Final concentrations of each component were: 20 mM HEPES pH 6.8, 1 mM of each rNTP, 1.5 U/μL T7 RNA polymerase, 250 nM polyU-IABkFQ, 500 nM polyA-IABkRQ, 22.5 nM LwaCas13a crRNA, 67.5 nM PsmCas13b crRNA, 45 nM LwaCas13a enzyme, 135 nM PsmCas13b enzyme, 750 mM betaine monohydrate, and 24 mM magnesium chloride.

After mixing, 18 μL of the multiplexed Cas reaction mixture was transferred to a 384-well-plate well, and 2 μL of the multiplexed RPA reaction was added. Fluorescent signals of FAM, ROX, and Cy5 were monitored using a fluorescence microplate reader (Infinite M Plex, Tecan) at 37 °C. Alternatively, FAM and ROX fluorescence can be visualized using an LED transilluminator (BluPAD Dual LED Blue/White light transilluminator) equipped with plastic lighting gels as excitation and emission filters (LEE Filters, filter no.101 Yellow, 106 Primary red, 119 Dark blue, 139 Primary green, 158 Deep orange).

Visualization	Light Source	Emission filter	Excitation filter
FAM-ROX	Blue Light	Blue	Orange and yellow
FAM	Blue Light	Blue	Orange and green
ROX	Blue Light	Green	Red
ROX	White Light	Green	Red

Specific RPA and Cas-based detection methods for relevant figures, see Table S3 and Table S4.

Lyophilized RT-RPA for multiplexed gene detection
An RT-RPA reaction buffer A was prepared from 500 μL 50% (w/v) PEG20000, 250 μL of 1 M Tris pH 7.4, and 100 μL of 100 mM DTT. The multiplexed RT-RPA reaction mixture was prepared by resuspending one RPA pellet (TwistAmp Basic kit, TwistDx) with 14.2 μL of RT-RPA reaction buffer A. 15 μL nuclease-free water, 1 μL EpiScript reverse transcriptase (200 U/μL stock; Lucigen), 0.36 μL RNase H (5 U/μL stock; NEB), 5 μL triglycine (570 mM stock, Sigma), 5 μL of multiplexed RPA primers mix were added to the RPA resuspension. 8.2 μL of

746 the RPA-primer-enzyme master-mix was aliquoted into precooled 1.5 mL Eppendorf tubes;
747 the recipe given was enough to make 5 aliquots. The mixture was snap frozen with liquid
748 nitrogen and lyophilized using a freeze dryer (Alpha 2-4 LDplus, Martin Christ) overnight.
749
750 To reconstitute and initiate the RT-RPA reaction, the lyophilized RT-RPA pellet was
751 resuspended with 12.7 µL of the RNA sample. Lastly, 1 µL of a solution composed of 196 mM
752 magnesium acetate and 1.5 M potassium acetate was added to each reaction. The reactions
753 were incubated at 42 °C for 25 min, then placed on ice before proceeding to the Cas-based
754 detection using Cas13a-based detection step containing crRNAs for both S and N genes as
755 previously described. The relative FAM fluorescence intensity was evaluated using a real-time
756 thermal cycler (CFX Connect Real-Time PCR System, Bio-Rad).
757
758 **One-pot, multiplexed RT-RPA/CRISPR-Cas13a detection**
759 We prepare the one-pot, monophasic detection reactions by preparing the multiplex RT-RPA
760 and CRISPR-Cas13a reaction mixes separately, before mixing them together, as follows.
761
762 RT-RPA reaction buffer and multiplexed RPA primers mix were prepared as described above.
763 crRNA-reporter solution was prepared from 24 µL DEPC-treated water, 4 µL of 100 ng/µL
764 LwaCas13a crRNA for *s* gene, 4 µL of 100 ng/µL LwaCas13a crRNA for *n* gene, and 2 µL of
765 100 µM FAM-PolyU reporter. Then, CRISPR-Cas13a reaction mix was prepared by
766 combining 2.8 µL rNTPs mix (25 mM each), 2 µL T7 RNA polymerase (50 U/µL), 7 µL
767 LwaCas13a (63 µg/mL), and 3 µL of the crRNA-reporter solution.
768
769 The multiplexed RT-RPA reaction mixture was prepared by resuspending one RPA pellet
770 (TwistAmp Basic kit, TwistDx) with 14.2 µL of RT-RPA reaction buffer A. 1 µL EpiScript
771 reverse transcriptase (200 U/µL stock; Lucigen), 0.36 µL RNase H (5 U/µL stock; NEB), 5 µL
772 triglycine (570 mM stock, Sigma), 5 µL of multiplexed RPA primers mix, and 15 µL of
773 CRISPR-Cas13a reaction mix were then added to the RPA resuspension. 8.2 µL of the RPA-
774 primer-enzyme master-mix was aliquoted into precooled 0.1 mL PCR strip tubes; the recipe
775 given was enough to make 5 aliquots.
776
777 To initiate amplification and detection, 5.3 µL of the RNA sample was added to each aliquot,
778 followed by 0.7 µL magnesium acetate (280 mM). The reactions were incubated at 39 °C and
779 generated FAM fluorescence was monitored using a real-time thermal cycler (CFX Connect
780 Real-Time PCR System - Bio-Rad).
781
782 **Standard (unoptimized) in-house RPA reaction**
783 Standard RPA reactions were set up as previously reported (Piepenburg et al., 2006) and
784 contained the following components: 50 mM Tris (pH 7.5), 100 mM potassium acetate, 14 mM
785 magnesium acetate, 2 mM DTT, 5% (w/v) PEG20000, 200 µM dNTPs, 3 mM ATP, 50 mM
786 phosphocreatine, 100 µg/mL creatine kinase, 120 µg/mL UvsX, 30 µg/mL UvsY, 900 µg/mL
787 Gp32, 30 µg/mL Bsu LF, 450 nM primers, and DNA templates. Reactions were performed in
788 20 µL volumes at 37 °C for 60 min, followed by inactivation at 65 °C for 10 min. Ten
789 microliters of each reaction were mixed with 2% (w/v) final concentration of sodium dodecyl
790 sulfate (SDS) and Novel Juice DNA staining reagent (BIO-HELIX), separated on 2% (w/v)
791 agarose gel and visualized under blue light (BluPAD, BIO-HELIX).
792
793 **Optimizing RPA through titration of protein components**
794 Concentrations of the main protein components of RPA (UvsX, UvsY, Gp32, and Bsu LF)
795 were varied as indicated in . We also switched to using RPA primers for the *n* gene

796 amplification (the F4/R1 pair) and pUC57-2019-nCoV-N plasmid (MolecularCloud cat no.
797 #MC_0101085) at 10,000 copies/µL as the DNA template. The RPA reaction conditions were
798 otherwise identical to the standard RPA reaction (see previous section), and were allowed to
799 proceed at 42°C for 60 min. Thereafter, 2 µL of the RPA products were mixed with 18 µL of
800 the Cas13a-based detection reaction, which contained 20 mM Tris-HCl pH 7.4, 60 mM NaCl,
801 6 mM MgCl$_2$, 1 mM of each rNTPs, 1.5 U/µL NxGen T7 RNA polymerase, 6.3 µg/mL
802 LwaCas13a, 0.5 ng/µL LwaCas13a crRNA, and 0.3 µM FAM-PolyU reporter. The generated
803 FAM fluorescence was monitored at 37 °C over 90 min using a fluorescence microplate reader
804 (Varioskan, Thermo Scientific or Infinite M Plex, Tecan).
805

806 **Optimized in-house RPA for single-gene detection**
807 The single-plexed RPA of the *n* gene was set up with the following components (20 µl total
808 reaction volume, consisting of 19 µL reagent mastermix and 1 µL RNA input): 50 mM Tris
809 (pH 7.5), 100 mM potassium acetate, 14 mM magnesium acetate, 2 mM DTT, 5% (w/v)
810 PEG20000, 200 µM dNTPs, 12 mM ATP, 50 mM phosphocreatine, 100 µg/mL creatine kinase,
811 150 µg/mL (3.3 µM) UvsX, 30 µg/mL (1.7 µM) UvsY, 900 µg/mL (26.5 µM) Gp32, 120
812 µg/mL (1.8 µM) Bsu LF, 40 mM triglycine (Sigma), and 700 nM *n* gene primers. One µL of
813 pUC57-2019-nCoV-N plasmid (MolecularCloud cat no. #MC_0101085) was used as a
814 template, and the RPA reactions were allowed to proceed at 42°C for 60 min. Thereafter, 2 µL
815 of the RPA products were mixed with 18 µL of the Cas13a-based detection reaction, which
816 contained 40 mM Tris-HCl pH 7.4, 60 mM NaCl, 6 mM MgCl$_2$, 1 mM of each rNTPs, 1.5
817 U/µL NxGen T7 RNA polymerase, 6.3 µg/mL LwaCas13a, 1 ng/µL LwaCas13a crRNA for *n*
818 gene, and 0.3 µM FAM-PolyU reporter. The generated FAM fluorescence was monitored at
819 37 °C over 90 min using a real-time thermal cycler (CFX Connect Real-Time PCR System,
820 Bio-Rad).
821

822 **Optimized in-house RT-RPA for single-gene and multiplexed Cas13-based detection**
823 The single-plexed RT-RPA of the *n* gene was set up with the following components (20 µL
824 total reaction volume, consisting of 14.5 µL reagent mastermix and 5.5 µL RNA input): 50
825 mM Tris (pH 7.5), 100 mM potassium acetate, 14 mM magnesium acetate, 2 mM DTT, 5%
826 (w/v) PEG20000, 200 µM dNTPs, 12 mM ATP, 50 mM phosphocreatine, 100 µg/mL creatine
827 kinase, 150 µg/mL (3.3 µM) UvsX, 30 µg/mL (1.7 µM) UvsY, 900 µg/mL (26.5 µM) Gp32,
828 120 µg/mL (1.8 µM) Bsu LF, 26.6 U/mL RNase H, 2.8 U/µL EpiScript Reverse Transcriptase,
829 40 mM triglycine (Sigma), and 700 nM *n* gene primers. 5.5 µL of serially diluted SARS-CoV-
830 2 RNA was used as a template, and the RT-RPA reactions were allowed to proceed at 42°C for
831 60 min.
832

833 The multiplexed RT-RPA to detect the *s* and *n* genes of SARS-CoV-2 was set up in a similar
834 condition as the single-plexed amplification, except for the concentration of specific primers,
835 and the amount of RNA template used. Here, we used the *n* gene and *s* gene RPA primers at
836 222 nM and 177 nM, respectively, and add 7 µL of serially diluted SARS-CoV-2 RNA as
837 input. RT-RPA reactions were performed at 42 °C for 60 min, and the RPA products monitored
838 through multiplexed Cas13a/b-based detection as described in the optimized multiplexed
839 Cas13-based detection methods section.
840

841 Thereafter, 2 µL of the RPA products were mixed with 18 µL of the Cas13a-based detection
842 reaction, which contained 40 mM Tris-HCl pH 7.4, 60 mM NaCl, 6 mM MgCl$_2$, 1 mM of each
843 rNTPs, 1.5 U/µL NxGen T7 RNA polymerase, 6.3 µg/mL LwaCas13a, 1 ng/µL LwaCas13a
844 crRNA (1 ng/µL LwaCas13a crRNA for single gene detection and 0.5 ng/µL LwaCas13a
845 crRNA for *s* gene, 0.5 ng/µL LwaCas13a crRNA for *n* gene for multiplexed detection), and 0.3

846 µM FAM-PolyU reporter. The generated FAM fluorescence was monitored at 37 °C over 90
847 min using a real-time thermal cycler (CFX Connect Real-Time PCR System, Bio-Rad).
848

849 **Lyophilized in-house RT-RPA for multiplexed gene detection**
850 The multiplexed RT-RPA reaction mixture was prepared by assembling all components as
851 described in the optimized in-house RT-RPA methods section, except that magnesium acetate
852 and potassium acetate were not included, and the mixture was further supplemented with 6%
853 (w/v) trehalose. The mixture was lyophilized using a freeze dryer (Alpha 2-4 LDplus, Martin
854 Christ).
855

856 To reconstitute and initiate the RT-RPA reaction, the lyophilized RT-RPA pellet was
857 resuspended in a solution consisting of 1 µL of 280 mM magnesium acetate, 0.4 µL of 5 M
858 potassium acetate, and 17.6 µL of SARS-CoV-2 RNA. The RT-RPA reaction was incubated at
859 42 °C for 60 min. A portion of the reaction was then transferred to the Cas13a-based detection
860 step containing crRNAs for both *s* and *n* genes as previously described. The generated FAM
861 fluorescence was monitored using a real-time thermal cycler (CFX Connect Real-Time PCR
862 System, Bio-Rad).
863

864 **Sample collection, RNA preparation, and ethical approval**
865 As previously described (Chaimayo et al., 2020), respiratory samples were collected from
866 patients with suspected SARS-CoV-2 infection at Siriraj Hospital and processed at the
867 Diagnostic Molecular Laboratory, Department of Microbiology, Faculty of Medicine, Siriraj
868 Hospital. Nasopharyngeal and throat swabs were collected in viral transport media (VTM,
869 Gibco). RNA was extracted from 200 µL of the respiratory swabs in VTM using magLEAD®
870 12gC automated extraction platform (Precision System Science, Japan), eluted in 100 µL
871 buffer, and either used directly for clinical laboratory diagnosis of SARS-CoV-2 via RT-qPCR
872 or stored at -70 °C for later use.
873

874 Excess RNA extracts from these samples were then used without any personally identifiable
875 information being collected for our studies. 91 samples with known positive results from RT-
876 PCR for SARS-CoV-2, 45 samples with known negative results from RT-PCR for SARS-CoV-
877 2, 20 Delta clinical samples, 10 Alpha clinical samples, 15 Omicron clinical samples, and 3
878 samples with positive results for human coronavirus OC43, NL63, and 229E were included for
879 the method validation. Samples were randomized upon giving to study staff, who were kept
880 blinded to the SARS-CoV-2 RT-PCR diagnostics results of the samples when they performed
881 validation experiments of CRISPR diagnostics.
882

883 Ethical approval of the study was given by the Siriraj Institutional Review Board (COA: Si
884 339/2020 and Si 424/2020).
885

886 **Cultured SARS-CoV-2 viral RNA extracts and serial dilutions**
887 SARS-CoV-2 Wuhan variant (clinical isolate hCoV-19/Thailand/Siriraj_5/2020; GISAID
888 accession ID: EPI_ISL_447908), Alpha variant (clinical isolate hCoV-
889 19/Thailand/Bangkok_R098/2021; GISAID accession ID: EPI_ISL_11000098), and Delta
890 variant (clinical isolate hCoV-19/Thailand/Bangkok_SEQ4389/2021; GISAID accession ID:
891 EPI_ISL_3038904) were propagated in Vero E6 cells cultured in MEM-E supplemented with
892 10% fetal bovine serum. The culture media were collected and extracted as described for the
893 clinical sample. The RNA extracts at given dilution were prepared by dilution with nuclease-
894 free water and stored at -70 °C for later use.
895

RT-qPCR

The RT-qPCR was performed according to a published protocol (Vogels et al., 2020). In brief, a 5 µL of the RNA sample was added to a 20-µL reaction prepared with Luna® Universal Probe One-Step RT-qPCR Kit (New England Biolabs) and nCoV_N1 primer-probe set (Integrated DNA Technologies). The reactions were monitored using CFX Connect Real-Time PCR System (Bio-Rad).

Allplex™ SARS-CoV-2 Variants I Assay (Seegene, Korea), which targets *RdRp* and *S*; delH69/V70, E484K and N501Y of SARS-CoV-2, was used for SARS-CoV-2 Alpha and Omicron variant screening. Allplex™ SARS-CoV-2 Variants II Assay (Seegene, Korea), which targets *RdRp* and *S*; K417N, K417T, L452R and W152C, was used for Delta variant screening. All identified variant samples were confirmed with full length spike sequencing.

Droplet digital RT-PCR (RT-ddPCR)

The RT-ddPCR was performed using One-Step RT-ddPCR Advanced Kit for Probes (Bio-Rad) according to the manufacturer's protocol and in line with RT-qPCR protocol described above. A 20-µL reaction consisted of 5 µL of RNA input, 5 µL of Supermix, 2 µL of reverse transcriptase, 1 µL of 300 mM DTT, 4 µL nuclease-free water, and each 1 µL of following component from nCoV_N1 primer-probe set (Integrated DNA Technologies): 10 µM forward primer, 10 µM reverse primer, and 10 µM probe. The reaction droplets were generated and read using a QX100™ Droplet Digital™ PCR system (Bio-Rad) connected to a T100™ Thermal Cycler (Bio-Rad). Thermocycling conditions were reverse transcription at 50 °C for 60 minutes, enzyme activation at 95 °C for 10 minutes, followed by 40 cycles of 95 °C for 15 seconds, 55 °C for 30 seconds, 58 °C for 10 seconds. The enzyme deactivation was done at 98 °C for 10 minutes. The quantification was carried out using QuantaSoft™ software (Bio-rad).

Standard curve of qPCR Ct versus ddPCR-derived copies/uL RNA input see Appendix 1

Data analysis and visualization

Statistical analyses were performed, and graphical representations created with GraphPad Prism 9, unless indicated otherwise. Schematic diagrams were created with Biorender.com and Adobe Illustrator CC 2017.

References

Aksamentov, I., Roemer, C., Hodcroft, E., & Neher, R. (2021). Nextclade: clade assignment, mutation calling and quality control for viral genomes. *Journal of Open Source Software*, *6*(67). https://doi.org/10.21105/joss.03773

Alexandersen, S., Chamings, A., & Bhatta, T. R. (2020). SARS-CoV-2 genomic and subgenomic RNAs in diagnostic samples are not an indicator of active replication. *Nature Communications*, *11*(1), 6059. https://doi.org/10.1038/s41467-020-19883-7

Arizti-Sanz, J., Bradley, A. D., Zhang, Y. B., Boehm, C. K., Freije, C. A., Grunberg, M. E., Kosoko-Thoroddsen, T.-S. F., Welch, N. L., Pillai, P. P., Mantena, S., Kim, G., Uwanibe, J. N., John, O. G., Eromon, P. E., Kocher, G., Gross, R., Lee, J. S., Hensley, L. E., Happi, C. T., . . . Myhrvold, C. (2021). Equipment-free detection of SARS-CoV-2 and Variants of Concern using Cas13. *medRxiv*, 2021.2011.2001.21265764. https://doi.org/10.1101/2021.11.01.21265764

Arizti-Sanz, J., Freije, C. A., Stanton, A. C., Petros, B. A., Boehm, C. K., Siddiqui, S., Shaw, B. M., Adams, G., Kosoko-Thoroddsen, T.-S. F., Kemball, M. E., Uwanibe, J. N., Ajogbasile, F. V., Eromon, P. E., Gross, R., Wronka, L., Caviness, K., Hensley, L. E.,

945   Bergman, N. H., MacInnis, B. L., . . . Myhrvold, C. (2020). Streamlined inactivation,
946   amplification, and Cas13-based detection of SARS-CoV-2. *Nature Communications*,
947   *11*(1), 5921. https://doi.org/10.1038/s41467-020-19097-x
948   Ball, C. S., Light, Y. K., Koh, C.-Y., Wheeler, S. S., Coffey, L. L., & Meagher, R. J. (2016).
949   Quenching of Unincorporated Amplification Signal Reporters in Reverse-Transcription
950   Loop-Mediated Isothermal Amplification Enabling Bright, Single-Step, Closed-Tube,
951   and Multiplexed Detection of RNA Viruses. *Analytical chemistry*, *88*(7), 3562-3568.
952   https://doi.org/10.1021/acs.analchem.5b04054
953   Bao, Y., Jiang, Y., Xiong, E., Tian, T., Zhang, Z., Lv, J., Li, Y., & Zhou, X. (2020). CUT-
954   LAMP: Contamination-Free Loop-Mediated Isothermal Amplification Based on the
955   CRISPR/Cas9 Cleavage. *ACS sensors*, *5*(4), 1082-1091.
956   Bi, K., Herrera-Diestra, J. L., Bai, Y., Du, Z., Wang, L., Gibson, G., Johnson-Leon, M., Fox,
957   S. J., & Meyers, L. A. (2022). The risk of SARS-CoV-2 Omicron variant emergence in
958   low and middle-income countries (LMICs). *medRxiv*, 2022.2001.2014.22268821.
959   https://doi.org/10.1101/2022.01.14.22268821
960   Brito, A. F., Semenova, E., Dudas, G., Hassler, G. W., Kalinich, C. C., Kraemer, M. U. G., Ho,
961   J., Tegally, H., Githinji, G., Agoti, C. N., Matkin, L. E., Whittaker, C., Howden, B. P.,
962   Sintchenko, V., Zuckerman, N. S., Mor, O., Blankenship, H. M., de Oliveira, T., Lin,
963   R. T. P., . . . Faria, N. R. (2021). Global disparities in SARS-CoV-2 genomic
964   surveillance. *medRxiv*. https://doi.org/10.1101/2021.08.21.21262393
965   Broughton, J. P., Deng, X., Yu, G., Fasching, C. L., Servellita, V., Singh, J., Miao, X.,
966   Streithorst, J. A., Granados, A., Sotomayor-Gonzalez, A., Zorn, K., Gopez, A., Hsu, E.,
967   Gu, W., Miller, S., Pan, C.-Y., Guevara, H., Wadford, D. A., Chen, J. S., & Chiu, C. Y.
968   (2020). CRISPR–Cas12-based detection of SARS-CoV-2. *Nature Biotechnology*,
969   *38*(7), 870-874. https://doi.org/10.1038/s41587-020-0513-4
970   Burki, T. K. (2021). Lifting of COVID-19 restrictions in the UK and the Delta variant. *The
971   Lancet   Respiratory   Medicine*,   *9*(8),   e85.   https://doi.org/10.1016/S2213-
972   2600(21)00328-3
973   Burki, T. K. (2022). Omicron variant and booster COVID-19 vaccines. *The Lancet Respiratory
974   Medicine*, *10*(2), e17. https://doi.org/10.1016/S2213-2600(21)00559-2
975   Chaibun, T., Puenpa, J., Ngamdee, T., Boonapatcharoen, N., Athamanolap, P., O'Mullane, A.
976   P., Vongpunsawad, S., Poovorawan, Y., Lee, S. Y., & Lertanantawong, B. (2021).
977   Rapid   electrochemical   detection   of   coronavirus   SARS-CoV-2.   *Nature
978   Communications*, *12*(1), 802. https://doi.org/10.1038/s41467-021-21121-7
979   Chaimayo, C., Kaewnaphan, B., Tanlieng, N., Athipanyasilp, N., Sirijatuphat, R.,
980   Chayakulkeeree, M., Angkasekwinai, N., Sutthent, R., Puangpunngam, N.,
981   Tharmviboonsri, T., Pongraweewan, O., Chuthapisith, S., Sirivatanauksorn, Y.,
982   Kantakamalakul, W., & Horthongkham, N. (2020). Rapid SARS-CoV-2 antigen
983   detection assay in comparison with real-time RT-PCR assay for laboratory diagnosis of
984   COVID-19 in Thailand. *Virol J*, *17*(1), 177. https://doi.org/10.1186/s12985-020-
985   01452-5
986   Chen, J. S., Ma, E., Harrington, L. B., Da Costa, M., Tian, X., Palefsky, J. M., & Doudna, J.
987   A. (2018). CRISPR-Cas12a target binding unleashes indiscriminate single-stranded
988   DNase activity. *Science*, *360*(6387), 436-439. https://doi.org/10.1126/science.aar6245
989   Chen, Y., Mei, Y., & Jiang, X. (2021). Universal and high-fidelity DNA single nucleotide
990   polymorphism detection based on a CRISPR/Cas12a biochip. *Chem Sci*, *12*(12), 4455-
991   4462. https://doi.org/10.1039/d0sc05717g
992   Dutta, N. K., Mazumdar, K., & Gordy, J. T. (2020). The Nucleocapsid Protein of SARS–CoV-
993   2: a Target for Vaccine Development. *Journal of Virology*, *94*(13), e00647-00620.
994   https://doi.org/10.1128/jvi.00647-20

995   Engler, C., Kandzia, R., & Marillonnet, S. (2008). A One Pot, One Step, Precision Cloning
996   Method with High Throughput Capability. *PLOS ONE*, *3*(11), e3647.
997   https://doi.org/10.1371/journal.pone.0003647

998   European Centre for Disease, P., Control, & World Health Organization. Regional Office for,
999   E. (2021). *Methods for the detection and characterisation of SARS-CoV-2 variants:*
1000   *first update, 20 December 2021* CC BY-NC-SA 3.0 IGO).
1001   https://apps.who.int/iris/handle/10665/351156

1002   Fasching, C. L., Servellita, V., McKay, B., Nagesh, V., Broughton, J. P., Sotomayor-Gonzalez,
1003   A., Wang, B., Brazer, N., Reyes, K., Streithorst, J., Deraney, R. N., Stanfield, E.,
1004   Hendriks, C. G., Miller, S., Ching, J., Chen, J. S., & Chiu, C. Y. (2022). COVID-19
1005   Variant Detection with a High-Fidelity CRISPR-Cas12 Enzyme. *medRxiv*,
1006   2021.2011.2029.21267041. https://doi.org/10.1101/2021.11.29.21267041

1007   Fozouni, P., Son, S., de León Derby, M. D., Knott, G. J., Gray, C. N., D'Ambrosio, M. V.,
1008   Zhao, C., Switz, N. A., Kumar, G. R., & Stephens, S. I. (2020). Amplification-free
1009   detection of SARS-CoV-2 with CRISPR-Cas13a and mobile phone microscopy. *Cell*.

1010   Gootenberg, J. S., Abudayyeh, O. O., Kellner, M. J., Joung, J., Collins, J. J., & Zhang, F.
1011   (2018). Multiplexed and portable nucleic acid detection platform with Cas13, Cas12a,
1012   and Csm6. *Science*, *360*(6387), 439-444.

1013   Gootenberg, J. S., Abudayyeh, O. O., Lee, J. W., Essletzbichler, P., Dy, A. J., Joung, J.,
1014   Verdine, V., Donghia, N., Daringer, N. M., & Freije, C. A. (2017). Nucleic acid
1015   detection with CRISPR-Cas13a/C2c2. *Science*, *356*(6336), 438-442.

1016   Harrington, L. B., Burstein, D., Chen, J. S., Paez-Espino, D., Ma, E., Witte, I. P., Cofsky, J. C.,
1017   Kyrpides, N. C., Banfield, J. F., & Doudna, J. A. (2018). Programmed DNA destruction
1018   by miniature CRISPR-Cas14 enzymes. *Science*, *362*(6416), 839-842.
1019   https://doi.org/10.1126/science.aav4294

1020   He, C., Lin, C., Mo, G., Xi, B., Li, A. a., Huang, D., Wan, Y., Chen, F., Liang, Y., Zuo, Q.,
1021   Xu, W., Feng, D., Zhang, G., Han, L., Ke, C., Du, H., & Huang, L. (2022). Rapid and
1022   accurate detection of SARS-CoV-2 mutations using a Cas12a-based sensing platform.
1023   *Biosensors and Bioelectronics*, *198*, 113857.
1024   https://doi.org/https://doi.org/10.1016/j.bios.2021.113857

1025   Jauset-Rubio, M., Tomaso, H., El-Shahawi, M. S., Bashammakh, A. S., Al-Youbi, A. O., &
1026   O'Sullivan, C. K. (2018). Duplex lateral flow assay for the simultaneous detection of
1027   Yersinia pestis and Francisella tularensis. *Analytical chemistry*, *90*(21), 12745-12751.

1028   Joung, J., Ladha, A., Saito, M., Kim, N.-G., Woolley, A. E., Segel, M., Barretto, R. P. J., Ranu,
1029   A., Macrae, R. K., Faure, G., Ioannidi, E. I., Krajeski, R. N., Bruneau, R., Huang, M.-
1030   L. W., Yu, X. G., Li, J. Z., Walker, B. D., Hung, D. T., Greninger, A. L., . . . Zhang, F.
1031   (2020). Detection of SARS-CoV-2 with SHERLOCK One-Pot Testing. *New England*
1032   *Journal of Medicine*, *383*(15), 1492-1494. https://doi.org/10.1056/NEJMc2026172

1033   Katoh, K., & Standley, D. M. (2013). MAFFT multiple sequence alignment software version
1034   7: improvements in performance and usability. *Mol Biol Evol*, *30*(4), 772-780.
1035   https://doi.org/10.1093/molbev/mst010

1036   Kellner, M. J., Koob, J. G., Gootenberg, J. S., Abudayyeh, O. O., & Zhang, F. (2019).
1037   SHERLOCK: nucleic acid detection with CRISPR nucleases. *Nat Protoc*, *14*(10),
1038   2986-3012. https://doi.org/10.1038/s41596-019-0210-2

1039   Konermann, S., Lotfy, P., Brideau, N. J., Oki, J., Shokhirev, M. N., & Hsu, P. D. (2018).
1040   Transcriptome engineering with RNA-targeting type VI-D CRISPR effectors. *Cell*,
1041   *173*(3), 665-676. e614.

1042   Lin, Y., Cradick, T. J., Brown, M. T., Deshmukh, H., Ranjan, P., Sarode, N., Wile, B. M.,
1043   Vertino, P. M., Stewart, F. J., & Bao, G. (2014). CRISPR/Cas9 systems have off-target

22

1044   activity with insertions or deletions between target DNA and guide RNA sequences.
1045   *Nucleic Acids Res*, *42*(11), 7473-7485. https://doi.org/10.1093/nar/gku402

1046 Liu, Y., & Rocklöv, J. (2021). The reproductive number of the Delta variant of SARS-CoV-2
1047   is far higher compared to the ancestral SARS-CoV-2 virus. *J Travel Med*, *28*(7).
1048   https://doi.org/10.1093/jtm/taab124

1049 Mayuramart, O., Nimsamer, P., Rattanaburi, S., Chantaravisoot, N., Khongnomnan, K.,
1050   Chansaenroj, J., Puenpa, J., Suntronwong, N., Vichaiwattana, P., Poovorawan, Y., &
1051   Payungporn, S. (2021). Detection of severe acute respiratory syndrome coronavirus 2
1052   and influenza viruses based on CRISPR-Cas12a. *Exp Biol Med (Maywood)*, *246*(4),
1053   400-405. https://doi.org/10.1177/1535370220963793

1054 Myhrvold, C., Freije, C. A., Gootenberg, J. S., Abudayyeh, O. O., Metsky, H. C., Durbin, A.
1055   F., Kellner, M. J., Tan, A. L., Paul, L. M., Parham, L. A., Garcia, K. F., Barnes, K. G.,
1056   Chak, B., Mondini, A., Nogueira, M. L., Isern, S., Michael, S. F., Lorenzana, I.,
1057   Yozwiak, N. L., . . . Sabeti, P. C. (2018). Field-deployable viral diagnostics using
1058   CRISPR-Cas13. *Science*, *360*(6387), 444-448. https://doi.org/10.1126/science.aas8836

1059 Nguyen, L. T., Rananaware, S. R., Pizzano, B. L. M., Stone, B. T., & Jain, P. K. (2020).
1060   Engineered CRISPR/Cas12a Enables Rapid SARS-CoV-2 Detection. *medRxiv*,
1061   2020.2012.2023.20248725. https://doi.org/10.1101/2020.12.23.20248725

1062 Nguyen, L. T., Smith, B. M., & Jain, P. K. (2020). Enhancement of trans-cleavage activity of
1063   Cas12a with engineered crRNA enables amplified nucleic acid detection. *Nature
1064   Communications*, *11*(1), 4906. https://doi.org/10.1038/s41467-020-18615-1

1065 Nimsamer, P., Mayuramart, O., Rattanaburi, S., Chantaravisoot, N., Saengchoowong, S.,
1066   Puenpa, J., Poovorawan, Y., & Payungporn, S. (2021). Comparative performance of
1067   CRISPR-Cas12a assays for SARS-CoV-2 detection tested with RNA extracted from
1068   clinical specimens. *J Virol Methods*, *290*, 114092.
1069   https://doi.org/10.1016/j.jviromet.2021.114092

1070 Ooi, K. H., Liu, M. M., Tay, J. W. D., Teo, S. Y., Kaewsapsak, P., Jin, S., Lee, C. K., Hou, J.,
1071   Maurer-Stroh, S., Lin, W., Yan, B., Yan, G., Gao, Y. G., & Tan, M. H. (2021). An
1072   engineered CRISPR-Cas12a variant and DNA-RNA hybrid guides enable robust and
1073   rapid COVID-19 testing. *Nat Commun*, *12*(1), 1739. https://doi.org/10.1038/s41467-
1074   021-21996-6

1075 Patchsung, M., Jantarug, K., Pattama, A., Aphicho, K., Suraritdechachai, S., Meesawat, P.,
1076   Sappakhaw, K., Leelahakorn, N., Ruenkam, T., Wongsatit, T., Athipanyasilp, N.,
1077   Eiamthong, B., Lakkanasirorat, B., Phoodokmai, T., Niljianskul, N., Pakotiprapha, D.,
1078   Chanarat, S., Homchan, A., Tinikul, R., . . . Uttamapinant, C. (2020). Clinical validation
1079   of a Cas13-based assay for the detection of SARS-CoV-2 RNA. *Nature Biomedical
1080   Engineering*, *4*(12), 1140-1149. https://doi.org/10.1038/s41551-020-00603-x

1081 Piepenburg, O., Williams, C. H., Stemple, D. L., & Armes, N. A. (2006). DNA detection using
1082   recombination proteins. *PLoS Biol*, *4*(7), e204.

1083 Priye, A., Ball, C. S., & Meagher, R. J. (2018). Colorimetric-Luminance Readout for
1084   Quantitative Analysis of Fluorescence Signals with a Smartphone CMOS Sensor. *Anal
1085   Chem*, *90*(21), 12385-12389. https://doi.org/10.1021/acs.analchem.8b03521

1086 Priye, A., Bird, S. W., Light, Y. K., Ball, C. S., Negrete, O. A., & Meagher, R. J. (2017). A
1087   smartphone-based diagnostic platform for rapid detection of Zika, chikungunya, and
1088   dengue viruses. *Sci Rep*, *7*, 44778. https://doi.org/10.1038/srep44778

1089 Qian, J., Boswell, S. A., Chidley, C., Lu, Z.-x., Pettit, M. E., Gaudio, B. L., Fajnzylber, J. M.,
1090   Ingram, R. T., Ward, R. H., Li, J. Z., & Springer, M. (2020). An enhanced isothermal
1091   amplification assay for viral detection. *Nature Communications*, *11*(1), 5920.
1092   https://doi.org/10.1038/s41467-020-19258-y

Quan, J., & Tian, J. (2011). Circular polymerase extension cloning for high-throughput cloning of complex and combinatorial DNA libraries. *Nature Protocols*, *6*(2), 242-251. https://doi.org/10.1038/nprot.2010.181

Rambaut, A., Holmes, E. C., O'Toole, A., Hill, V., McCrone, J. T., Ruis, C., du Plessis, L., & Pybus, O. G. (2020). A dynamic nomenclature proposal for SARS-CoV-2 lineages to assist genomic epidemiology. *Nat Microbiol*, *5*(11), 1403-1407. https://doi.org/10.1038/s41564-020-0770-5

Samacoits, A., Nimsamer, P., Mayuramart, O., Chantaravisoot, N., Sitthi-amorn, P., Nakhakes, C., Luangkamchorn, L., Tongcham, P., Zahm, U., & Suphanpayak, S. (2021). Machine Learning-Driven and Smartphone-Based Fluorescence Detection for CRISPR Diagnostic of SARS-CoV-2. *ACS Omega*.

Schindelin, J., Arganda-Carreras, I., Frise, E., Kaynig, V., Longair, M., Pietzsch, T., Preibisch, S., Rueden, C., Saalfeld, S., Schmid, B., Tinevez, J. Y., White, D. J., Hartenstein, V., Eliceiri, K., Tomancak, P., & Cardona, A. (2012). Fiji: an open-source platform for biological-image analysis. *Nat Methods*, *9*(7), 676-682. https://doi.org/10.1038/nmeth.2019

Shinoda, H., Taguchi, Y., Nakagawa, R., Makino, A., Okazaki, S., Nakano, M., Muramoto, Y., Takahashi, C., Takahashi, I., Ando, J., Noda, T., Nureki, O., Nishimasu, H., & Watanabe, R. (2021). Amplification-free RNA detection with CRISPR-Cas13. *Commun Biol*, *4*(1), 476. https://doi.org/10.1038/s42003-021-02001-8

Subsoontorn, P., Lohitnavy, M., & Kongkaew, C. (2020). The diagnostic accuracy of isothermal nucleic acid point-of-care tests for human coronaviruses: A systematic review and meta-analysis. *Scientific Reports*, *10*(1), 22349. https://doi.org/10.1038/s41598-020-79237-7

Tang, Y. W., Schmitz, J. E., Persing, D. H., & Stratton, C. W. (2020). Laboratory Diagnosis of COVID-19: Current Issues and Challenges. *J Clin Microbiol*, *58*(6). https://doi.org/10.1128/JCM.00512-20

Teng, F., Guo, L., Cui, T., Wang, X. G., Xu, K., Gao, Q., Zhou, Q., & Li, W. (2019). CDetection: CRISPR-Cas12b-based DNA detection with sub-attomolar sensitivity and single-base specificity. *Genome Biol*, *20*(1), 132. https://doi.org/10.1186/s13059-019-1742-z

Vogels, C. B. F., Brito, A. F., Wyllie, A. L., Fauver, J. R., Ott, I. M., Kalinich, C. C., Petrone, M. E., Casanovas-Massana, A., Catherine Muenker, M., Moore, A. J., Klein, J., Lu, P., Lu-Culligan, A., Jiang, X., Kim, D. J., Kudo, E., Mao, T., Moriyama, M., Oh, J. E., . . . Grubaugh, N. D. (2020). Analytical sensitivity and efficiency comparisons of SARS-CoV-2 RT–qPCR primer–probe sets. *Nature Microbiology*, *5*(10), 1299-1305. https://doi.org/10.1038/s41564-020-0761-6

Waterhouse, A. M., Procter, J. B., Martin, D. M., Clamp, M., & Barton, G. J. (2009). Jalview Version 2--a multiple sequence alignment editor and analysis workbench. *Bioinformatics*, *25*(9), 1189-1191. https://doi.org/10.1093/bioinformatics/btp033

Welch, N. L., Zhu, M., Hua, C., Weller, J., Mirhashemi, M. E., Nguyen, T. G., Mantena, S., Bauer, M. R., Shaw, B. M., Ackerman, C. M., Thakku, S. G., Tse, M. W., Kehe, J., Uwera, M. M., Eversley, J. S., Bielwaski, D. A., McGrath, G., Braidt, J., Johnson, J., . . . Myhrvold, C. (2022). Multiplexed CRISPR-based microfluidic platform for clinical testing of respiratory viruses and identification of SARS-CoV-2 variants. *Nat Med*. https://doi.org/10.1038/s41591-022-01734-1

Yin, K., Ding, X., Li, Z., Zhao, H., Cooper, K., & Liu, C. (2020). Dynamic Aqueous Multiphase Reaction System for One-Pot CRISPR-Cas12a-Based Ultrasensitive and Quantitative Molecular Diagnosis. *Analytical chemistry*, *92*(12), 8561-8568. https://doi.org/10.1021/acs.analchem.0c01459

24

1143 Zhou, T., Huang, R., Huang, M., Shen, J., Shan, Y., & Xing, D. (2020). CRISPR/Cas13a
1144 Powered Portable Electrochemiluminescence Chip for Ultrasensitive and Specific
1145 MiRNA Detection. *Adv Sci (Weinh)*, *7*(13), 1903661.
1146 https://doi.org/10.1002/advs.201903661
1147

Acknowledgments

1161

Author contributions

1163 Conceptualization: MP, AH, SS, KA, CU, DP, NH
1164 Methodology: MP, AH, SS, KA, CU, DP, NH, SC, CC
1165 Investigation: MP, AH, SS, KA, AP, KS, PM, TWo, AA, KJ, NAt, SV, TWa
1166 Material support: NN, PC, RT, NW, SM, MAC, PSF, JJ, AL, OA, JG, FZ, SC
1167 Clinical study support: AP, NAt, JB, RS, NAn, NH
1168 Supervision: CU, DP, NH
1169 Writing—original draft: MP, AH, SS, KA, CU, DP
1170 Writing—reviewing and editing: all authors

1171

Competing interests

1173 O.A., J.G., and F.Z. are co-founders of Sherlock Biosciences and Pine Trees Health. M.A.C.
1174 and P.S.F. have acted as consultants for Analytik Jena GmbH. M.P., A.H., K.A., S.S., D.P.,
1175 and C.U. have filed a patent in Thailand on the formulations for multiplexed detection of
1176 SARS-CoV-2 RNA. The remaining authors declare no competing interests.

1177
1178

Data availability

1180 The main data supporting the results in this study are available within the paper and its
1181 supplementary information. Raw datasets generated and analysed during the study are available
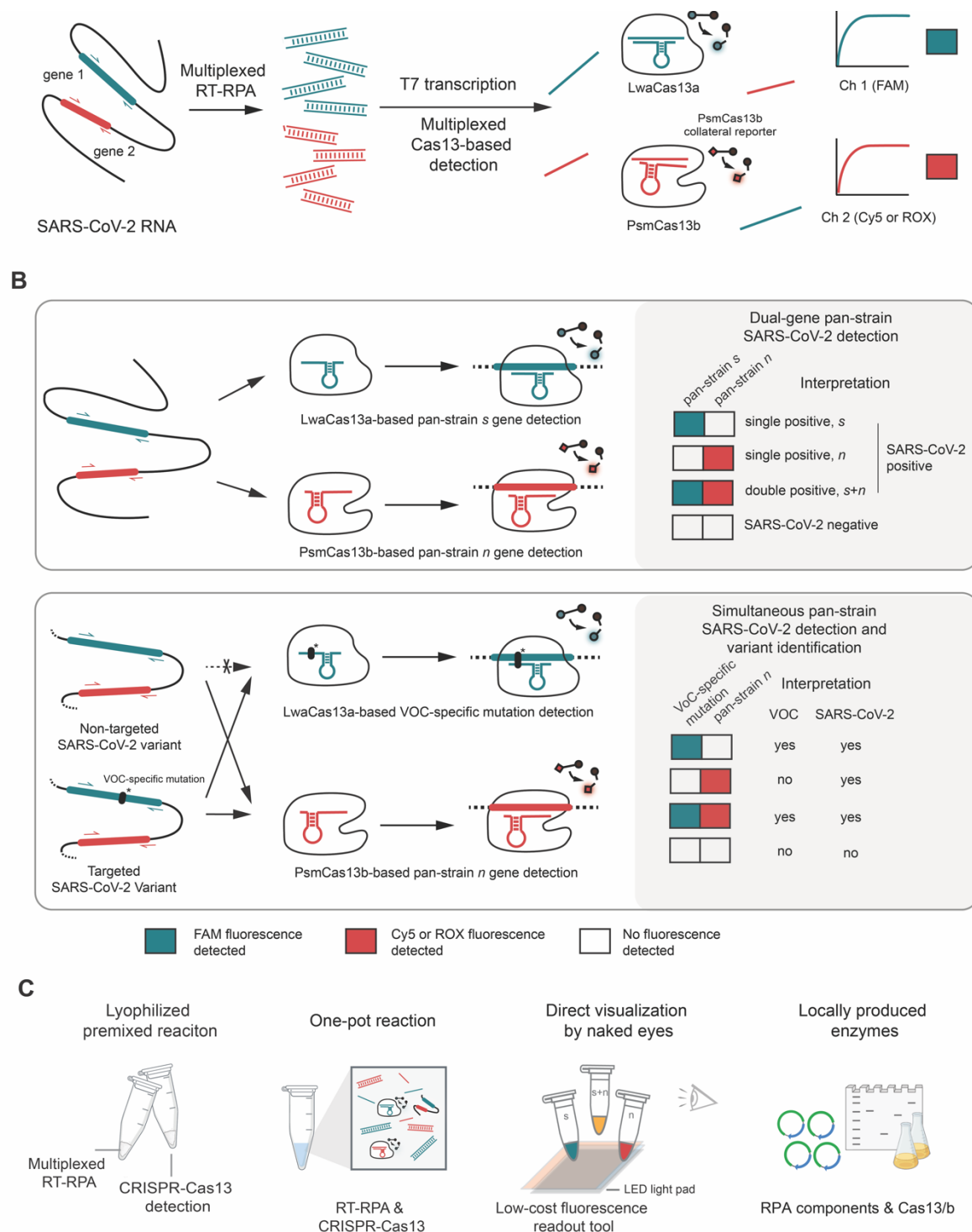1182 from the corresponding authors upon reasonable request.
1183

25

Figure 1. A multiplexed Cas13-based assay for simultaneous SARS-CoV-2 detection and variant identification.
(**A**) Regions of interest in SARS-CoV-2 RNA, such as the *s* and *n* genes, are isothermally amplified by multiplexed RT-RPA. T7 transcription then converts and amplifies DNA amplicons to RNAs, which are recognized by cognate Cas13a-crRNA and Cas13b-crRNA complexes with orthogonal collateral cleavage preferences. Cleavage of orthogonal RNA reporters by target-activated Cas enzymes elicits multicolored fluorescence, which can be monitored with standard fluorescence detection instruments.

(**B**) Top, dual-gene detection via CRISPR-Cas13a/b for COVID-19 diagnosis. Bottom, dual-gene detection for simultaneous COVID-19 diagnosis and SARS-CoV-2 variant identification. LwaCas13a is used to detect a universal, pan-strain region (top) or a variant-specific region (bottom) of the SARS-CoV-2 *s* gene. PsmCas13b is used to detect a pan-strain region of the *n* gene. The amplified regions of the S and N genes are shown in red and green respectively.

(**C**) Developing simple-to-use SARS-CoV-2 variant surveillance tools which can be locally manufactured. Our multiplexed CRISPR-based detection reactions can be premixed and lyophilized for convenient use and storage; multiplexed RPA and Cas13-based reactions can be combined in one tube; result readouts can be directly observed by eye with low-cost light sources; and RPA and Cas13a/b can be locally produced and formulated.
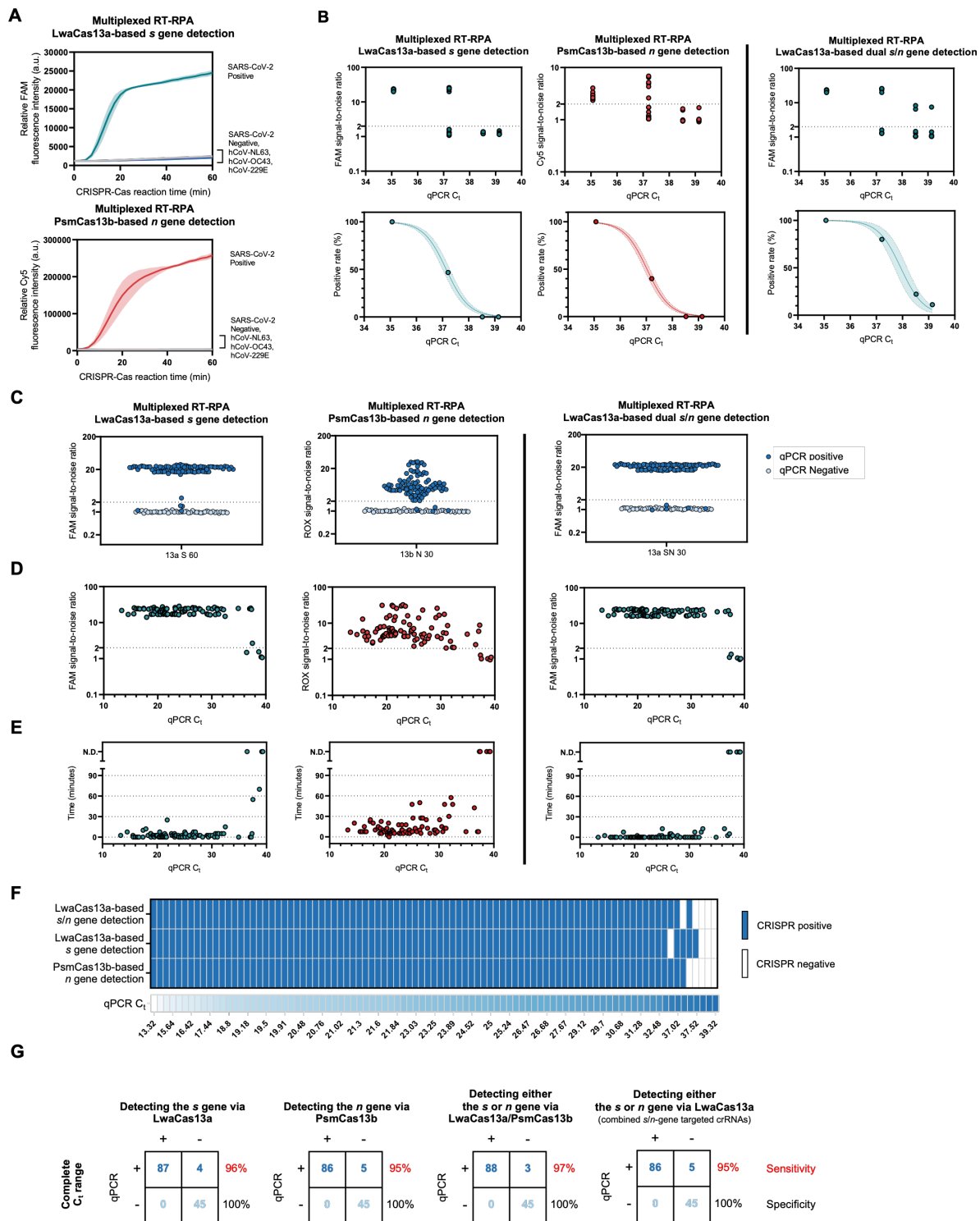
Figure 2. Specificity and sensitivity of the multiplexed CRISPR-based detection of SARS-CoV-2 RNA.

(A) Clinical specificity. Kinetics of FAM (top) and Cy5 (bottom) fluorescence signal generation from the SARS-CoV-2 *s* (top) and *n* gene (bottom) detection via a multiplexed CRISPR-Cas reaction, using RNA extracts from clinical samples verified to be positive with different coronaviruses via RT-qPCR. The SARS-CoV-2 negative sample is an extract from a clinical sample confirmed to be SARS-CoV-2-negative by RT-qPCR. Data are mean ± s.d. from 3 replicates. **(B)** The limit of detection. Multiplexed RT-RPA followed by multiplexed Cas-based detection were performed with serially diluted SARS-CoV-2 RNA, whose Ct

values were determined using a Luna one-step RT-qPCR assay targeting the *n* gene of SARS-CoV-2. At least three independent replicates of the amplification/detection reactions were performed for each SARS-CoV-2 RNA dilution. Top: signal-to-noises (S/N) of FAM (from LwaCas13a-mediated *s* gene detection) and Cy5 (from PsmCas13b-mediated *n* gene detection) fluorescence intensities are shown. The S/N threshold for a positive result was set at 2. Noise is defined as the fluorescence intensity generated from a negative sample with water as input performed in parallel. Bottom: positive rates of the detection of the *s* and *n* genes from multiplexed CRISPR-based detection at different SARS-CoV-2 RNA input concentrations. **(C)-(G)**, clinical sensitivity. **(C)** Summary of S/N obtained from multiplexed CRISPR-based detection results on 136 clinical samples (91 are COVID-19-positive by RT-qPCR; 45 are negative). **(D)** Relation of S/N obtained from multiplexed CRISPR-based detection to C_t values of COVID-19-positive samples. **(E)** Time to positive CRISPR detection results vs C_t values of COVID-19-positive samples. **(F)** Results of multiplexed CRISPR-based detection for 91 COVID-19-positive samples ordered by C_t values from RT-qPCR. **(G)** Concordance between RT-qPCR and multiplexed CRISPR-based detection of SARS-CoV-2 RNA. On the right of each concordance box, sensitivity values (%) for the detection of the *s* and *n* genes under a given scheme are shown in red; specificity values (%) are shown in black.
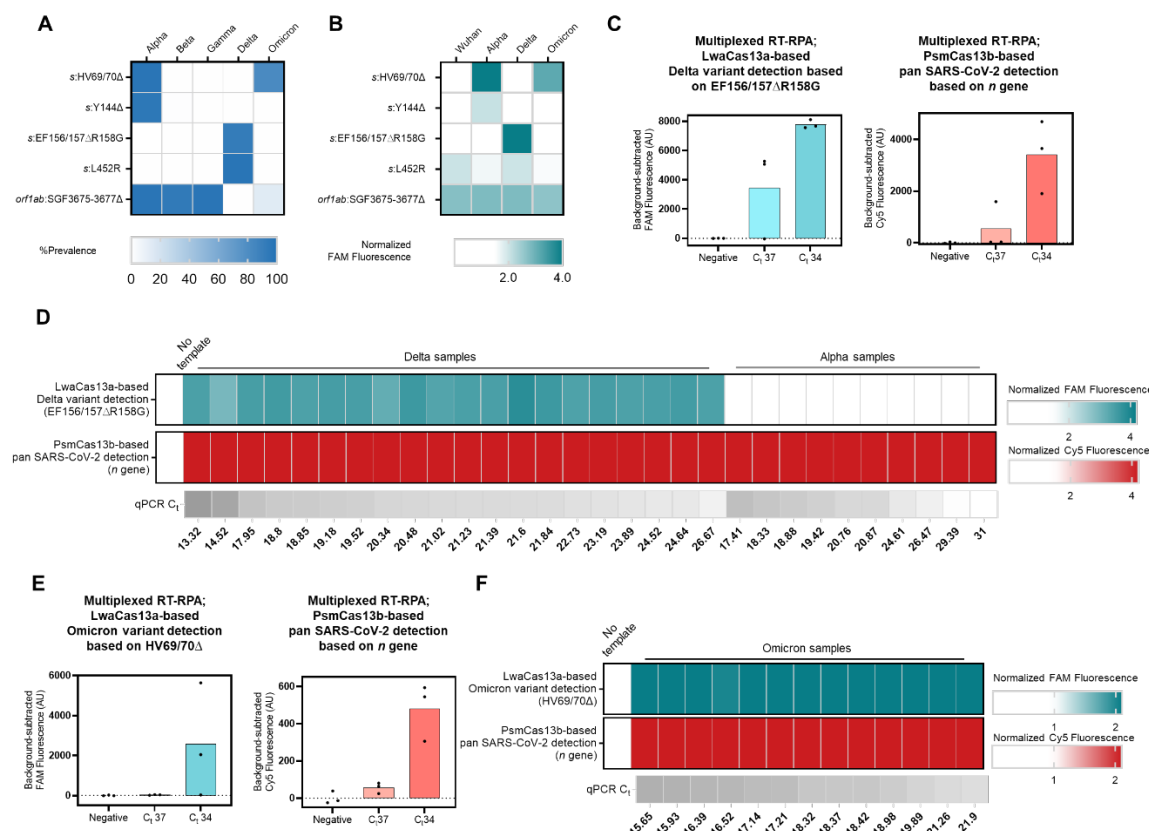
Figure 3. Multiplexed CRISPR-based detection for SARS-CoV-2 variant surveillance
(**A**) Prevalence of the target mutations in five major SARS-CoV-2 variants of concern (obtained from https://outbreak.info on , 15 March 2022, Alpha (n = 1,155,468), Beta (n = 41,428), Gamma (n = 120,775), Delta (n = 4,239,814), and Omicron (n = 2,150,574)) (**B**) Selectivity of singleplexed CRISPR-based SARS-CoV-2 variant detection targeting different mutations of interest. FAM fluorescence intensities at 60 minutes were normalized against intensities obtained from the no template control. Data are mean of two replicates. Raw kinetic traces are shown in Figure 3–figure supplement 4 (**C**) Multiplexed CRISPR-based detection for the Delta variant. The Delta *s* gene was detected via its EF156/157ΔR158G mutation and LwaCas13a. Pan-strain SARS-CoV-2 detection was performed via PsmCas13b-based detection of a conserved region in the *n* gene. Relative FAM (from LwaCas13a-mediated *s* gene detection) and Cy5 (from PsmCas13b-mediated *n* gene detection) fluorescence intensities are shown. Data are mean ± s.d. from 3 replicates. Raw kinetic traces are shown in Figure 3–figure supplement 7A (**D**) Clinical performance of the multiplexed CRISPR-based detection for the Delta variant. Each cell represents a COVID-19-positive clinical sample from Delta (left, n = 20) or Alpha (right, n = 10) lineage. FAM and Cy5 fluorescence intensities at 60 minutes were normalized against intensities obtained from the no template control. (**E**) Multiplexed CRISPR-based detection for the Omicron variant. The Omicron *s* gene was detected via its HV69/70Δ mutation and LwaCas13a. Pan-strain SARS-CoV-2 detection was performed via PsmCas13b-based detection of the *n* gene. Relative FAM (from LwaCas13a-mediated *s* gene detection) and Cy5 (from PsmCas13b-mediated *n* gene detection) fluorescence intensities are shown. Data are mean ± s.d. from 3 replicates. Raw kinetic traces are shown in Figure 3–figure supplement 7B (**F**) Clinical performance of the multiplexed CRISPR-based detection for

Omicron. FAM and Cy5 fluorescence intensities at 30 minutes were normalized against intensities obtained from the no template control.
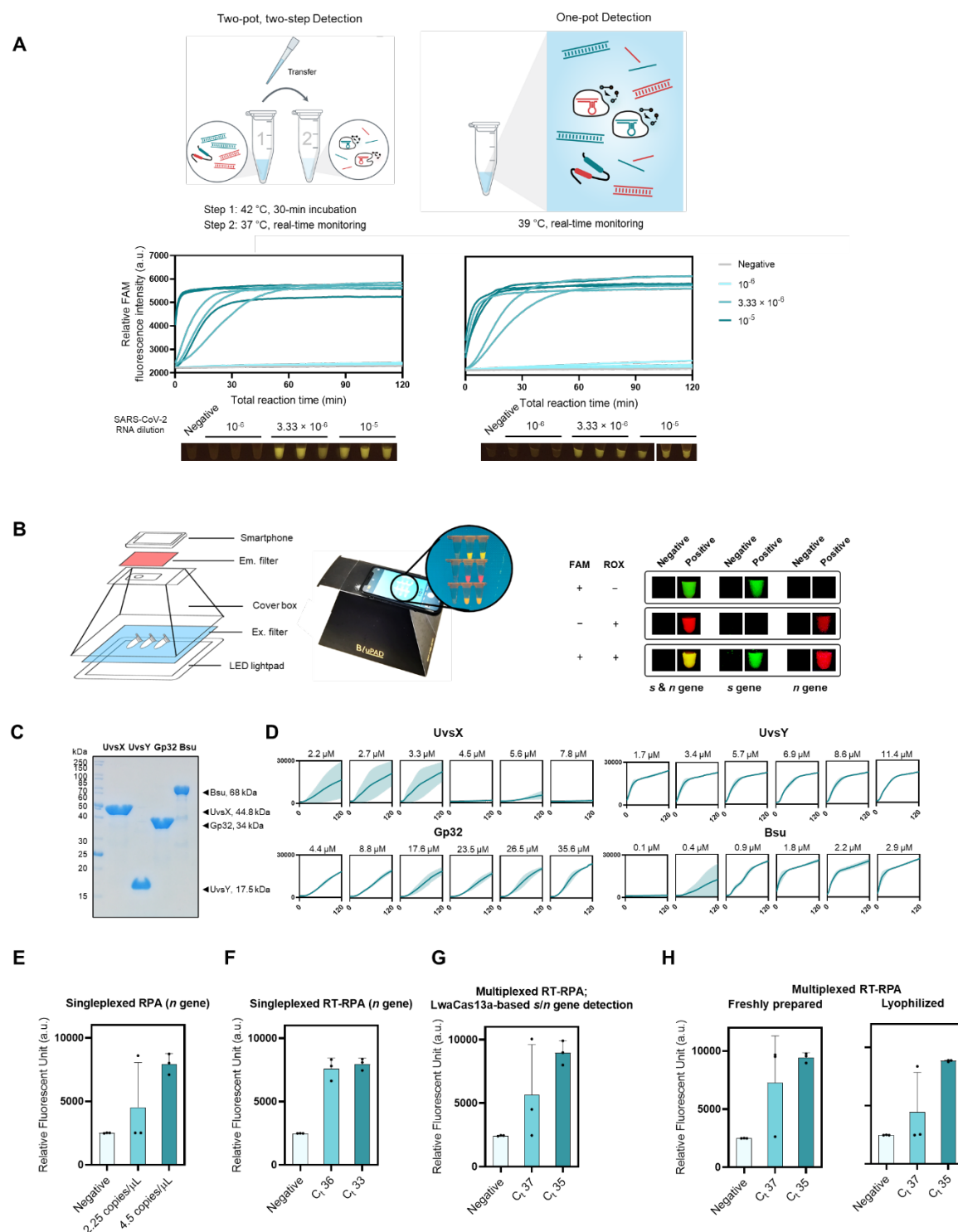
Figure 4. One-pot formulation, easy visualization, and local production of components for RPA and multiplexed CRISPR-based detection.

(**A**) The one-pot reaction scheme and its analytical sensitivity compared to the standard two-pot setup. For all, *s*- and *n*-gene amplicons generated from multiplexed RPA were detected with LwaCas13a-based reaction programmed with *s*- and *n*-targeted crRNAs. Data from 3 independent replicates at each RNA input dilution are shown. (**B**) Easy visualization of multiplexed Cas13-based detection. A sample equipment setup with a LED transilluminator, appropriate lighting gels for visualization of fluorescein (FAM) and rhodamine X (ROX),

and a smartphone for image capturing is shown. Smartphone-captured images of FAM and ROX signal generated from multiplexed Cas13a/b-based detection of the *s* and *n* genes of SARS-CoV-2. (**C**) SDS-PAGE analysis of locally produced and purified RPA components: UvsX, UvsY, Gp32, and Bsu polymerase large fragment (Bsu LF). (**D**) Optimizations of protein concentrations in in-house RPA. RPA reactions with varying concentrations of UvsX, UvsY, Gp32, and Bsu LF were performed with pUC57-2019-nCoV-N plasmid as a DNA template (at 10,000 copies/µl). Thereafter, the RPA products were used in a LwaCas13a-based detection. FAM fluorescence generated over 120 min for each RPA condition is shown. (**E, F**) Optimally formulated in-house RPA in amplification of N gene of SARS-CoV-2 from pUC57-2019-nCoV-N plasmid (**E**) and serially diluted SARS-CoV-2 RNA (**F**). LwaCas13a-based detection was then used to detect *n*-gene amplicons, with FAM fluorescence intensity generated after 90 min at 37°C shown. (**G**) Optimized in-house RT-RPA for multiplexed detection. Multiplexed RT-RPA to amplify the *s* and *n* genes of SARS-CoV-2 was performed using serially diluted SARS-CoV-2 RNA as a template. Detection of *s* and *n* amplicons was monitored through FAM fluorescence signal generated by Cas13a-mediated *s* and *n* gene detection. The reaction was measured after 90 min at 37°C. (**H**) Lyophilized multiplexed in-house RT-RPA has similar sensitivity as freshly prepared reactions. Amplification and detection of the SARS-CoV-2 *s* and *n* gene are as in (**G**). Data are mean ± s.d. from 3 replicates. RNase-free water was used as input of all negative control reactions.

Supplementary Materials

A multiplexed Cas13-based assay with point-of-care attributes for simultaneous COVID-19 diagnosis and variant surveillance

Maturada Patchsung[1,†], Aimorn Homchan[1,2,†], Kanokpol Aphicho[1,†], Surased Suraritdechachai[1,†], Thanyapat Wanitchanon[1,5], Archiraya Pattama[3], Khomkrit Sappakhaw[1], Piyachat Meesawat[1], Thanakrit Wongsatit[1], Artittaya Athipanyasilp[1,3], Krittapas Jantarug[1], Niracha Athipanyasilp[3], Supapat Visanpattanasin[2], Nootaree Niljianskul[4], Pimchai Chaiyen[1], Ruchanok Tinikul[2], Nuanjun Wichukchinda[5], Surakameth Mahasirimongkol[5], Rujipas Sirijatuphat[6], Nasikarn Angkasekwinai[6], Michael A. Crone[7,8,9], Paul S. Freemont[7,8,9], Julia Joung[10,11,12,13,14], Alim Ladha[10,11,12,13,14], Omar Abudayyeh[12], Jonathan Gootenberg[12], Feng Zhang[10,11,12,13,14], Claire Chewapreecha[15,16], Sittinan Chanarat[2], Navin Horthongkham[3,*], Danaya Pakotiprapha[2,*], Chayasith Uttamapinant[1,*]

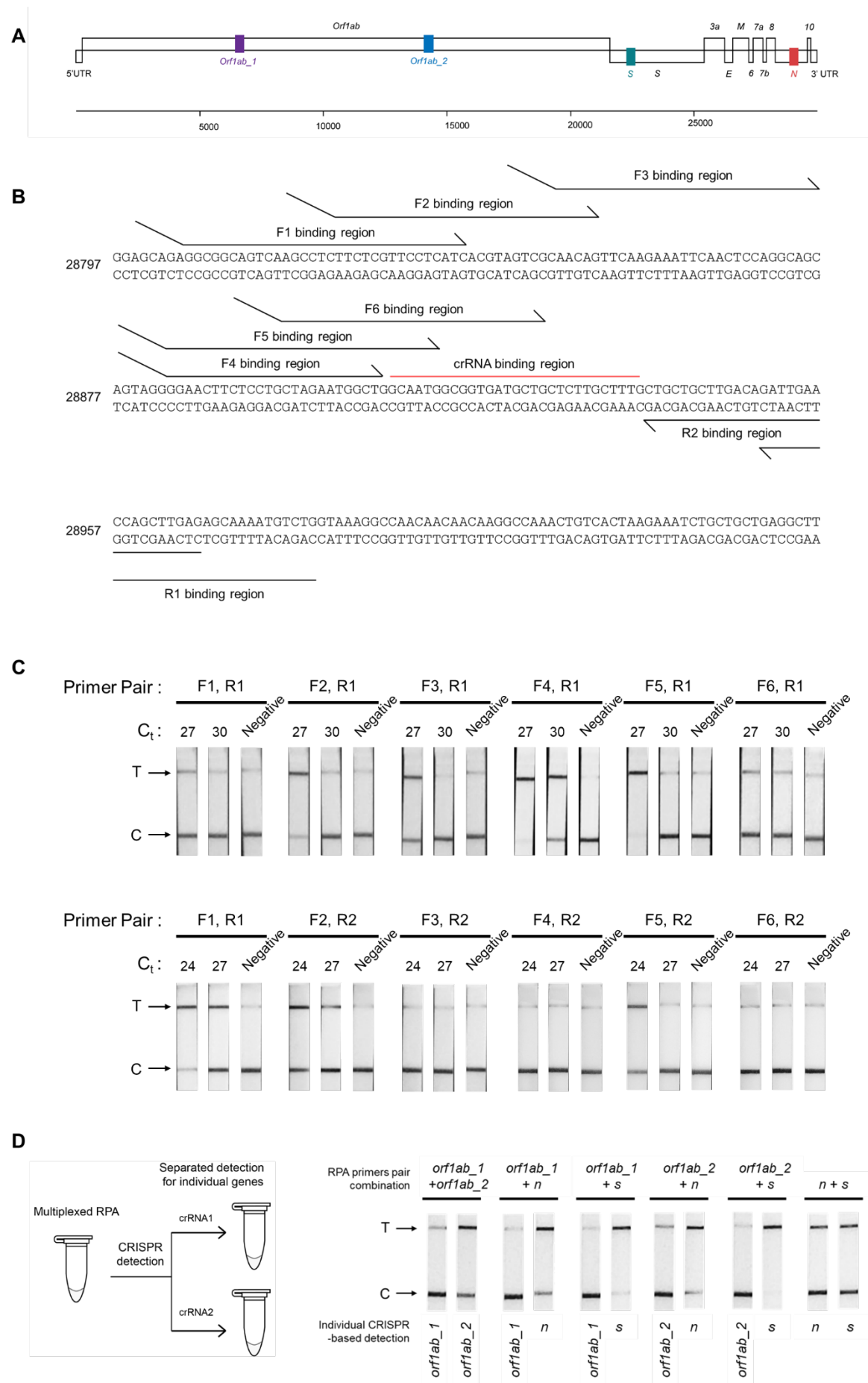*Corresponding authors: danaya.pak@mahidol.ac.th; navin.hor@mahidol.edu; chayasith.u@vistec.ac.th

A

Orf1ab

Orf1ab_1   Orf1ab_2

5'UTR   S   S   E   3a   M   6 7b 7a 8   N   10   3' UTR

5000   10000   15000   20000   25000

B

F3 binding region

F2 binding region

F1 binding region

28797 GGAGCAGAGGCGGCAGTCAAGCCTCTTCTCGTTCCTCATCACGTAGTCGCAACAGTTCAAGAAATTCAACTCCAGGCAGC
CCTCGTCTCCGCCGTCAGTTCGGAGAAGAGCAAGGAGTAGTGCATCAGCGTTGTCAAGTTCTTTAAGTTGAGGTCCGTCG

F6 binding region

F5 binding region

F4 binding region   crRNA binding region

28877 AGTAGGGGAACTTCTCCTGCTAGAATGGCTGGCAATGGCGGTGATGCTGCTCTTGCTTTGCTGCTGCTTGACAGATTGAA
TCATCCCCTTGAAGAGGACGATCTTACCGACCGTTACCGCCACTACGACGAGAACGAAACGACGACGAACTGTCTAACTT

R2 binding region

28957 CCAGCTTGAGAGCAAAATGTCTGGTAAAGGCCAACAACAACAAGGCCAAACTGTCACTAAGAAATCTGCTGCTGAGGCTT
GGTCGAACTCTCGTTTTACAGACCATTTCCGGTTGTTGTTGTTCCGGTTTGACAGTGATTCTTTAGACGACGACTCCGAA

R1 binding region

C

Primer Pair: F1, R1   F2, R1   F3, R1   F4, R1   F5, R1   F6, R1

C_t: 27 30 Negative   27 30 Negative   27 30 Negative   27 30 Negative   27 30 Negative   27 30 Negative

T →

C →

Primer Pair: F1, R1   F2, R2   F3, R2   F4, R2   F5, R2   F6, R2

C_t: 24 27 Negative   24 27 Negative   24 27 Negative   24 27 Negative   24 27 Negative   24 27 Negative

T →

C →

D

Multiplexed RPA

Separated detection for individual genes

crRNA1

crRNA2

CRISPR detection

RPA primers pair combination   orf1ab_1 +orf1ab_2   orf1ab_1 + n   orf1ab_1 + s   orf1ab_2 + n   orf1ab_2 + s   n + s

T →

C →

Individual CRISPR-based detection   orf1ab_1   orf1ab_2   orf1ab_1   n   orf1ab_1   s   orf1ab_2   n   orf1ab_2   s   n   s

Figure 1–figure supplement 1: **Optimizing the RT-RPA amplification of SARS-CoV-2 *n* gene.**
(**A**) Four regions within the *orf1ab*, *s*, and *n* genes of SARS-CoV-2 genome selected for detection are
highlighted. (**B**) Binding positions of different primers to the SARS-CoV-2 *n* gene. (**C**) Testing efficiency
of different primer pairs on SARS-CoV-2 RNA. RT-RPA using each primer pair was performed with
SARS-CoV-2 RNA at two different concentrations as a template. Cas13a-based detection with lateral-
flow readout was then used to assess successful amplification. Experiments with R1 reverse primers
(Qian et al.) and R2 reverse primers (bottom) were performed using different SARS-CoV-2 RNA
dilutions, but with an identical control primer pair (F1, R1) included in both sets of experiments, allowing
us to compare relative performance of all primer pairs. Based on this screening, we selected the (F4, R1)
primer pair for subsequent *n* gene amplifications. **D**) Multiplexed RPA reactions with pairwise
combinations of RPA primers (4 different primer pairs; 6 pairwise combinations). A multiplexed RPA
is individually assessed with a LwaCas13a-based detection reaction, each programmed with a specific
crRNA for the SARS-CoV-2 gene, and lateral-flow readout. Successful amplification was marked by
production of a strong-colored band at a test band (T), which indicates target-activated Cas13a activity
and resulting in efficient cleavage of the FAM-biotin reporter.
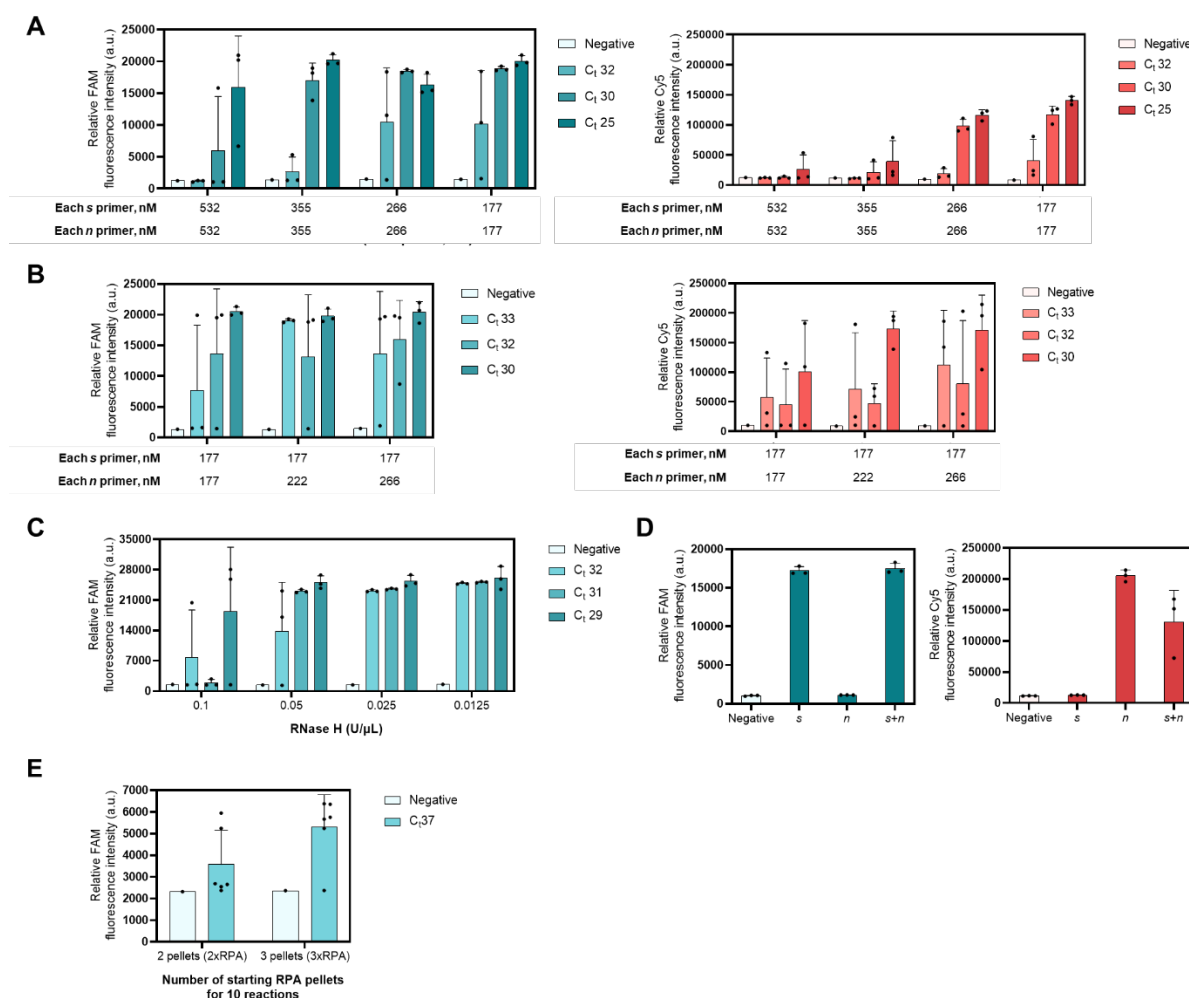
Figure 1–figure supplement 2: Evaluation of the sensitivity and specificity of the Multiplexed RT-RPA assay with real-time fluorescence detection.

(**A**) Optimizing total primer concentrations in multiplexed RPA with 1:1 malar ratio of *n* to *s* primer. Multiplexed RPA for the *s* and *n* gene of SARS-CoV-2 was performed using indicated primer concentrations and serially diluted SARS-CoV-2 genomic RNA template. In the second step, generated *s* and *n* amplicons were detected using a multiplexed CRISPR-Cas reaction containing LwaCas13a and PsmCas13b enzymes. LwaCas13a is programmed with a crRNA targeting the *s* amplicon and cleaves a FAM/IABkFQ -functionalized polyU reporter once target-activated (left), while PsmCas13b is programmed with a crRNA targeting the *n* amplicon and cleaves a Cy5/IABkRQ-functionalized polyA reporter (right). (**B**) Fine-tuning primer concentrations in the multiplexed RPA reaction. Multiplexed RPA for the *s* and *n* gene of SARS-CoV-2 was performed using indicated primer concentrations, with serially diluted SARS-CoV-2 genomic RNA as a template. Amplicons were detected in a multiplexed CRISPR-Cas reaction, via FAM fluorescence generated from *s*-targeted LwaCas13a (left) and Cy5 fluorescence from N-targeted PsmCas13b (right). (**C**) Optimizing RNase H concentrations in the RT-RPA reaction. RT-RPA for *s* gene amplification from serially diluted SARS-CoV-2 RNA, followed by LwaCas13a-based detection, was used. (**D**) Orthogonality of LwaCas13a and PsmCas13b in a multiplexed CRISPR-Cas detection. RPA reactions were performed with only *s* primers (*s*), only

n primers (*n*), or combined *s* and *n* primers (*s+n*). Endpoint fluorescence intensities of the multiplexed detection reactions (90 min) containing all components for LwaCas13-based detection of the *s* gene and PsmCas13b-based detection of the *n* gene were shown. Generated FAM (left) and Cy5 (right) fluorescence indicated cleavage of the reporters by the *s*-targeted LwaCas13a and the *n*-targeted PsmCas13b, respectively. For C-F, negative controls have no SARS-CoV-2 RNA template input. Data are mean ± s.d. from 3 replicates. (**E**) Analytical sensitivity of increasing of RPA pellet. Multiplexed RT-RPA for the *s* and *n* gene of SARS-CoV-2 was performed using indicated number of RPA pellets, with diluted SARS-CoV-2 genomic RNA at C_t 37 as a template. Subsequently, the amplicons were detected via FAM fluorescence generated from LwaCas13a-based reaction programmed with *s*- and *n*-targeted crRNAs.
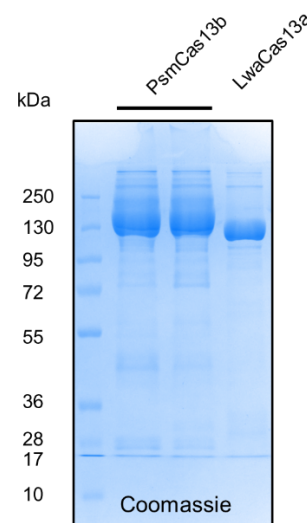
Figure 1–figure supplement 3: Protein purification of LwaCas13a and PsmCas13b.
12% SDS-PAGE gel of purified PsmCas13b and LwaCas13a. Each lane was loaded with 6 µg of protein. PsmCas13b was loaded twice.
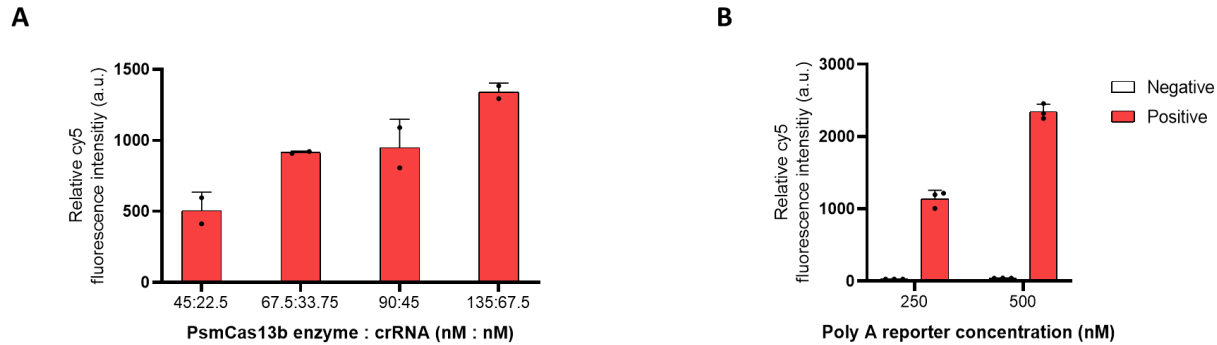
Figure 1–figure supplement 4: Optimizing PsmCas13b-based detection of the SARS-CoV-2 N gene.
(**A**) Varying PsmCas13b enzyme and crRNA amount in the detection reaction. The concentration of Cy5-functionalized polyA reporter was 250 nM in all conditions in (A). (**B**) Varying the amount of Cy5-polyA reporter in the detection reaction. 135 nM PsmCas13b and 67.5 nM crRNA were used for all conditions in (B). The *n* amplicon from the same RPA reaction was used as a substrate for all PsmCas13b-based detection reactions, which were performed for 90 min at 37 ºC, without any special additive in the RPA nor the CRISPR-Cas reactions. Endpoint fluorescence intensities were shown. Negative control reactions in (B) have no SARS-CoV-2 RNA template input. Error bars, ± s.d. from 2 replicates (A) and 3 replicates (B).

A

B

C

	C_t	25	28	31	34
FAM 13a		3/3	3/3	3/3	1/3
Cy5 13b		3/3	2/3	2/3	0/3
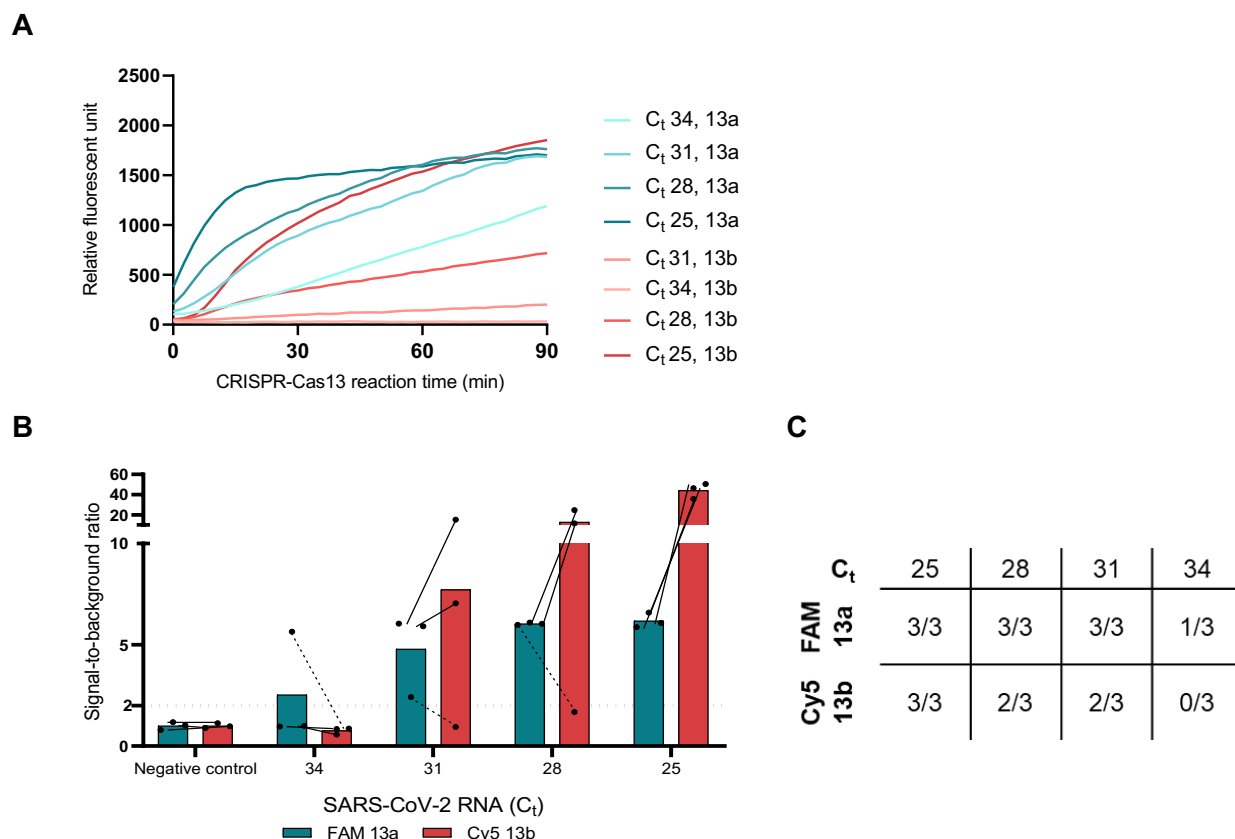
Figure 1–figure supplement 5: Comparison of LwaCas13a- and PsmCas13b-based detection. The *n* amplicons from the RPA reactions performed with serially diluted SARS-CoV-2 RNA were used as substrates for all Cas13-based detection reactions, which were performed for 90 min at 37 ºC. The concentrations of all other components in the CRISPR-Cas reactions were identical, and no special additive was added to the RPA nor the CRISPR-Cas reactions. (**A**) Kinetics of fluorescence signal generation from PsmCas13b-mediated detection is slower than that of LwaCas13a. (**B**) When we calculated signal-to-noise (S/N, with noise defined as fluorescence intensity obtained from a no input sample performed in parallel), PsmCas13b generates higher signal-to-noise than LwaCas13a, primarily due to lower background fluorescence in the negative control sample for PsmCas13b. However, LwaCas13a-mediated detection still has higher positive rates (**B, C**) than PsmCas13b. Error bars, ± s.d. from 3 replicates.
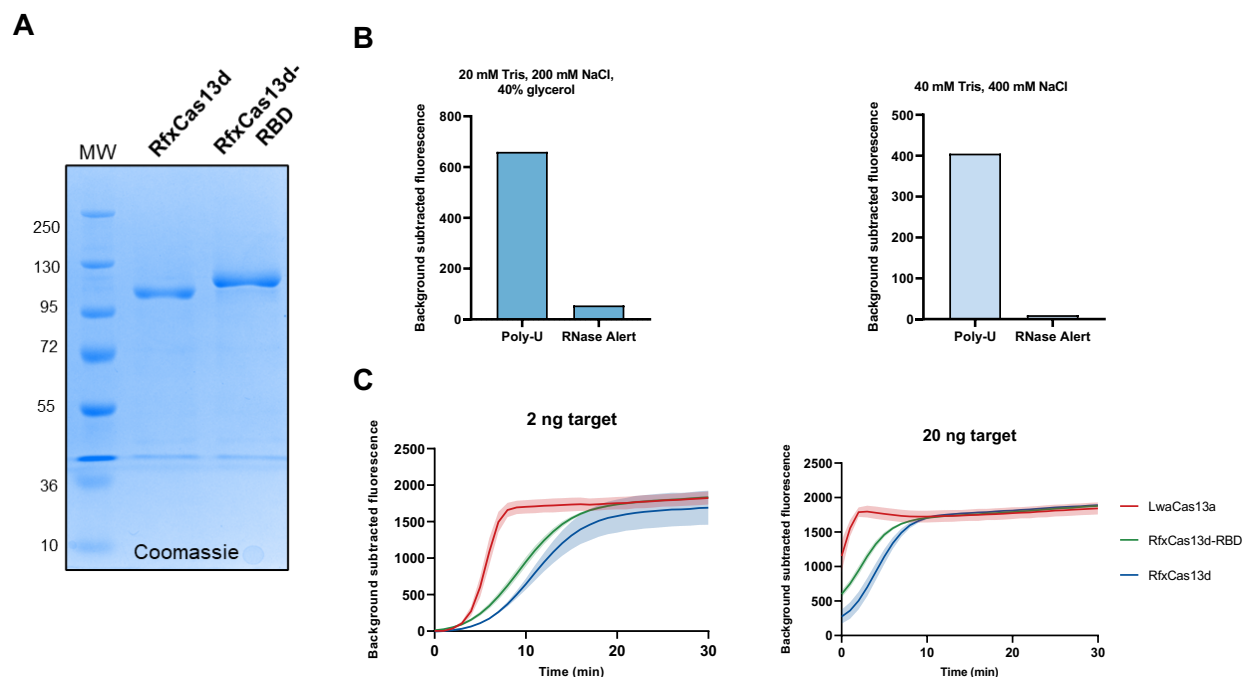
Figure 1–figure supplement 6: RfxCas13d-based detection of SARS-CoV-2 RNA.
(**A**) SDS-PAGE gel of purified RfxCas13d (112 kDa) and RfxCas13d-RBD (120 kDa). Each lane was loaded with 2 ng of protein. (**B**) RfxCas13d exhibited collateral cleavage preference in degrading a polyU reporter over RNaseAlert®. An *n* gene amplicon of SARS-CoV-2 was used as a substrate in a Cas13d-mediated detection. Two reaction conditions as well as two potential collateral reporters of RfxCas13d were tested. Fluorescence signal generated after 60 min of the CRISPR-Cas reaction for each condition (performed once) is shown. (**C**) Comparison of LwaCas13a, RfxCas13d, and RfxCas13d-RBD in SHERLOCK detection of the SARS-CoV-2 *n* gene. RfxCas13d-RBD has improved collateral cleavage efficiency over RfxCas13d, but still does not match LwaCas13a. Fluorescence signal generated over time using the FAM-polyU reporter is shown, at 2 ng (left) and 20 ng (right) RNA input amount. Error bands in (C) ± s.d. from 3 replicates.
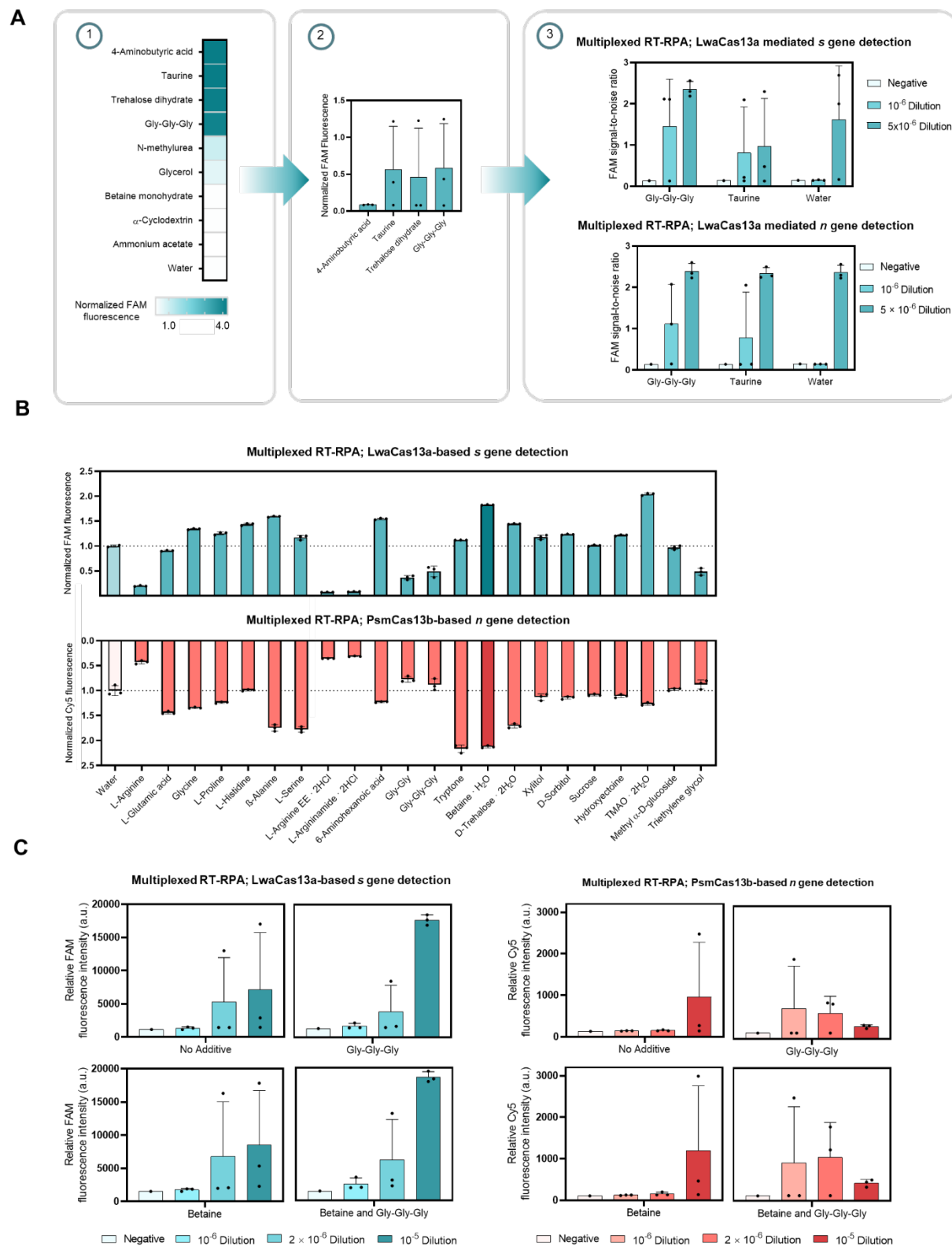
Figure 1–figure supplement 7: Screening of additives to enhance multiplexed RPA and CRISPR-Cas reactions.

(**A**) Screening for additives that enhance multiplexed RT-RPA. Left: nine additives were assessed in a conventional two-step (RPA, then LwaCas13a-based CRISPR-Cas) SHERLOCK detection for the *s* gene of SARS-CoV-2. Middle: four active additives were evaluated further in triplicates, using less RNA input. Right: two best-performing additives—triglycine and taurine—were finally assessed in a multiplexed RPA reaction for the *s* and *n* gene of SARS-CoV-2. Two serial dilutions of SARS-CoV-2 RNA were used as a template; negative control has no SARS-CoV-2 RNA template input. Generated *s* and *n* amplicons were detected in separate LwaCas13a-based detection reactions, whose FAM fluorescence signal is shown. (**B**) Screening for additives that improve the multiplexed CRISPR reaction. Twenty-two additives were assessed in the multiplexed CRISPR-Cas detection, using an RPA product from a multiplexed. Endpoint FAM (Qian et al.) and Cy5 (bottom) fluorescence intensities were normalized against intensities obtained from the no-additive controls. Data are mean ± s.d. from 3 replicates. L-Arginine EE. 2HCl, L-Arginine ethyl ester dihydrochloride. TMAO, trimethylamine N-oxide. (**C**) Cumulative benefits of triglycine additive in the multiplexed RPA and betaine monohydrate additive in the multiplexed CRISPR-Cas reaction. Multiplexed RPA to amplify the *s* and *n* genes of SARS-CoV-2 was performed in the presence or absence of 40 mM triglycine, using serially diluted SARS-CoV-2 RNA as a template, and multiplexed RPA was allowed to proceed for 25 min at 42 ºC. Multiplexed CRISPR-Cas reactions to detect the *s* and *n* amplicons were then performed in the presence or absence of 500 mM betaine. FAM and Cy5 fluorescence signal (indicative of Cas13a-mediated *s* gene and Cas13b-mediated *n* gene detection respectively) is shown. RNase-free water was used as input of all negative control reactions. Data are mean ± s.d. from 3 replicates.
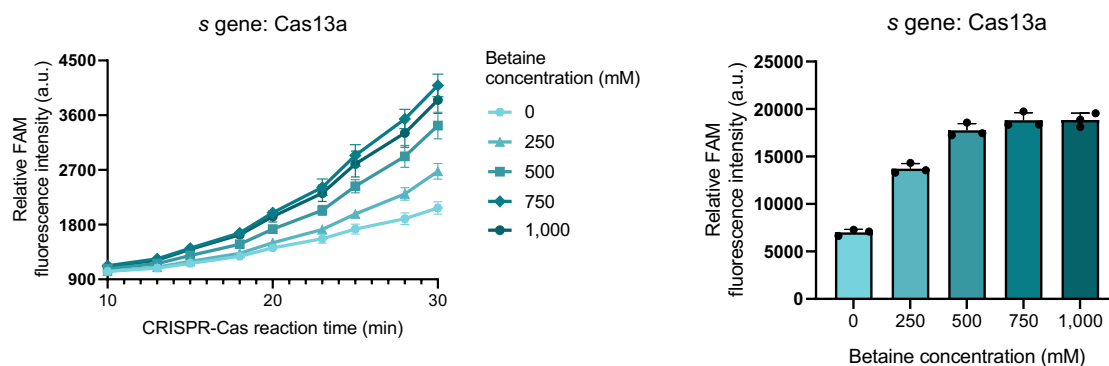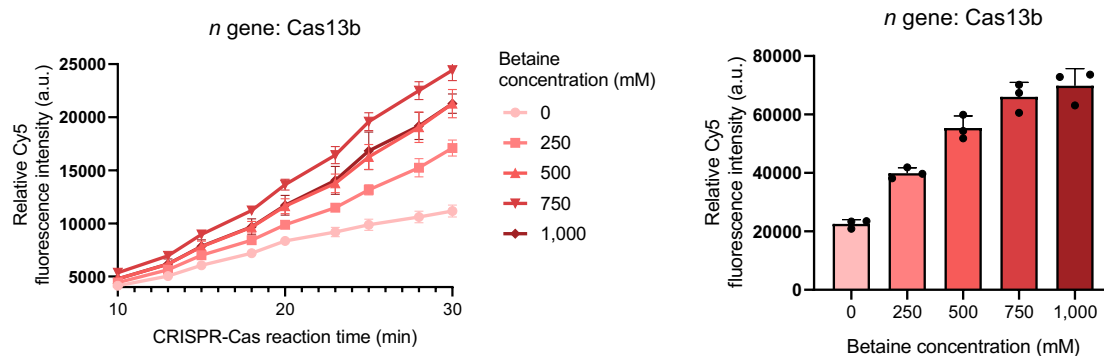
Figure 1–figure supplement 8: Optimizing betaine monohydrate concentration in multiplexed CRISPR-Cas detection.
FAM fluorescence indicated cleavage of the FAM reporter by the *s*-targeted LwaCas13a, while Cy5 fluorescence was from cleavage of the Cy5 reporter by the *n*-targeted PsmCas13b. FAM (**A**) and Cy5 (**B**) fluorescence signal generated after 30 min of the multiplexed CRISPR-Cas reaction for each condition are shown. The target was a diluted RPA product at 1:300 dilution. Error bars, ± s.d. from 3 replicates.
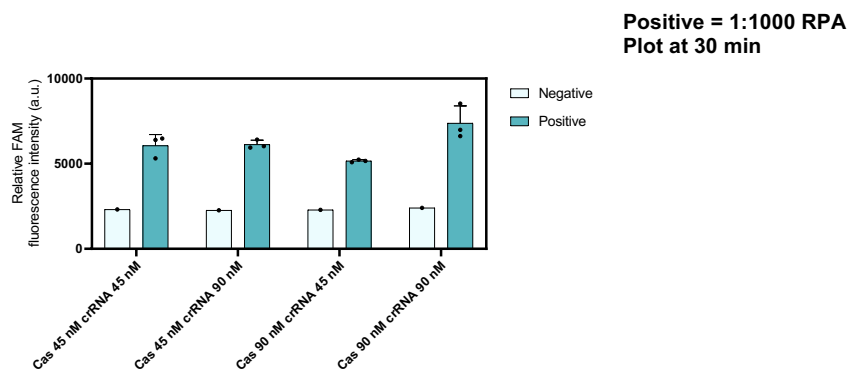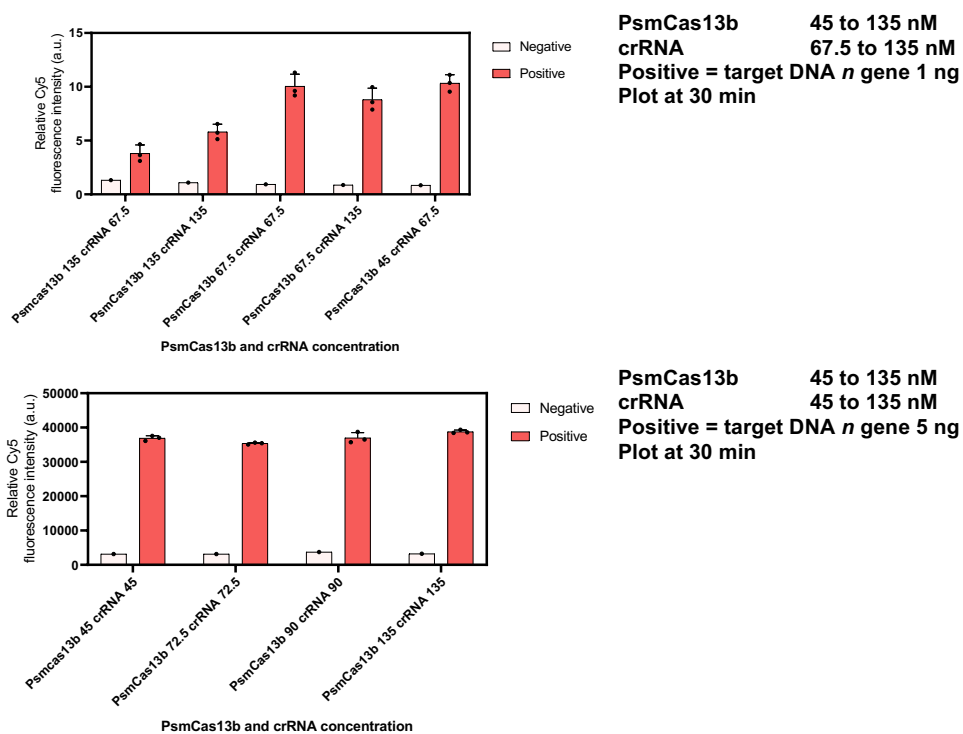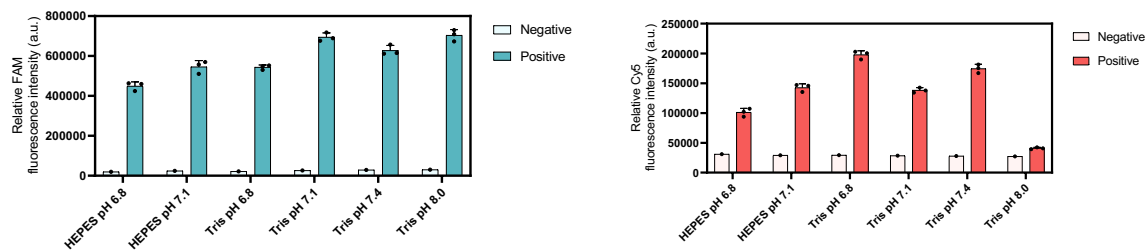
A

Positive = 1:1000 RPA
Plot at 30 min

B

PsmCas13b   45 to 135 nM
crRNA   67.5 to 135 nM
Positive = target DNA *n* gene 1 ng
Plot at 30 min

PsmCas13b   45 to 135 nM
crRNA   45 to 135 nM
Positive = target DNA *n* gene 5 ng
Plot at 30 min

C

Figure 1–figure supplement 9: Effect of crRNA ratio and pH in multiplexed CRISPR-Cas 13 based detection

(**A**) LwaCas13a-based detection of a diluted RPA product at different concentration of LwaCas13a (45 – 90 nM) and LwaCas13a-crRNA (45 – 90 nM) for the *s* gene.

(**B**) PsmCas13b-based detection of purified N amplicon at different concentration of PsmCas13b (45 – 135 nM) and PsmCas13b-crRNA (45 – 135 nM) for the *n* gene.

(**C**) Identifying optimal buffer conditions for LwaCas13a and PsmCas13b. The multiplexed CRISPR-based detection reaction prepared in Tris-HCl or HEPES buffer (pH 6.8 – 8.0) were performed using a diluted multiplexed RPA product as input. Error bars, ± s.d. from 3 replicates.

No cryoprotectant

5% PEG20000

6% Trehalose

5% PEG20000 + 6% Trehalose

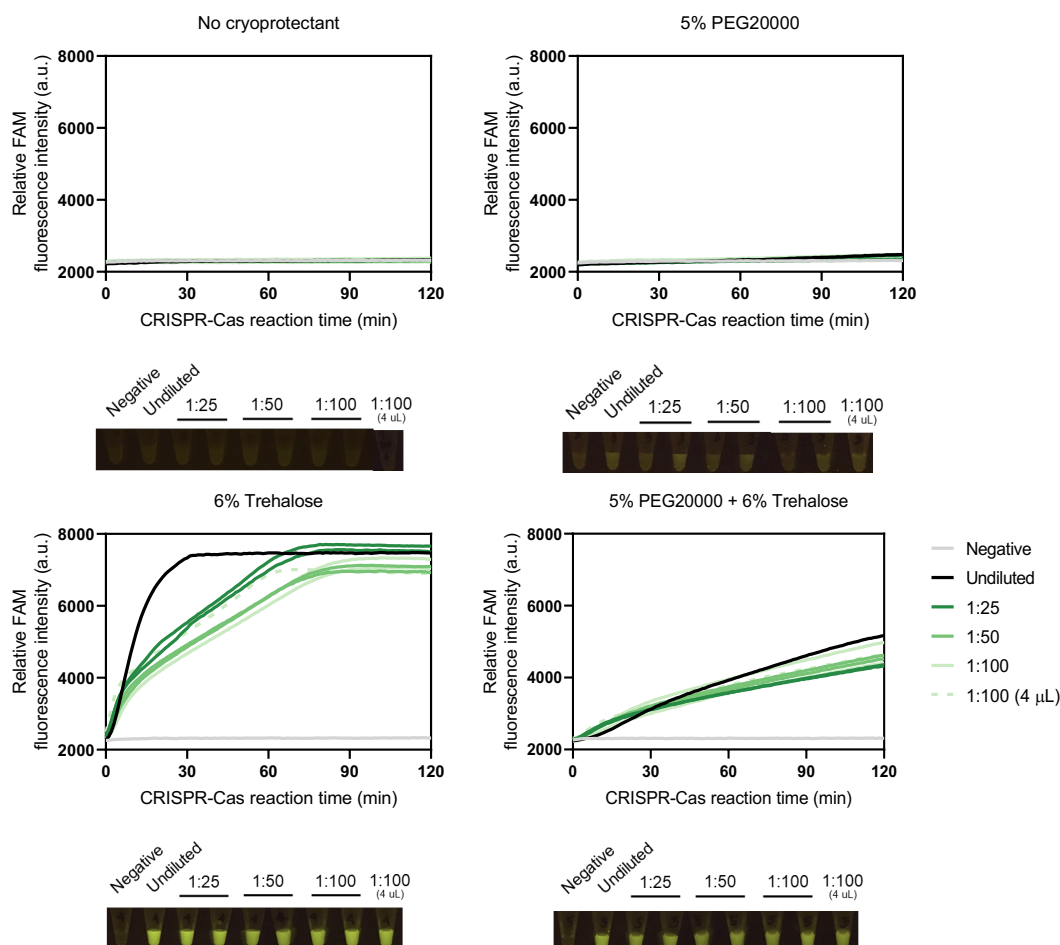Negative
Undiluted
1:25
1:50
1:100
1:100 (4 μL)

Figure 1–figure supplement 10: Effects of cryoprotectants on lyophilized CRISPR-Cas13a reactions.

LwaCas13a-based detection reactions were prepared with or without 5% (w/v) PEG20000 and 6% (w/v) trehalose added as a cryoprotectant. $MgCl_2$ was omitted from all reactions and was added at the rehydration step. The detection was performed at 37 °C using *n* gene RPA product at various dilution levels and monitored under FAM channel using a real-time thermal cycler. The input volume of the RPA dilutions was 2 μL except for the 1:100 dilution sample in which we used either 2-μL or 4-μL input volume. The end-point fluorescence in tubes was visualized using a BluPAD transilluminator.
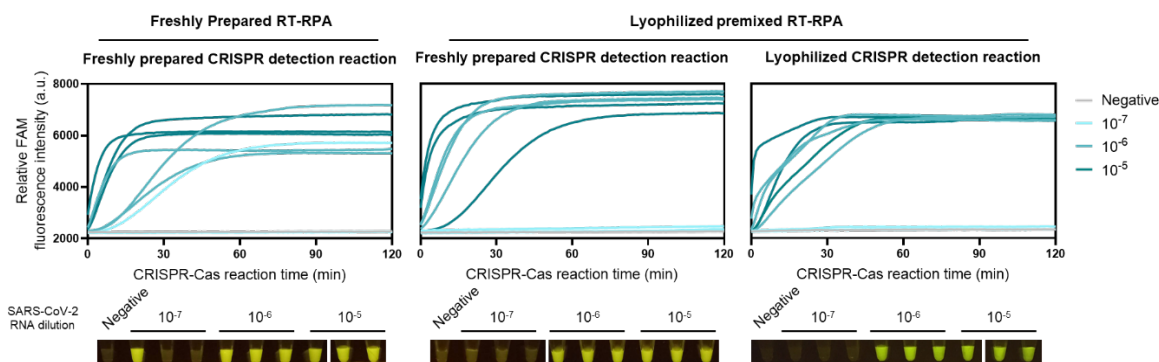
Figure 1–figure supplement 11: lyophilized RT-RPA for multiplexed amplification of the S and N genes

Left vs middle graphs: all-in-one lyophilized RT-RPA for multiplexed amplification of the *s* and *n* genes has similar sensitivity as freshly prepared RT-RPA. Non-volatile salt KOAc (the high concentration of which likely destabilizes protein components of RT-RPA upon lyophilization) and the typical reaction initiator $Mg(OAc)_2$ were excluded, while all other components required for multiplexed RT-RPA including all protein components for RPA, reverse transcriptase, RNase H, primer pairs, and other substrates and buffering/crowding compounds can be lyophilized together. The lyophilized RT-RPA pellets were reconstituted with 12.7 µl of serially diluted SARS-CoV-2 RNA, $Mg(OAc)_2$, and KOAc, and incubated at 42°C for 25 min. Thereafter, the multiplexed RPA products were used in a freshly prepared Cas13a-based detection with *s*- and *n*-targeted crRNAs. FAM fluorescence generated over 120 min for each condition is shown. Middle vs right graphs: lyophilized LwaCas13a-based detection reaction has similar sensitivity as freshly prepared reactions.
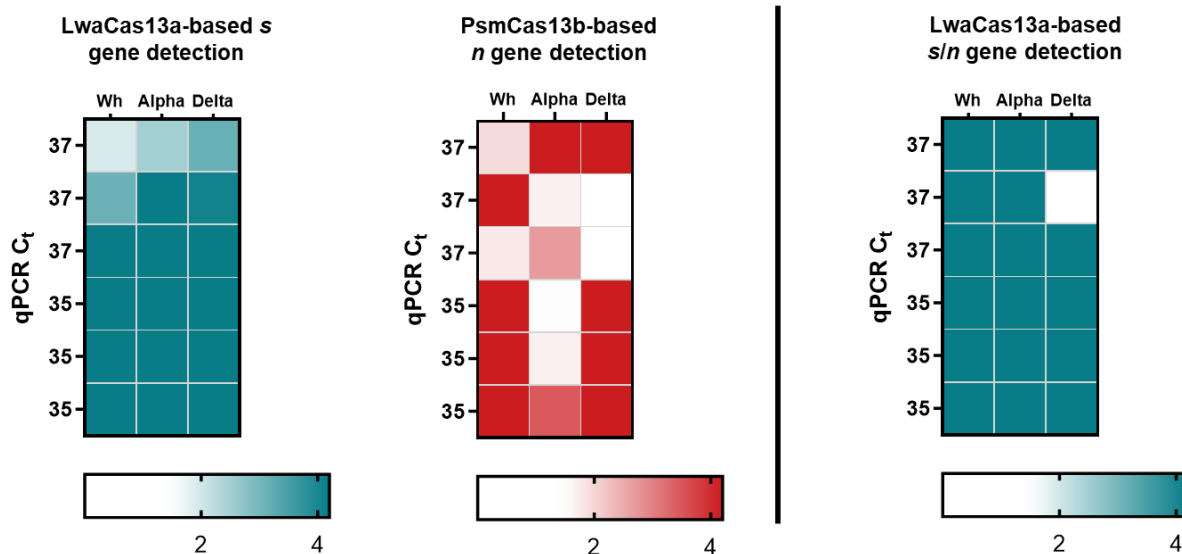
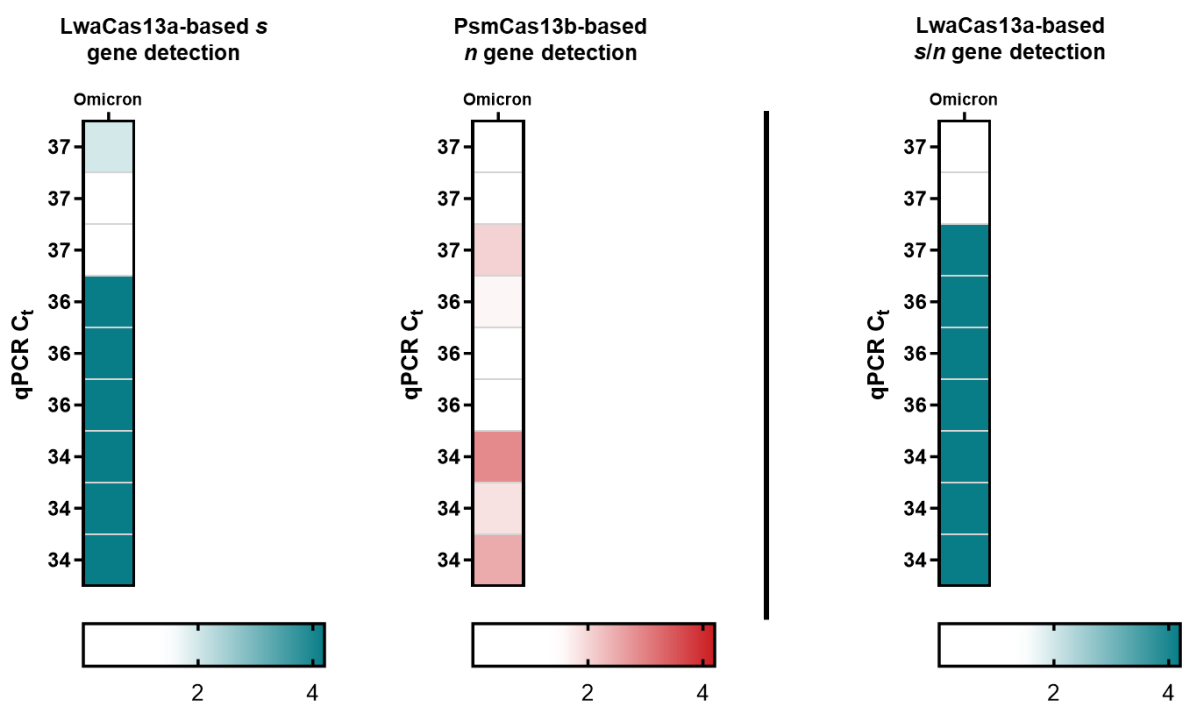**Figure 2–figure supplement 1: The lyophilized multiplexed CRISPR-based detection is robust across major SARS-CoV-2 variants.** Performance of the multiplexed CRISPR-based detection for **(A)** ancestral Wuhan strain, Alpha variant, Delta variant, and **(B)** Omicron variant.

FAM and Cy5 fluorescence intensities at 60 minutes were normalized against averaged intensities obtained from the no template control.
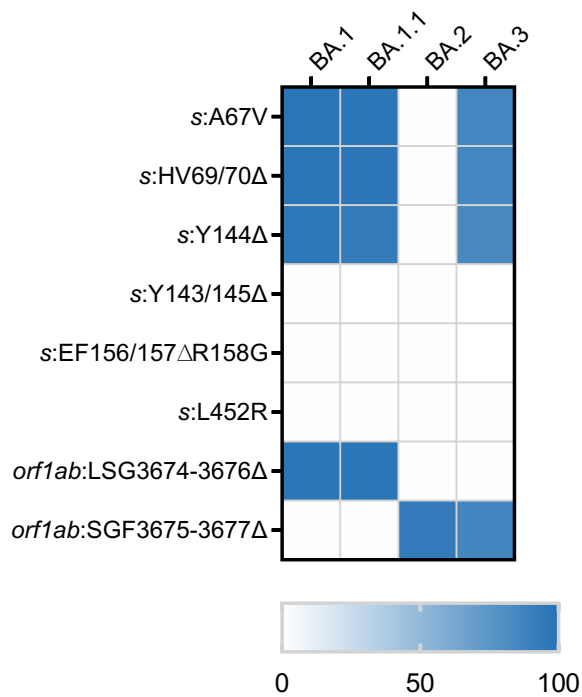

Figure 3–figure supplement 1: Mutation prevalence across Omicron sub-lineages
Percentages of mutations prevalence across four SARS-CoV-2 Omicron sub-lineages (BA.1, BA.1.1, BA.2, and BA.3) were obtained from Outbreak.info as of 15 March 2022; BA.1 (n = 1,005,355), BA.1.1 (n = 827,907), BA.2 (n = 316,708), and BA.3 (n = 694))

			crRNA		%F
SGF3675-3677Δ	3'	**tatgatcaaac---------ttcgattttctgacaca**		5'	–
Wuhan	5'	atactagtttg`tctggttttt`aagctaaaagactgtgt		3'	–
<u>Alpha</u>	5'	<u>atactagtttg---------aagctaaaagactgtgt</u>		3'	<u>94.0</u>
<u>Beta</u>	5'	<u>atactagtttg---------aagctaaaagactgtgt</u>		3'	<u>96.2</u>
<u>Gamma</u>	5'	<u>atactagtttg---------aagctaaaagactgtgt</u>		3'	<u>93.1</u>
Delta	5'	atactagtttg`tctggttttt`aagctaaaagactgtgt		3'	99.0
Omicron	5'	<u>atactagttt`t`---------aagctaaaagactgtgt</u>		3'	85.4
HV69/70Δ	3'	**aaccaaggtacgat------agagaccctggtta**		5'	–
Wuhan	5'	ttggttccatgcta`tacatg`tctctgggaccaat		3'	–
<u>Alpha</u>	5'	<u>ttggttccatgcta------tctctgggaccaat</u>		3'	<u>88.1</u>
Beta	5'	ttggttccatgcta`tacatg`tctctgggaccaat		3'	92.3
Gamma	5'	ttggttccatgcta`tacatg`tctctgggaccaat		3'	96.6
Delta	5'	ttggttccatgcta`tacatg`tctctgggaccaat		3'	96.9
<u>Omicron</u>	5'	<u>ttggttccatg`t`ta------tctctgggaccaat</u>		3'	84.5*
*%F for sublineage; BA.1 (95) and BA.2 (0)					
Y144Δ	3'	**aaaacccacaaa---tggtgtttttgttgtt**		5'	–
Wuhan	5'	ttttgggtgttt`att`accacaaaaacaacaa		3'	–
<u>Alpha</u>	5'	<u>ttttgggtgttt---accacaaaaacaacaa</u>		3'	<u>86.1</u>
Beta	5'	ttttgggtgttt`att`accacaaaaacaacaa		3'	100
Gamma	5'	ttttgggtgttt`att`accacaaaaacaacaa		3'	100
Delta	5'	ttttgg`a`tgtttattaccacaaaaacaacaa		3'	62.8
Omicron	5'	ttttgg---------accacaaaaacaacaa		3'	85.0
EF156/157ΔR158G	3'	**ttcaacctacctttcac------ctcaaataaga**		5'	–
Wuhan	5'	aagttggatggaaagtg`agttca`gagtttattct		3'	–
Alpha	5'	aagttggatggaaagtg`agttca`gagtttattct		3'	99.0
Beta	5'	aagttggatggaaagtg`agttca`gagtttattct		3'	100
Gamma	5'	aagttggatggaaagtg`agttca`gagtttattct		3'	100
<u>Delta</u>	5'	<u>aagttggatggaaagtg------gagtttattct</u>		3'	<u>98.8</u>
Omicron	5'	aagttggatggaaagtg`agttca`gagtttattct		3'	100
L452R	3'	**ttccaaccaccattaatattaatagcca**		5'	–
Wuhan	5'	aaggttggtggtaattataatta`c`c`t`gt		3'	–
Alpha	5'	aaggttggtggtaattataatta`c`c`t`gt		3'	98.0
Beta	5'	aaggttggtggtaattataatta`c`c`t`gt		3'	100
Gamma	5'	aaggttggtggtaattataatta`c`c`t`gt		3'	96.6
<u>Delta</u>	5'	<u>aaggttggtggtaattataatta`c`cggt</u>		3'	<u>96.8</u>
Omicron	5'	aaggtt`a`gtggtaattataatta`c`c`t`gt		3'	84.7

Figure 3–figure supplement 2: Multiple sequence alignments of the guide RNA spacer targeting a specific mutation representative of SARS-CoV-2 variant sequences. %F, frequency of the sequence among the variant genomes. The associated dataset was given in Figure 3–source data 2. *Black shading highlights the mismatches to the corresponding crRNA. The underlines highlight the anticipated targeted variants and targeted sequences of each design.*

	Forward Primer		%F	Reverse Primer		%F
SGF3675-3677Δ	5' **agttgggtgatgcgtattatgacatggttg** 3'		–	3' **catacgtagtcgacatcacaatgattagga** 5'		–
Wuhan	5' agttgggtgatgcgtattatgacatggttg 3'		–	5' gtatgcatcagctgtagtgttactaatcct 3'		–
<u>Alpha</u>	5' agttgggtgatgcgtattatgacatggttg 3'		100	5' gtatgcatcagctgtagtgttactaatcct 3'		99.0
Beta	5' agttgggtgatgcgtattatgacatggttg 3'		100	5' gtatgcatcagctgtagtgttactaatcct 3'		100
Gamma	5' agttgggtgatgcgtattatgacatggttg 3'		100	5' gtatgcatcagctgtagtgttactaatcct 3'		100
Delta	5' agttgggtgatgcgtattatgacatggttg 3'		100	5' gtatgcatcagctgt gtgttactaatcct 3'		90.0
Omicron	5' agttgggtgatgcgtattatgacatggttg 3'		100	5' gtatgcatcagctgtagtgttactaatcct 3'		99.8
HV69/70Δ	5' **attaccctgacaaagttttcagatcctcag** 3'		–	3' **ggacaggatggtaaattactaccacaaata** 5'		–
Wuhan	5' attaccctgacaaagttttcagatcctcag 3'		–	5' cctgtcctaccatttaatgatggtgtttat 3'		–
<u>Alpha</u>	5' attaccctgacaaagttttcagatcctcag 3'		100	5' cctgtcctaccatttaatgatggtgtttat 3'		99.0
Beta	5' attaccctgacaaagttttcagatcctcag 3'		100	5' cctgtcctaccatttaatgatggtgtttat 3'		100
Gamma	5' attaccctgacaaagttttcagatcctcag 3'		100	5' cctgtcctaccatttaatgatggtgtttat 3'		100
Delta	5' attaccctgacaaagttttcagatcctcag 3'		99.8	5' cctgtcctaccatttaatgatggtgtttat 3'		99.0
<u>Omicron</u>	5' attaccctgacaaagttttcagatcctcag 3'		99.8	5' cctgtcctaccatttaatgatggtgtttat 3'		99.8
Y144Δ	5' **acgctactaatgttgttattaaagtctgtg** 3'		–	3' **tcaaataagatcacgcttattaacgtgaaa** 5'		–
Wuhan	5' acgctactaatgttgttattaaagtctgtg 3'		–	5' agtttattctagtgcgaataattgcacttt 3'		–
<u>Alpha</u>	5' acgctactaatgttgttattaaagtctgtg 3'		99.0	5' agtttattctagtgcgaataattgcacttt 3'		100
Beta	5' acgctactaatgttgttattaaagtctgtg 3'		100	5' agtttattctagtgcgaataattgcacttt 3'		100
Gamma	5' acgctactaatgttgttattaaagtctgtg 3'		100	5' agtttattctagtgcgaataattgcacttt 3'		100
Delta	5' acgctactaatgttgttattaaagtctgtg 3'		99.4	5' agtttattctagtgcgaataattgcacttt 3'		99.6
Omicron	5' acgctactaatgttgttattaaagtctgtg 3'		100	5' agtttattctagtgcgaataattgcacttt 3'		99.8
EF156/157ΔR158G	5' **Same as Y144Δ** 3'		–	3' **attaacgtgaaaacttatacagagagtcgg** 5'		–
Wuhan	5' Same as Y144Δ 3'		x	5' taattgcacttttgaatatgtctctcagcc 3'		–
Alpha	5' Same as Y144Δ 3'		x	5' taattgcacttttgaatatgtctctcagcc 3'		100
Beta	5' Same as Y144Δ 3'		x	5' taattgcacttttgaatatgtctctcagcc 3'		100
Gamma	5' Same as Y144Δ 3'		x	5' taattgcacttttgaatatgtctctcagcc 3'		100
<u>Delta</u>	5' Same as Y144Δ 3'		x	5' taattgcacttttgaatatgtctctcagcc 3'		99.1
Omicron	5' Same as Y144Δ 3'		x	5' taattgcacttttgaatatgtctctcagcc 3'		100
L452R	5' **acaggctgcgttatagcttggaattctaac** 3'		–	3' **ccatatctaacaaatccttcagattagagt** 5'		–
Wuhan	5' acaggctgcgttatagcttggaattctaac 3'		–	5' gtatagattgtttaggaagtctaatctca 3'		–
Alpha	5' acaggctgcgttatagcttggaattctaac 3'		100	5' gtatagattgtttaggaagtctaatctca 3'		100
Beta	5' acaggctgcgttatagcttggaattctaac 3'		96.2	5' gtatagattgtttaggaagtctaatctca 3'		100
Gamma	5' acaggctgcgttatagcttggaattctaac 3'		100	5' gtatagattgtttaggaagtctaatctca 3'		100
<u>Delta</u>	5' acaggctgcgttatagcttggaattctaac 3'		99.8	5' ggtatagattgtttaggaagtctaatctca 3'		98.8
Omicron	5' acaggctgcgttatagcttggaattctaac 3'		99.5	5' gtatagattgtttaggaagtctaatctca 3'		99.8

Figure 3–figure supplement 3: Multiple sequence alignments of primer pairs targeting a specific mutation representative of SARS-CoV-2 variant sequences. %F, frequency of the sequence among the variant isolates. The associated dataset was given in Figure 3–source data 2. *Black shading highlights the mismatches to the corresponding crRNA. The underlines highlight the anticipated targeted variants and targeted sequences of each design.*
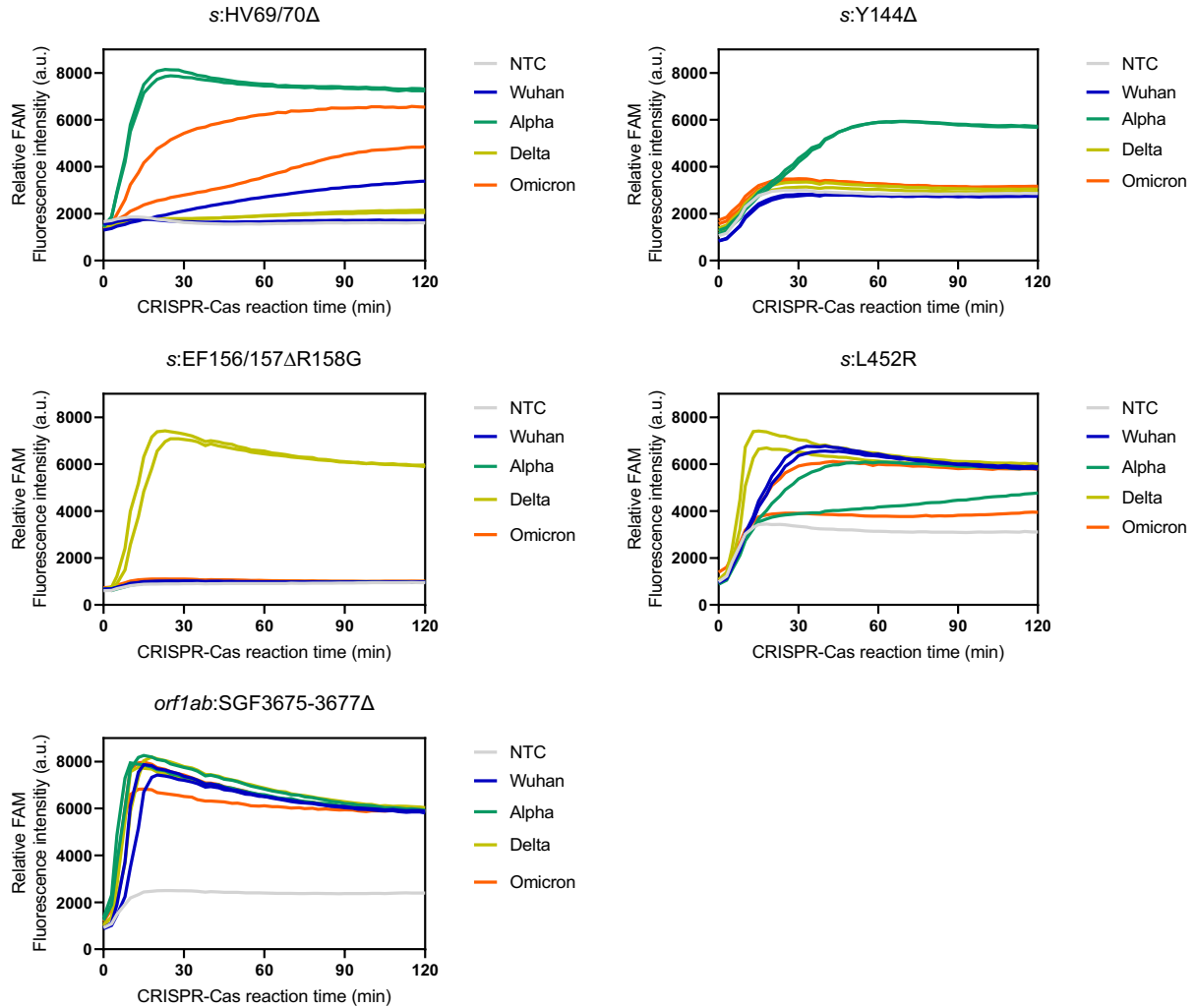
Figure 3–figure supplement 4: **Kinetic tracing of CRISPR-Cas13a detection reaction underlying Figure 3B**

Screening of primer sets and crRNA for cross-reactivity against the high viral RNA titers (C_t 28) of ancestral Wuhan, the alpha, and the delta strains, as well as the omicron strain. Kinetics of FAM fluorescence signal generation from the SARS-CoV-2 gene detection (as indicated) via a singleplexed CRISPR-Cas13a reaction, using cultured SARS-CoV-2 viral RNA extracts, except the omicron RNA extract from clinical sample, verified to be positive with different coronaviruses via RT-qPCR. Data are mean ± s.d. from 3 replicates. RNase-free water was used as input of all negative control reactions.
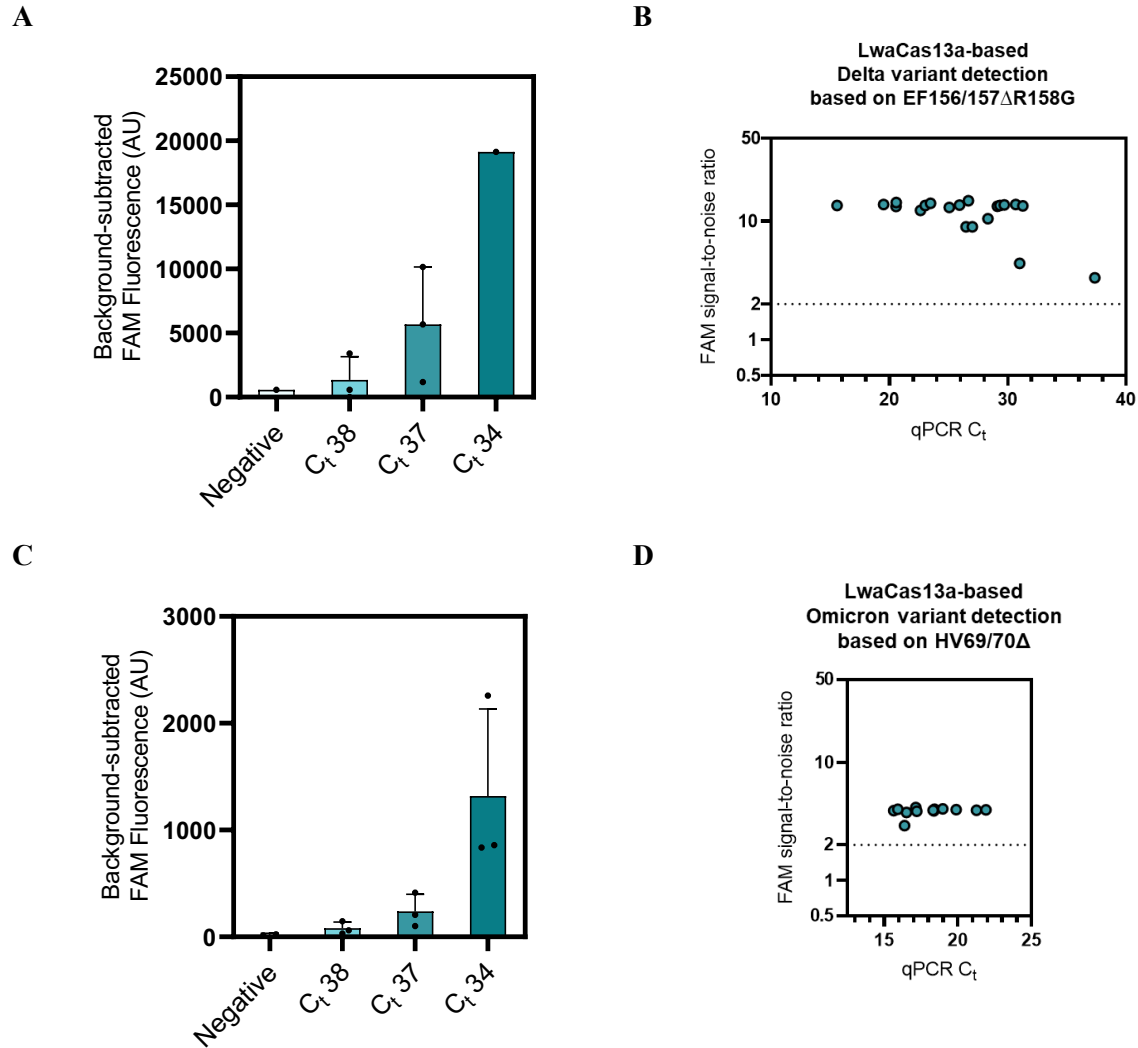
A

B

LwaCas13a-based
Delta variant detection
based on EF156/157ΔR158G

C

D

LwaCas13a-based
Omicron variant detection
based on HV69/70Δ

Figure 3–figure supplement 5: Singleplexed Detection of SARS-CoV-2 Delta and Omicron variants.
(A) LwaCas13a-based Delta variant detection based on EF156/157ΔR158G performed on a dilution series of a SARS-CoV-2 Delta RNA extract with determined C_t value. FAM fluorescence at 60 minutes were subtracted with background signal generated in negative control whose input is RNase-free water. Data are mean ± s.d. from 3 replicates. **(B)** LwaCas13a-based Delta variant detection based on EF156/157ΔR158G performed on Clinical Delta samples with determined C_t value. FAM fluorescence at 60 minutes were normalized against intensities obtained from the no template control. Data are mean ± s.d. from 3 replicates. **(C)** LwaCas13a-based Omicron variant detection based on HV69/70Δ performed on a dilution series of a SARS-CoV-2 Omicron RNA extract with determined C_t value. FAM fluorescence at 60 minutes were subtracted with background signal generated in negative control whose input is RNase-free water. Data are mean ± s.d. from 3 replicates. **(D)** LwaCas13a-based Omicron variant detection based on HV69/70Δ performed on Clinical Delta samples with determined C_t value. FAM fluorescence at 60 minutes were normalized against intensities obtained from the no template control. Data are mean ± s.d. from 3 replicates.
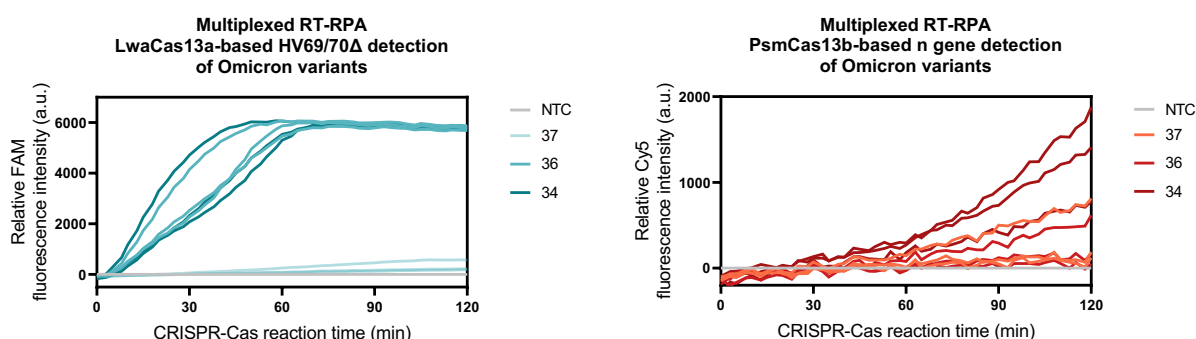
A

B
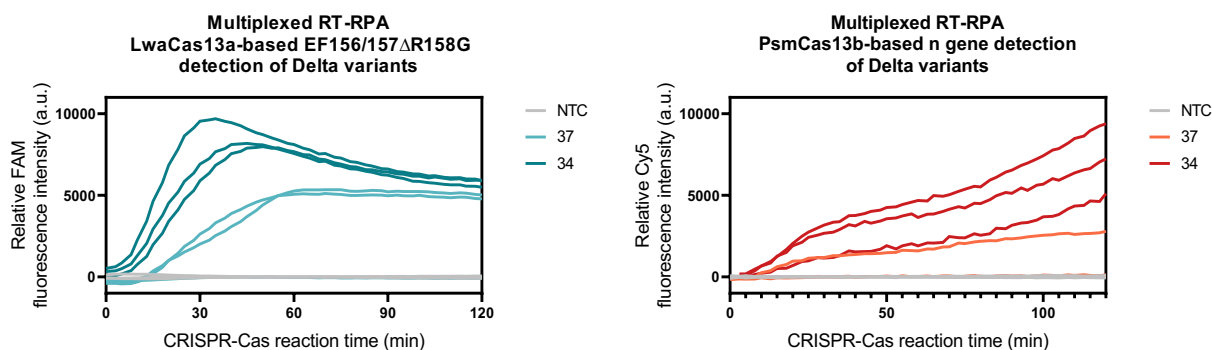
Figure 3–figure supplement 6: Kinetic traces of CRISPR-Cas13a/b detection reactions for Figure 3C and 3E.
(A) Multiplexed LwaCas13a-mediated EF156/157ΔR158G (s gene) and PsmCas13b-mediated pan-SARS-CoV-2 (n gene) detection **(B)** Multiplexed LwaCas13a-mediated HV69/70Δ (s gene) and PsmCas13b-mediated pan-SARS-CoV-2 (n gene) detection. Kinetics of FAM (left) and Cy5 (right) fluorescence signal generation via a multiplexed CRISPR-Cas13a/b reaction performed on a dilution series with determined C_t value of Delta RNA extracts from laboratory culture **(A)** or Omicron RNA extracts from clinical samples **(B)** were shown. RNase-free water was used as input of all no template control (NTC) reactions.
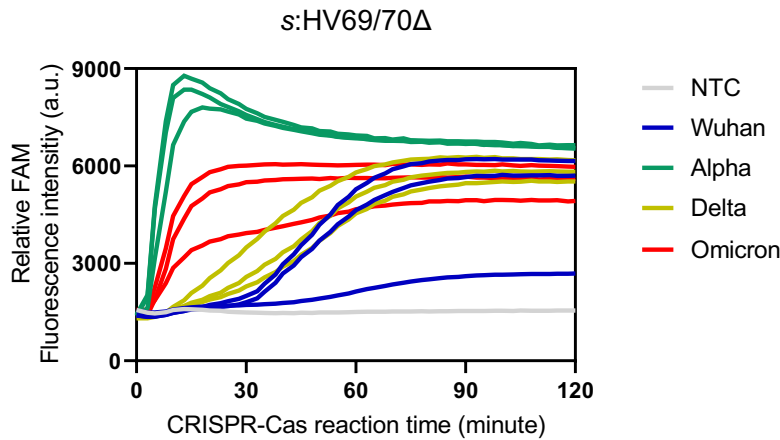
s:HV69/70Δ

Figure 3–figure supplement 7: Exclusivity (cross-reactivity) testing of primer and crRNA targeting HV69/70Δ detection against the high viral RNA titers (C_t 25) of ancestral Wuhan, the alpha, and the delta strains, as well as the omicron strain
Kinetics of FAM fluorescence signal generation from the SARS-CoV-2 s gene harboring HV69/70Δ mutation detection via a singleplexed CRISPR-Cas13a reaction, using cultured SARS-CoV-2 viral RNA extracts, except the omicron RNA extract from clinical sample, verified to be positive with different coronaviruses via RT-qPCR. Data are mean ± s.d. from 3 replicates. RNase-free water was used as input for negative control reactions.
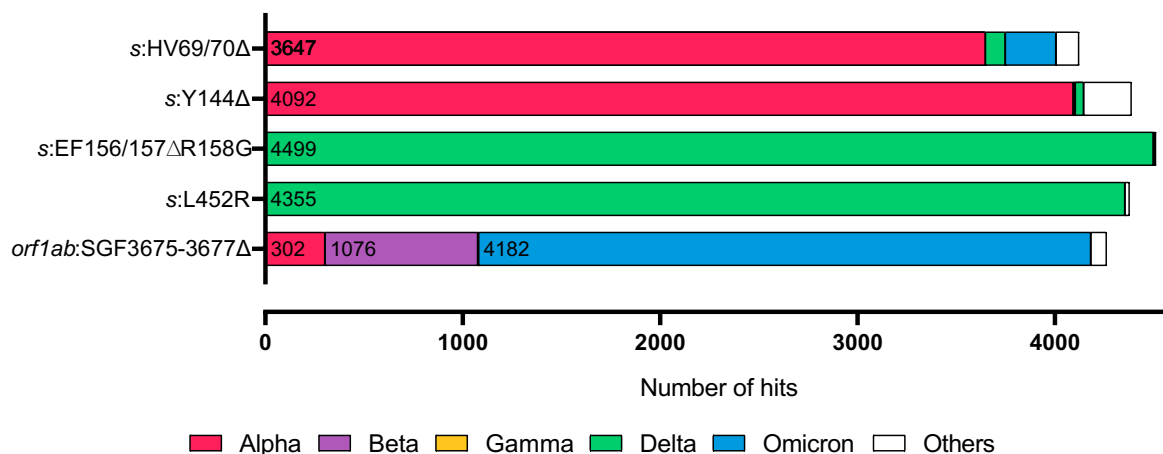
Figure 3–figure supplement 8: Exclusivity evaluation of designed crRNAs
Distribution of the SARS-COV-2 variant genome hits from BLAST search using crRNA spacer
complementary sequences as queries. The associated dataset was given in Figure 3–source data
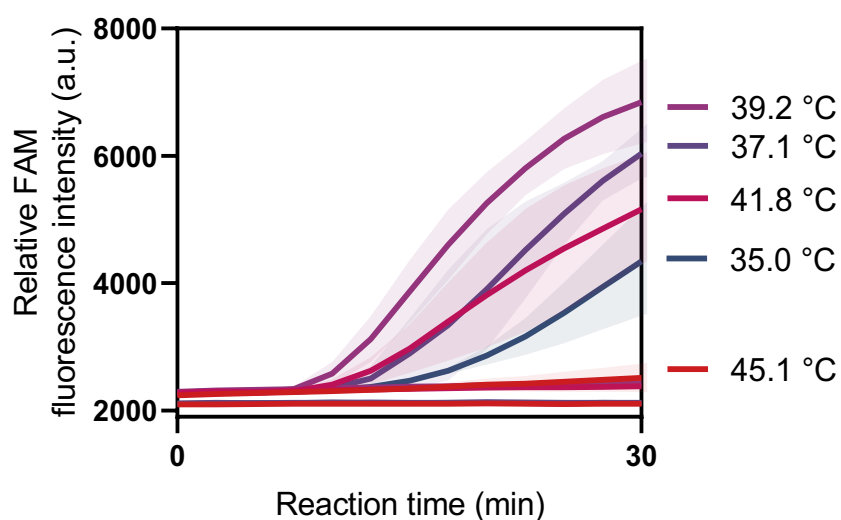1.

Figure 4–figure supplement 1: Effects of the reaction temperature on SHINE protocol.
A one-pot SHINE detection was performed using *s* gene primers and LwaCas13a-crRNA targeting *s* gene at varying temperature ranging from 35.0 - 45.1 °C. FAM fluorescence was monitored using a real-time PCR (CFX Connect Real-Time PCR System, Bio-Rad). Error bars, ± s.d. from 3 replicates.
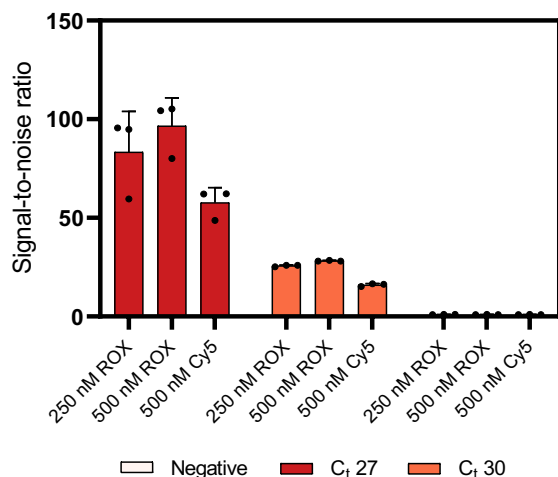
Figure 4–figure supplement 2: **Comparing ROX-based vs Cy5-based polyA reporter for PsmCas13b-based detection.**

PsmCas13b-based detection of RT-RPA products with serially diluted SARS-CoV-2 RNA as input was performed with either 250 nM Rhodamine X (ROX)-PolyA reporter, 500 nM ROX-PolyA, or 500 nM Cy5-PolyA reporter. Signal-to-noise ratios (defined as fluorescence intensities of the samples divided by those from negative input samples) generated after 22.5 min of the CRISPR-Cas reaction for each condition are shown. Error bars, ± s.d. from 3 replicates.
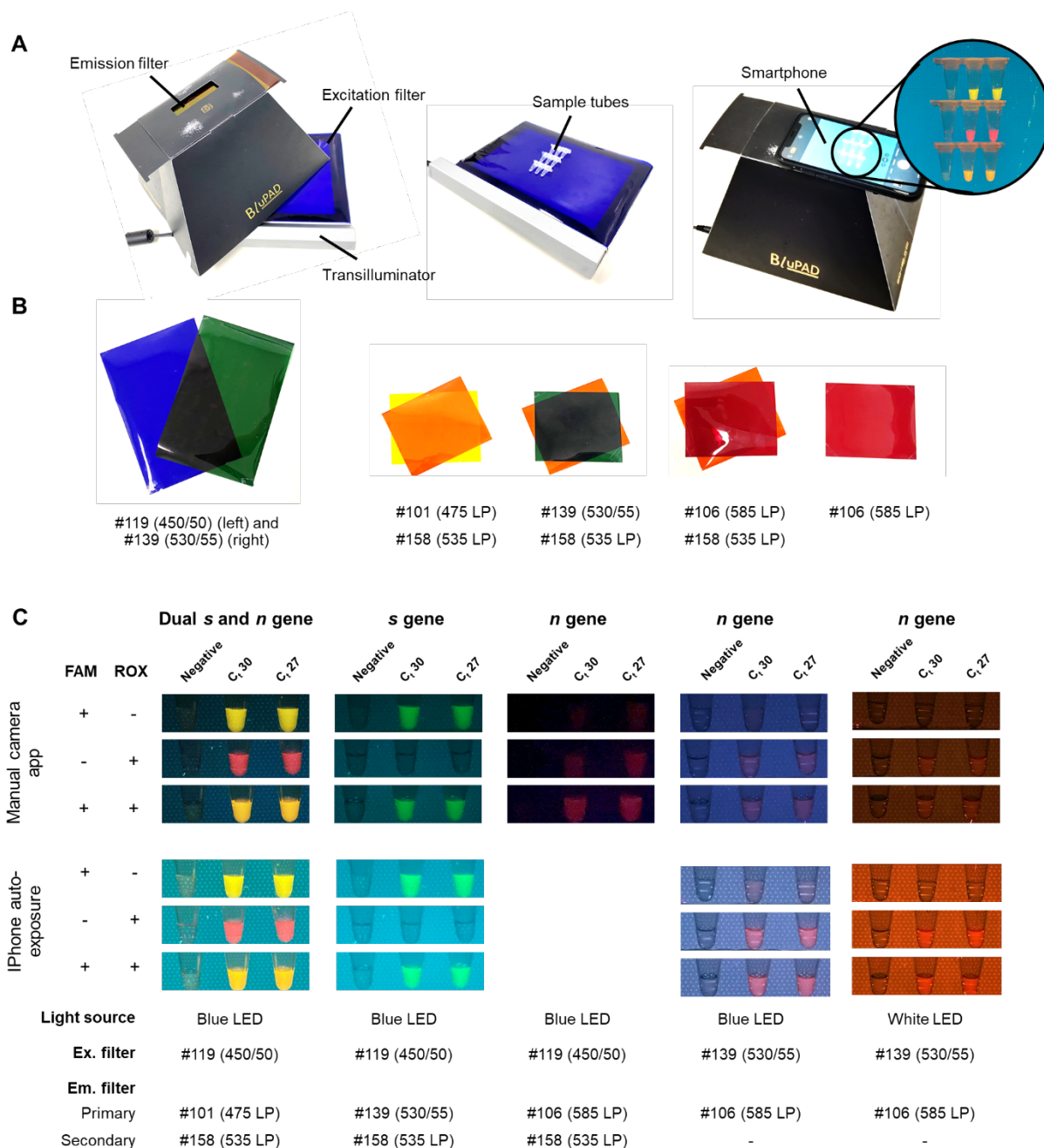
Figure 4–figure supplement 3: Direct-eye and smartphone-based visualization of multiplexed CRISPR-based detection.
(**A**) An example of equipment setup. We used a dual blue/white LED transilluminator. (**B**) Lighting gels with appropriate light filtering for visualization of FAM and ROX. (**C**) Images taken by manual camera application (Qian et al.) and auto-exposure (bottom) using different combinations of LED light source, excitation filters, emission filters, and phone-based image acquisition for visualization of FAM and ROX signals generated from multiplexed CRISPR-based detection reactions.

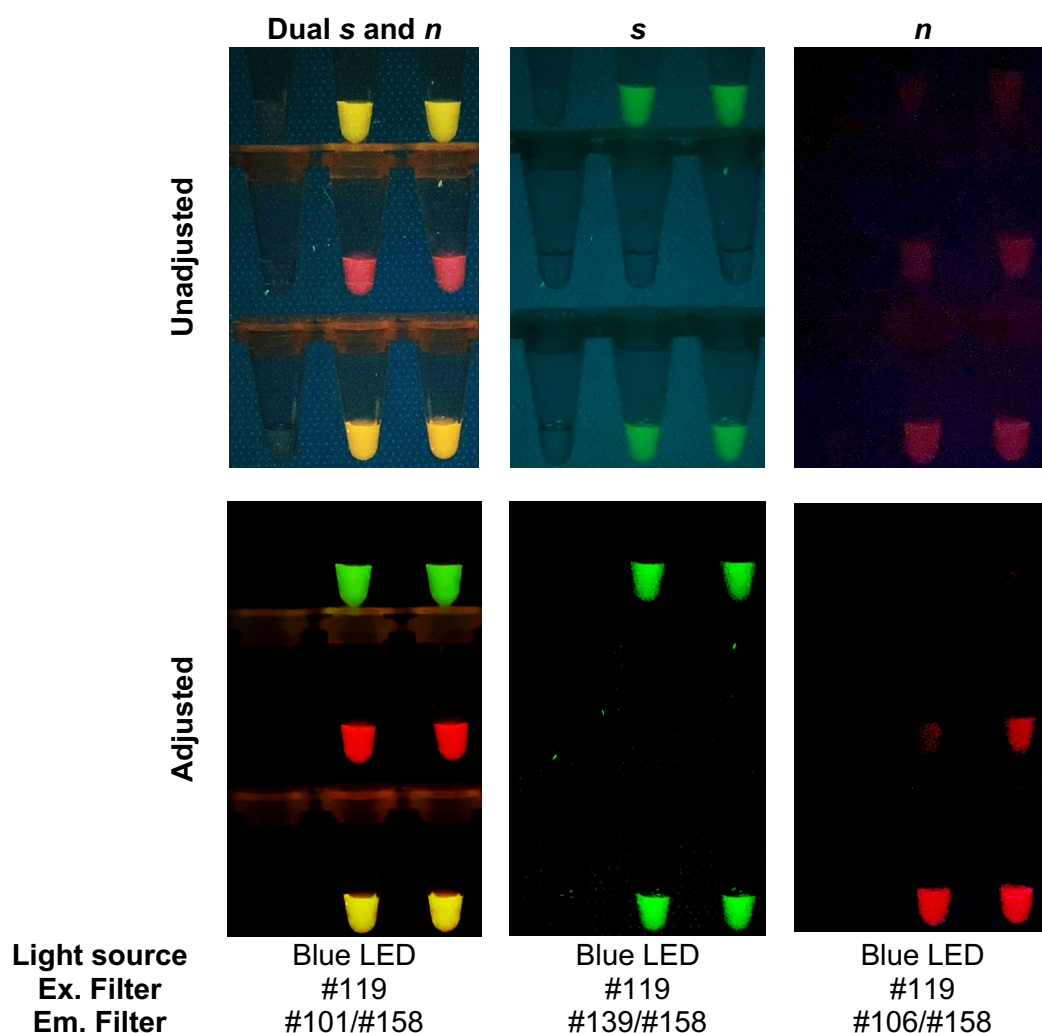| Light source | Blue LED | Blue LED | Blue LED |
| Ex. Filter | #119 | #119 | #119 |
| Em. Filter | #101/#158 | #139/#158 | #106/#158 |

Figure 4–figure supplement 4: Raw smartphone images vs processed images of FAM/ROX-labeled multiplexed detection samples.

The acquired images were processed using Curves adjustment menu and Channel mixers adjustment menu in Photoshop CC 2017 (Adobe Systems) to improve contrast and filter out blue color background, respectively.
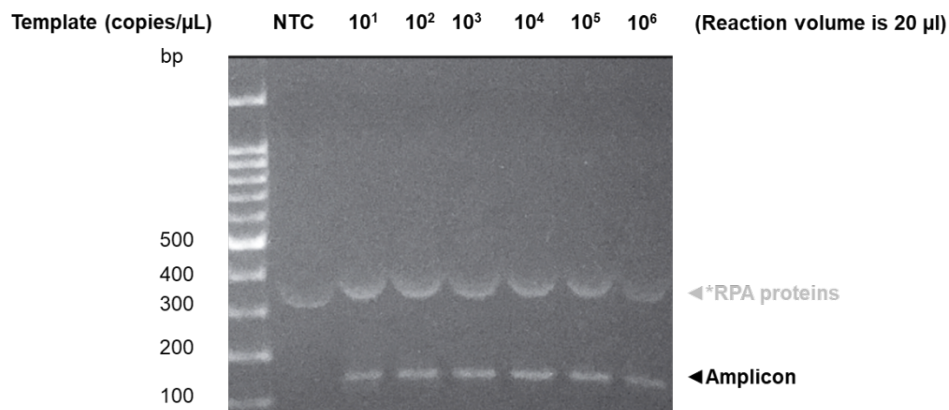
Figure 4–figure supplement 5: Activity of in-house RPA under standard reaction conditions.

RPA amplification reactions using in-house enzyme components were performed based on the standard reaction condition as described in the methods section. The copy number of the DNA template (T7 promoter linked to the SARS-CoV-2 *s* gene) used as input was varied as indicated. NTC is a negative control with RNase-free water as input. After incubation at 37°C for 60 min, RPA products were mixed with Novel Juice DNA staining reagent (BIO-HELIX), separated on 2% (w/v) agarose gel and visualized under blue light (BluPAD, BIO-HELIX). Positions of DNA template (T7 promoter-*s* gene, 137 bp) and amplicons were indicated with black arrowheads. The Novel Juice DNA stain also weakly stains proteins present in the reaction (white arrowheads).

Table S1. Nomenclature of the SARS-CoV-2 lineages referenced in this study

This study	WHO label	NextStrain clade	PANGO lineage
Alpha	Alpha	20I (Alpha, V1)	B.1.1.7
Beta	Beta	20H (Beta, V2)	B.1.351
Gamma	Gamma	20J (Gamma, V3)	P.1
Delta	Delta	21A (Delta) 21I (Delta) 20J (Delta)	B.1617.2
Omicron	Omicron	21K (Omicron) 21L (Omicron) 20M (Omicron)	BA.1 BA.1.1 BA.2 BA.3

Table S2. Oligonucleotides used in this study

Name	Sequence	Sources	Ref.
RT-RPA primer			
SL_s-RPA-Forward_v1	gaaattaatacgactcactatagggAGGTTTCAAACTTTACTTGCTTTACATAGA	IDT	Patchsung et al., 2020
SL_s-RPA-Reverse_v1	TCCTAGGTTGAAGATAACCCACATAATAAG	IDT	Patchsung et al., 2020
SL_orf1a-RPA-Forward_v1	gaaattaatacgactcactatagggCGAAGTTGTAGGAGACATTATACTTAAACC	IDT	Patchsung et al., 2020
SL_orf1a-RPA-Reverse_v1	TAGTAAGACTAGAATTGTCTACATAAGCAGC	IDT	Patchsung et al., 2020
SI_orf1b-RPA-Forward_v1	gaaattaatacgactcactatagggTGATGCCATGCGAAATGCTGGTATTGTTGG	IDT	Patchsung et al., 2020
SI_orf1b-RPA-Reverse_v1	CTGCAGTTAAAGCCCTGGTCAAGGTTAATA	IDT	Patchsung et al., 2020
SI_n-RPA-Forward_v1	gaaattaatacgactcactatagggCGGCAGTCAAGCCTCTTCTCGTTCCTCATC	IDT	Patchsung et al., 2020
SI_n-RPA-Reverse_v1	CAGACATTTTGCTCTCAAGCTGGTTCAATC	IDT	Patchsung et al., 2020
SI-n-RPA-Forward_v2	gaaattaatacgactcactatagggTTCTCGTTCCTCATCACGTAGTCGCAACAG	IDT	This study
SI-n-RPA-Forward_v3	gaaattaatacgactcactatagggAACAGTTCAAGAAATTCAACTCCAGGCAGC	IDT	This study
SI-n-RPA-Forward_v4	gaaattaatacgactcactatagggGAACTTCTCCTGCTAGAATGGCTG	IDT	This study
SI-n-RPA-Forward_v5	gaaattaatacgactcactatagggGAACTTCTCCTGCTAGAATGGCTGGCAATG	IDT	This study
SI-n-RPA-Forward_v6	gaaattaatacgactcactatagggCTAGAATGGCTGGCAATGGCGGTGATGCTG	IDT	This study
SGF3675-3677Del_F	gaaattaatacgactcactataggAGTTGGGTGATGCGTATTATGACATGGTTG	IDT	This study
SGF3675-3677Del_R	AGGATTAGTAACACTACAGCTGATGCATAC	IDT	This study
HV69-70Del_F	gaaattaatacgactcactataggATTACCCTGACAAAGTTTTCAGATCCTCAG	IDT	This study
HV69-70Del_R	ATAAACACCATCATTAAATGGTAGGACAGG	IDT	This study
Y144Del_F	gaaattaatacgactcactataggACGCTACTAATGTTGTTATTAAAGTCTGTG	IDT	This study
Y144Del_R	AAAGTGCAATTATTCGCACTAGAATAAACT	IDT	This study
EF156-157Del_R	GGCTGAGAGACATATTCAAAAGTGCAATTA	IDT	This study
L452R_F	gaaattaatacgactcactataggACAGGCTGCGTTATAGCTTGGAATTCTAAC	IDT	This study
L452R_R	TGAGATTAGACTTCCTAAACAATCTATACC	IDT	This study
crRNA			
13a_SL_s-crRNA_v1	gauuuagacuaccccaaaaacgaaggggacuaaaacGCAGCACCAGCUGUCCAACCUGAAGAAG	Synthego	Patchsung et al., 2020
13a_SL_orf1a-crRNA_v1	gauuuagacuaccccaaaaacgaaggggacuaaaacCCAACCUCUUCUGUAAUUUUUAAACUAU	Synthego	Patchsung et al., 2020

Name	Sequence	Sources	Ref.
13a_SI_orf1b-crRNA_v1	gauuuagacuaccccaaaaacgaaggggacuaaaacGGAACUCCACUACCUGGCGUGGUUUGUA	Synthego	Patchsung et al., 2020
13a_SI_n-crRNA_v1	gauuuagacuaccccaaaaacgaaggggacuaaaacAAAGCAAGAGCAGCAUCACCGCCAUUGC	Synthego	Patchsung et al., 2020
Psm13b_SI_n-crRNA-v1	aaagcaagagcagcaucaccgccauugccaGUUGUAGAAGCUUAUCGUUUGGAUAGGUAUGACAAC	Genscript	This study
crRNA template for IVT			
SGF3675-3677Del	ATACTAGTTTGAAGCTAAAAGACTGTGTgttttagtccccttcgtttttggggtagtctaaatcCCTATAGTGAGTCGTATTAATTTC	IDT	This study
HV69-70Del	TTGGTTCCATGCTATCTCTGGGACCAATgttttagtcccccttcgtttttggggtagtctaaatcCCTATAGTGAGTCGTATTAATTTC	IDT	This study
Y144Del	TTTTGGGTGTTTACCACAAAAACAACAAgttttagtcccccttcgtttttggggtagtctaaatcCCTATAGTGAGTCGTATTAATTTC	IDT	This study
EF156-157Del	AAGTTGGATGGAAAGTGGAGTTTATTCTgttttagtccccttcgtttttggggtagtctaaatcCCTATAGTGAGTCGTATTAATTTC	IDT	This study
L452R	AAGGTTGGTGGTAATTATAATTATCGGTgttttagtcccccttcgttttgggtagtctaaatcCCTATAGTGAGTCGTATTAATTTC	IDT	This study
Reporter		IDT	
Cas13a_reporter	/FAM/mArArUrGrGrCmAmArArUrGrGrCmA/Bio/	IDT	Patchsung et al., 2020
FAM PolyU reporter	/FAM/rUrUrUrUrUrC/IABkFQ/	IDT	Patchsung et al., 2020
Cy5 PolyA reporter	/Cy5/rArArArArA/IAbRQSp/	IDT	This study
ROX PolyA reporter	/ROX/rArArArArA/IAbRQSp/	IDT	This study

Table S3. Specific RT-RPA conditions for each figure. Aside from parameters shown in the table which were varied during optimizations, all other parameters are as given in the "Optimized multiplexed RT-RPA" methods section.

Figure #	Primer identity and concentrations	RNase H Concentrations	Additive	RNA input
Figure 2A	177 nM each *s* primer and 222 nM *n* primer	0.025 U/μL	40 mM Triglycine	5.3
Figure 2B-2E	177 nM each *s* primer and 222 nM n primer	0.025 U/μL	40 mM Triglycine	12.4
Figure 2F	177 nM each *s* primer and 222 nM *n* primer	0.025 U/μL	40 mM Triglycine	12.4
Figure 3A-3B	704 nM each primer for each variant	0.025 U/μL	40 mM Triglycine	12.4
Figure 3C	177 nM each *s*(EF156/157ΔR158G) primer and 177 nM *n* primer	0.025 U/μL	40 mM Triglycine	12.4
Figure 3D	177 nM each *s*(EF156/157ΔR158G) primer and 177 nM *n* primer	0.025 U/μL	40 mM Triglycine	12.4
Figure 3E	177 nM each HV69/70Δ primer and 177 nM *n* primer	0.025 U/μL	40 mM Triglycine	12.4
Figure 3F	177 nM each HV69/70Δ primer and 177 nM *n* primer	0.025 U/μL	40 mM Triglycine	12.4
Figure 4A	177 nM each *s* primer and 222 nM *n* primer	0.025 U/μL	40 mM Triglycine	5.3
Figure 1–figure supplement 1C	709 nM each *n* primer	-	-	6.3 μL
Figure 1–figure supplement 1D	355 nM each primer for each gene	-	-	6.3 μL
Figure 1–figure supplement 2A, 2B	varying concentration of *s* and N primer pair	0.025 U/μL	-	6.3 μL
Figure 1–figure supplement 2C	709 nM each *s* primer	Varying RNase H concentrations	-	6.3 μL

Figure #	Primer identity and concentrations	RNase H Concentrations	Additive	RNA input
Figure 1–figure supplement 2D	704 nM each *n* primer, 704 each *s* primer, and 177 nM each *s* priemr and 222 nM *n* primer for s, n and s+n respectively	0.025 U/μL	40 mM Triglycine	5.3 μL
Figure 1–figure supplement 2E	704 nM each *n* primer	0.025 U/μL	40 mM Triglycine	5.3 μL
Figure 1–figure supplement 4	709 nM each *n* primer	-	-	6.3 μL
Figure 1–figure supplement 5	709 nM each *n* primer	1 U/μL	-	6.3 μL
Figure 1–figure supplement 6	709 nM each *n* primer	-	-	6.3 μL
Figure 1–figure supplement 7A	177 nM each *s* and *n* primer	0.025 U/μL	Varying additives	3.2 μL
Figure 1–figure supplement 7B	177 nM each *s* and *n* primer	0.025 U/μL	-	6.3 μL
Figure 1–figure supplement 7C	177 nM each *s* and *n* primer	0.025 U/μL	With and without 40 mM Triglycine	3.2 μL
Figure 1–figure supplement 8	177 nM each *s* primer and 222 nM *n* primer	0.025 U/μL	40 mM Triglycine	5.3 μL
Figure 1–figure supplement 10	704 nM each *n* primer	0.025 U/μL	40 mM Triglycine	5.3 μL
Figure 1–figure supplement 11	177 nM each *s* primer and 222 nM *n* primer	0.025 U/μL	40 mM Triglycine	5.3 μL
Figure 2–figure supplement 1	177 nM each s primer and 222 nM *n* primer	0.025 U/μL	40 mM Triglycine	12.4 μL
Figure 3–figure supplement 4	704 nM each primer for each variant	0.025 U/μL	40 mM Triglycine	12.4 μL
Figure 3–figure supplement 5	704 nM each *s*(EF156/157ΔR158G) primer	0.025 U/μL	40 mM Triglycine	12.4 μL
Figure 3–figure supplement 6	177 nM each *s*(EF156/157ΔR158G or HV69/70Δ) primer and 177 nM *n* primer	0.025 U/μL	40 mM Triglycine	12.4 μL
Figure 3–figure supplement 7	704 nM each *s*(HV69/70Δ) primer	0.025 U/μL	40 mM Triglycine	12.4 μL

Table S4.Specific Cas13-based reaction conditions for each figure. Aside from parameters shown in the table which were varied during optimizations, all other parameters are as given in the "Optimized multiplexed Cas13-based detection with fluorescence readout" methods section.

Figure	Buffer identity and concentration	Cas enzyme identity and concentration	crRNA identity and concentration	RNA reporter identity and concentration	additive	MgCl$_2$ concentration	Equipment used to monitor Cas-based reactions
Figure 2 Multiplexed LwaCas13a-PsmCas13b detection	20 mM HEPES pH 6.8	45 nM LwaCas13a, 135 nM PsmCas13b,	22.5 nM LwaCas13a crRNA targeting *s* gene, 67.5 nM PsmCas13b crRNA targeting *n* gene	250 nM PolyU-FAM, 500 nM PolyA-ROX	750 mM betaine	24 mM	Tecan microplate reader
Figure 2 LwaCas13a Dual S/N detection	20 mM HEPES pH 6.8	45 nM LwaCas13a	22.5 nM LwaCas13a crRNA targeting *s* gene, 22.5 nM LwaCas13a crRNA targeting *n* gene	250 nM PolyU-FAM	750 mM betaine	24 mM	Tecan microplate reader
Figure 3A-3B	40 mM Tris pH 7.4	45 nM LwaCas13a	22.5 nM LwaCas13a crRNA targeting each variant	250 nM PolyU-FAM	-	6 mM	Tecan microplate reader
Figure 3C	40 mM Tris pH 7.4	45 nM LwaCas13a, 135 nM PsmCas13b,	22.5 nM LwaCas13a crRNA targeting each variant, 67.5 nM PsmCas13b crRNA targeting *n* gene	250 nM PolyU-FAM, 500 nM PolyA-ROX	750 mM betaine	24 mM	Tecan microplate reader
Figure 3D	40 mM Tris pH 7.4	45 nM LwaCas13a,	22.5 nM LwaCas13a crRNA targeting	250 nM PolyU-FAM,	750 mM betaine	24 mM	Tecan microplate reader

Figure	Buffer identity and concentration	Cas enzyme identity and concentration	crRNA identity and concentration	RNA reporter identity and concentration	additive	MgCl₂ concentration	Equipment used to monitor Cas-based reactions
		135 nM PsmCas13b	each variant, 67.5 nM PsmCas13b crRNA targeting n gene	500 nM PolyA-ROX			
Figure 3E	40 mM Tris pH 6.8	45 nM LwaCas13a, 135 nM PsmCas13b	22.5 nM LwaCas13a crRNA targeting HV69/70Δ, 67.5 nM PsmCas13b crRNA targeting n gene	250 nM PolyU-FAM, 500 nM PolyA-ROX	-	24 mM	Tecan microplate reader
Figure 3F	40 mM Tris pH 6.8	45 nM LwaCas13a, 135 nM PsmCas13b	22.5 nM LwaCas13a crRNA targeting HV69/70Δ, 67.5 nM PsmCas13b crRNA targeting n gene	250 nM PolyU-FAM, 500 nM PolyA-ROX	-	24 mM	Tecan microplate reader
Figure 4A	40 mM Tris pH 7.4	45 nM LwaCas13a	22.5 nM LwaCas13a crRNA targeting *s* gene, 22.5 nM LwaCas13a crRNA targeting *n* gene	250 nM PolyU-FAM	-	6 mM	Real-time PCR
Figure 4B	20 mM HEPES pH 6.8	45 nM LwaCas13a, 135 nM PsmCas13b,	22.5 nM LwaCas13a crRNA targeting *s* gene, 67.5 nM PsmCas13b crRNA targeting *n* gene	Only 250 nM PolyU-FAM, only 500 nM PolyA-ROX, or both	750 mM betaine	24 mM	Naked eye visualization

Figure	Buffer identity and concentration	Cas enzyme identity and concentration	crRNA identity and concentration	RNA reporter identity and concentration	additive	MgCl$_2$ concentration	Equipment used to monitor Cas-based reactions
Figure 1– figure supplement 1C, 1D	40 mM Tris pH 7.4	45 nM LwaCas13a	22.5 nM LwaCas13a crRNA for each gene	1 µM FAM-Bio	-	6 mM	Lateral flow strip
Figure 1– figure supplement 2A, 2B, 2D	20 mM HEPES pH 6.8	45 nM LwaCas13a, 135 nM PsmCas13b,	22.5 nM LwaCas13a crRNA targeting *s* gene, 67.5 nM PsmCas13b crRNA targeting *n* gene	250 nM PolyU-FAM, 500 nM PolyA-Cy5	-	24 mM	Tecan microplate reader
Figure 1– figure supplement 2C	40 mM Tris pH 7.4	45 nM LwaCas13a	22.5 nM LwaCas13a crRNA for *s* gene	250 nM PolyU-FAM	-	6 mM	Tacan microplate reader
Figure 4B	20 mM HEPES pH 6.8	45 nM LwaCas13a, 135 nM PsmCas13b,	22.5 nM LwaCas13a crRNA targeting *s* gene, 67.5 nM PsmCas13b crRNA targeting *n* gene	Only 250 nM PolyU-FAM, only 500 nM PolyA-ROX, or both	750 mM betaine	24 mM	Naked eye visualization
Figure 4D, 4E, and 4F	40 mM Tris pH 7.4	45 nM LwaCas13a	22.5 nM LwaCas13a crRNA for *n* gene	250 nM PolyU-FAM	-	6 mM	Tacan microplate reader
Figure 4G	40 mM Tris pH 7.4	45 nM LwaCas13a	22.5 nM LwaCas13a crRNA targeting S gene, 22.5 nM LwaCas13a crRNA targeting *n* gene	250 nM PolyU-FAM	-	6 mM	Real-time PCR
Figure 4H	40 mM Tris pH 7.4	45 nM LwaCas13a	22.5 nM LwaCas13a	250 nM PolyU-FAM		6 mM	Real-time PCR

Figure	Buffer identity and concentration	Cas enzyme identity and concentration	crRNA identity and concentration	RNA reporter identity and concentration	additive	MgCl$_2$ concentration	Equipment used to monitor Cas-based reactions
			crRNA targeting S gene, 22.5 nM LwaCas13a crRNA targeting n gene				
Figure 1– figure supplement 1	40 mM Tris pH 7.4	45 nM LwaCas13a	22.5 nM LwaCas13a crRNA for each gene	1 µM FAM-Bio	-	6 mM	Lateral flow strip
Figure 1– figure supplement 1D	40 mM Tris pH 7.4	45 nM LwaCas13a	22.5 nM LwaCas13a crRNA for each gene	1 µM FAM-Bio	-	6 mM	Lateral flow strip
Figure 1– figure supplement 2A, 2B, 2D	20 mM HEPES pH 6.8	45 nM LwaCas13a, 135 nM PsmCas13b,	22.5 nM LwaCas13a crRNA targeting s gene, 67.5 nM PsmCas13b crRNA targeting n gene	250 nM PolyU-FAM, 500 nM PolyA-Cy5	-	24 mM	Tecan microplate reader
Figure 1– figure supplement 2C	40 mM Tris pH 7.4	45 nM LwaCas13a	22.5 nM LwaCas13a crRNA for s gene	250 nM PolyU-FAM	-	6 mM	Tacan microplate reader
Figure 1– figure supplement 2D	40 mM Tris pH 7.4	45 nM LwaCas13a	22.5 nM LwaCas13a crRNA for s gene or n gene	250 nM PolyU-FAM	-	6 mM	Tacan microplate reader
Figure 1– figure supplement 2E	40 mM Tris pH 7.4	45 nM LwaCas13a	22.5 nM LwaCas13a crRNA for n gene	250 nM PolyU-FAM	-	6 mM	Tacan microplate reader

Figure	Buffer identity and concentration	Cas enzyme identity and concentration	crRNA identity and concentration	RNA reporter identity and concentration	additive	MgCl$_2$ concentration	Equipment used to monitor Cas-based reactions
Figure 1–figure supplement 4A	20 mM HEPES pH 6.8	Varying PsmCas13b amount	Varying PsmCas13b crRNA	250 nM PolyA-Cy5	-	6 mM	Varioskan microplate reader
Figure 1–figure supplement 4B	20 mM HEPES pH 6.8	135 nM PsmCas13b	67.5 nM PsmCas13b crRNA	varying PolyA-Cy5 amount	-	6 mM	Varioskan microplate reader
Figure 1–figure supplement 5 LwaCas13a	20 mM HEPES pH 6.8	45 nM LwaCas13a	22.5 nM LwaCas13a crRNA for *n* gene	250 nM PolyU-FAM	-	6 mM	Varioskan microplate reader
Figure 1–figure supplement 5 PsmCas13b	20 mM HEPES pH 6.8	135 nM PsmCas13b	67.5 nM PsmCas13b crRNA	500 nM PolyA-Cy5	-	6 mM	Varioskan microplate reader
Figure 1–figure supplement 6B	40 mM Tris pH 7.4	45 nM RfxCas13d	28.4 nM RfxCas13d crRNA	250 nM PolyU-FAM reporter or 125 nM RNase Alert	-	6 mM	Varioskan microplate reader
Figure 1–figure supplement 6C	40 mM Tris pH 7.4	45 nM RfxCas13d or RfxCas13d-RBD or LwaCas13a	22.5 nM LwaCas13a crRNA or 28.4 nM RfxCas13d crRNA	500 nM PolyU/FAM reporter	-	6 mM	Tecan microplate reader
Figure 1–figure supplement 7A	40 mM Tris pH 7.4	45 nM LwaCas13a	22.5 nM LwaCas13a crRNA for target gene	250 μM PolyU-FAM	-	6 mM	Tacan microplate reader
Figure 1–figure supplement 7B	20 mM HEPES pH 6.8	45 nM LwaCas13a, 135 nM PsmCas13b,	22.5 nM LwaCas13a crRNA targeting *s* gene, 67.5 nM PsmCas13b	250 nM PolyU-FAM, 500 nM PolyA-Cy5	Varying additives	24 mM	Tecan microplate reader

Figure	Buffer identity and concentration	Cas enzyme identity and concentration	crRNA identity and concentration	RNA reporter identity and concentration	additive	MgCl$_2$ concentration	Equipment used to monitor Cas-based reactions
			crRNA targeting n gene				
Figure 1–figure supplement 7C	20 mM HEPES pH 6.8	45 nM LwaCas13a, 135 nM PsmCas13b,	22.5 nM LwaCas13a crRNA targeting s gene, 67.5 nM PsmCas13b crRNA targeting n gene	250 nM PolyU-FAM, 500 nM PolyA-Cy5	With and without 500 mM betaine	24 mM	Tecan microplate reader
Figure 1–figure supplement 8	20 mM HEPES pH 6.8	45 nM LwaCas13a, 135 nM PsmCas13b,	22.5 nM LwaCas13a crRNA targeting s gene, 67.5 nM PsmCas13b crRNA targeting n gene	250 nM PolyU-FAM, 500 nM PolyA-Cy5	Varying betaine amount	24 mM	Tecan microplate reader
Figure 1–figure supplement 9A	40 mM Tris pH 7.4	Varying amount of LwaCas13a	Varying amount of LwaCas13a crRNA targeting s gene	250 nM PolyU-FAM	-	6 mM	RT-PCR machine
Figure 1–figure supplement 9B	20 mM HEPES pH 6.8	Varying amount of PsmCas13b	Varying amount of PsmCas13b crRNA targeting n gene	500 nM PolyA-Cy5	-	6 mM	Varioskan microplate reader
Figure 1–figure supplement 9C	Varying type of buffers	45 nM LwaCas13a, 45 nM PsmCas13b	45 nM LwaCas13a crRNA targeting s gene, 45 nM PsmCas13b crRNA targeting n gene	250 nM PolyU-FAM, 500 nM PolyA-Cy5	-	6 mM	Tecan microplate reader

Figure	Buffer identity and concentration	Cas enzyme identity and concentration	crRNA identity and concentration	RNA reporter identity and concentration	additive	MgCl$_2$ concentration	Equipment used to monitor Cas-based reactions
Figure 1– figure supplement 10	40 mM Tris pH 7.4	45 nM LwaCas13a	22.5 nM LwaCas13a crRNA targeting n gene		-	6 mM	Real-time PCR
Figure 1– figure supplement 11	40 mM Tris pH 7.4	45 nM LwaCas13a	22.5 nM LwaCas13a crRNA targeting S gene, 22.5 nM LwaCas13a crRNA targeting n gene (s/n gene detection)	250 nM PolyU-FAM	750 mM betaine	24 mM	Tecan microplate reader
Figure 4– figure supplement 2	20 mM HEPES pH 6.8	45 nM LwaCas13a, 135 nM PsmCas13b,	22.5 nM LwaCas13a crRNA targeting *s* gene, 67.5 nM PsmCas13b crRNA targeting *n* gene	250 nM PolyU-FAM with 500 nM PolyA-Cy5, 250 nM or 500 nM PolyA-ROX	750 mM betaine	24 mM	Tecan microplate reader

Table S5. The limit of detection (LoD) of the multiplexed CRISPR-based detection of SARS-CoV-2 RNA. Estimated LoDs at 95% positive rate (95% LoD) from LwaCas13a-mediated *s* gene detection, PsmCas13b-mediated *n* gene detection, LwaCas13a-mediated *s* and *n* gene detection, or combined LwaCas13a-mediated *s* gene and PsmCas13b-mediated *n* gene detection determined using Probit regression. Calculation was performed using MedCalc (MedCalc software Ltd).

95% LoD qPCR C_t (95% CI)	At 60 minutes CRISPR reaction time
Detecting the *s* gene via LwaCas13a	36.83*
Detecting the *n* gene via PsmCas13b	36.78*
Detecting either the *s* or *n* gene via LwaCas13a	36.48 (35.99 – 36.97)
Detecting either the *s* or *n* gene via LwaCas13a/PsmCas13b	37.01*

*The margins of error were negligible.

Appendix 1

The linear correlation between qPCR Ct value and RNA copy number obtained from ddPCR.

RT-qPCR or ddPCR analyses were performed on paired samples from a dilution series of RNA extract from the cultured SARS-CoV-2 Wuhan strain. The experiment was carried out in triplicate (Appendix Table 1). Associated instructions were described in the *Materials and Methods* section. Linear regression analysis was performed. (Appendix Figure 1)
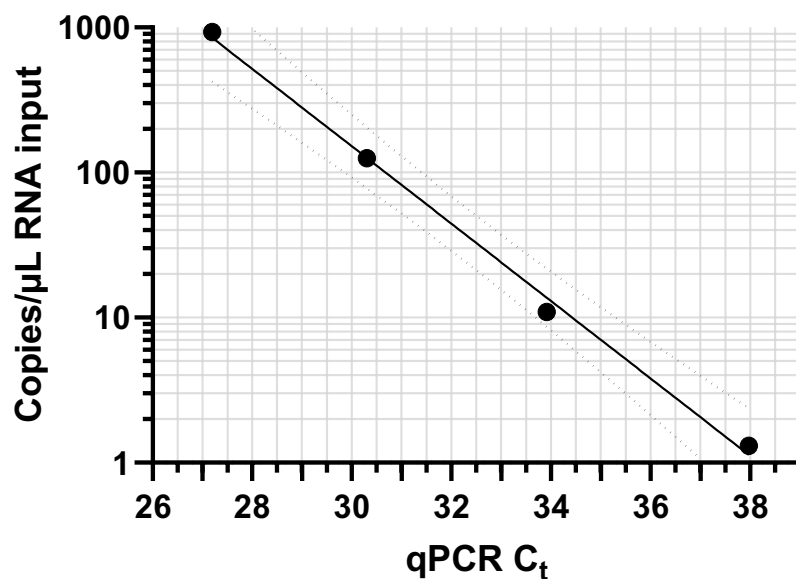
Appendix Figure 1 A standard plot of qPCR Ct value versus copies per µL obtained from ddPCR. Data are mean from three replicates. Linear regression equation: $\log_{10}$ (Copies per µL input) = -0.2669 (qPCR C_t) + 10.187, R^2 = 0.9967. *Dashed lines represent the 95% confidence intervals*

Appendix Table 1 Raw data underlying Appendix Figure 1

Dilution	qPCR Ct			Mean	SD	Copies per µL input			Mean	SD
	Triplicates					Triplicates				
1x	27.15	27.20	27.23	27.19	0.04	912	896	984	930.67	46.88
10x	30.31	30.30	30.30	30.30	0.01	114.8	137.2	123.6	125.20	11.29
100x	34.12	33.75	33.86	33.91	0.19	8.4	12.4	12	10.93	2.20
1000x	38.30	38.25	37.36	37.97	0.53	1.12	0.4	2.4	1.31	1.01